

# **Applications of Perturbative Quantum Chromodynamics to Processes with Heavy Quarks**

by

Alexander Mitov

Submitted in Partial Fulfillment  
of the  
Requirements for the Degree

Doctor of Philosophy

Supervised by  
Professor Lynne H. Orr

Department of Physics and Astronomy  
The College  
Arts and Sciences

University of Rochester

Rochester, New York

2003

*To my wife and true friend Milena Mitova,  
in appreciation for all her support.*

## **Curriculum Vitae**

The author was born in Sofia, Bulgaria. He attended Sofia University of St. Kliment Ohridski from 1990 to 1996. He graduated with a Master of Science degree in Physics in 1996 under the supervision of Professor D. Stoyanov. The author came to the University of Rochester in the fall of 1999. He pursued his research in elementary particle physics under the direction of Professor L. H. Orr and received the Master of Arts degree in 2001.

## Acknowledgments

First, I would like to thank my advisor Professor Lynne H. Orr for opening the doors of perturbative QCD to me and for her entire support during my research and study at the University of Rochester. I would like to thank Dr. Gennaro Corcella for his collaboration on the three papers that became the backbone of this thesis and for his consistency and hard work, and for the numerous important discussions that we have had while working together. I would also like to thank Dr. Matteo Cacciari for his collaboration on one of the papers that shaped this thesis, for the many useful discussions and for supplying us with his numerical code for performing inverse Mellin transformation and fits of hadronization models to  $e^+e^-$  data.

I would also like to thank Dr. S. Catani for very useful discussions on the subject of soft-gluon resummation, as well as Dr. A. Bodek and Dr. S. Kretzer for the helpful insights on the subject of DIS. It is also my pleasure to thank Dr. A. Das and Dr. D. Wackerlo for the many discussions on this and related topics.

# Applications of Perturbative Quantum Chromodynamics to Processes with Heavy Quarks

by

Alexander Mitov

## Abstract

In this thesis we apply perturbative QCD to make precision predictions for some observables in high-energy processes involving heavy quarks.

The first application we consider is a prediction for the spectrum of  $b$ -flavored hadrons in top quark decay. For that purpose we calculate at NLO the QCD corrections for bottom fragmentation in top decay with the  $b$ -mass fully taken into account. Using the perturbative fragmentation function formalism we then resum with NLL accuracy large collinear logs of the ratio of bottom-to-top mass, which leads to an essential improvement of the results. Next we perform the threshold resummation for the coefficient function for top decay with NLL accuracy. That resummation leads to an important improvement of the  $b$  spectrum in the region where the produced bottom in top decay carries a large fraction of the momentum of the parent top. Finally, we extract information for the non-perturbative  $b$ -fragmentation into hadrons from  $e^+e^-$  data and make a prediction for the spectrum of those  $b$ -flavored hadrons produced in top-quark decay.

Our second application is to charm production in charged-current DIS. We first calculate with NLL accuracy the soft-gluon resummed coefficient function for heavy quark production (initiated by a light quark) in inclusive DIS. Our result is applicable for the case of low momentum transfer that is of the order of the mass of the heavy quark. We also make a connection of this result to the known result for massless quark production. We then apply this result for charm quark production at NuTeV and HERA for a wide range of the transferred momentum, and present the effect of the threshold resummation on the charm structure functions.

# Contents

<b>Table of Contents</b>	<b>vii</b>
<b>List of Tables</b>	<b>x</b>
<b>List of Figures</b>	<b>xi</b>
<b>1 Introduction</b>	<b>1</b>
<b>2 Preliminaries: Perturbative QCD</b>	<b>7</b>
2.1 QCD as a Fundamental Model for the Strong Interactions . . . . .	7
2.1.1 Quark Hypothesis . . . . .	8
2.1.2 Parton Model . . . . .	9
2.1.3 QCD: the Dynamical Theory of Color . . . . .	10
2.1.4 Strong Coupling Constant . . . . .	13
2.2 QCD Factorization Theorem . . . . .	15
2.3 Perturbative Evolution: DGLAP Equations . . . . .	20
2.3.1 The Case of Space-like Evolution . . . . .	21
2.3.2 The Case of Time-like Evolution . . . . .	28
2.4 Infrared Effects . . . . .	29
2.4.1 Heavy Quark Masses . . . . .	32
2.4.2 Perturbative Fragmentation Function Formalism . . . . .	34

2.4.3	Soft-gluon Threshold Resummation . . . . .	39
<b>3</b>	<b><i>b</i>-quark Fragmentation in <i>t</i>-quark Decay</b>	<b>48</b>
3.1	Motivation: Top Physics . . . . .	48
3.2	$t \rightarrow bW$ in NLO QCD . . . . .	51
3.2.1	Calculation with $m_b \neq 0$ . . . . .	53
3.2.2	Calculation with $m_b=0$ . . . . .	59
3.3	NLL Resummation of $\log(m_b^2/m_t^2)$ . . . . .	61
3.4	NLL Threshold Resummation . . . . .	66
3.5	Energy Spectrum of <i>b</i> -flavored Hadrons in Top Decay . . . . .	75
<b>4</b>	<b>Charged–Current Deep Inelastic Scattering</b>	<b>81</b>
4.1	CC DIS: Notation and Overview . . . . .	81
4.2	Behavior of the Coefficient Function in the Soft Limit . . . . .	88
4.3	Soft-gluon Resummation for the Quark-initiated Coefficient Function	91
4.3.1	The case $m^2 \sim Q^2$ . . . . .	94
4.3.2	The case $m^2 \ll Q^2$ . . . . .	98
4.4	Phenomenological Results for Charm Quark Production . . . . .	100
<b>5</b>	<b>Conclusions</b>	<b>110</b>
	<b>Bibliography</b>	<b>113</b>
<b>A</b>	<b>Some Supplementary Results</b>	<b>121</b>
A.1	Relevant Feynman Rules . . . . .	121
A.2	Phase Space for Top Decay at NLO . . . . .	122
A.3	Spence Functions . . . . .	124
A.4	Plus Prescription . . . . .	126
A.5	Mellin-Space Results . . . . .	127

A.6	$N$ -space Result for the Coefficient Function and $D_q^{ini}$	128
A.7	$N$ -space Expressions for the Kernels $P_N^{(0,1)}$	129
A.8	Derivation of the Factors $K_i$ in Eqns.(4.47) and (4.58)	129

# List of Tables

3.1	Results of fits to $e^+e^- \rightarrow b\bar{b}$ ALEPH data, using matched coefficient function and initial condition, with NLL DGLAP evolution and NLL soft-gluon resummation. We set $\Lambda^{(5)} = 200$ MeV, $\mu_{0F} = \mu_0 = m_b = 5$ GeV and $\mu_F = \mu = \sqrt{s} = 91.2$ GeV. $\alpha$ and $\beta$ are the parameters in the power law (3.39), $\delta$ refers to (3.40), $\epsilon$ to (3.41). The fits have been performed neglecting the correlations between the data points. . . . .	78
3.2	Experimental data for the moments $\sigma_N^B$ from DELPHI [89], the resummed $e^+e^-$ perturbative calculations for $\sigma_N^b$ [43], the extracted non-perturbative contribution $D_N^{np}$ . Using the perturbative results $\Gamma_N^b$ , a prediction for the physical observable moments $\Gamma_N^B$ is given. Set [A]: $\Lambda^{(5)} = 0.226$ GeV and $m_b = 4.75$ GeV, set [B]: $\Lambda^{(5)} = 0.2$ GeV and $m_b = 5$ GeV. The experimental error should of course be propagated to the final prediction. . . . .	80

# List of Figures

3-1	Tree level (Born) diagram. . . . .	54
3-2	Contributing virtual emission diagrams. . . . .	54
3-3	Contributing real emission diagrams. . . . .	54
3-4	<i>b</i> -quark energy distribution in top decay according to the perturbative fragmentation approach, with (solid line) and without (dashes) NLL soft-gluon resummation in the initial condition of the perturbative fragmentation function, and according to the exact NLO calculation, with (dot-dashes) and without (dots) inclusion of powers of $m_b/m_t$ . In the inset figure, we show the same curves on a logarithmic scale. . . . .	64
3-5	(a): $x_b$ spectrum for $\mu_F = m_t$ and $\mu_{0F} = m_b/2$ (dots), $\mu_{0F} = m_b$ (solid) and $\mu_{0F} = 2m_b$ (dashes); (b): $\mu_{0F} = m_b$ and $\mu_F = m_t/2$ (dots), $\mu_F = m_t$ (solid) and $\mu_F = 2m_t$ (dashes). The renormalization scales are kept at $\mu = m_t$ and $\mu_0 = m_b$ . Though not visible, all distributions show a finite, sharp peak once $x_b$ is close to 1. . . . .	65
3-6	<i>b</i> -quark energy distribution in top decay according to the perturbative fragmentation approach, with (solid line) and without (dashes) NLL soft-gluon resummation. In the inset figure, we show the same curves on a logarithmic scale, for $x_b > 0.8$ . We have set $\mu_F = \mu = m_t$ and $\mu_{0F} = \mu_0 = m_b$ . . . . .	72

3-7	<i>b</i> -quark energy spectrum for different values of the factorization scale $\mu_F$ , with (solid) and without (dashes) NLL soft-gluon resummation. The other scales are fixed at $\mu = m_t$ , $\mu_0 = \mu_{0F} = m_b$ . As in Fig. 1, in the inset figure, we present the same plots for large values of $x_b$ , on a logarithmic scale. . . . .	73
3-8	As in Fig. 3-7, but for different values of $\mu_{0F}$ . The other scales are fixed at $\mu = \mu_F = m_t$ , $\mu_0 = m_b$ . . . . .	73
3-9	As in Fig. 3-7, but for different values of the renormalization scale $\mu$ . The other scales are fixed at $\mu_F = m_t$ , $\mu_0 = \mu_{0F} = m_b$ . . . . .	74
3-10	As in Fig. 3-7, but for different values of the renormalization scale $\mu_0$ . The other scales are fixed at $\mu = \mu_F = m_t$ , $\mu_{0F} = m_b$ . . . . .	74
3-11	$x_B$ spectrum in top decay, with the hadronization modelled according to a power law (solid lines), the Kartvelishvili et al. (dashes) and the Peterson (dots) model, with the relevant parameters fitted to the ALEPH data. The plotted curves are the edges of bands at one-standard-deviation confidence level. NLL soft-gluon resummation is included. We set $\mu_F = \mu = m_t$ and $\mu_{0F} = \mu_0 = m_b$ . . . . .	79
4-1	Deep Inelastic Scattering. . . . .	82
4-2	Results for $F_2^c(x, Q^2)$ for charm quark production in neutrino scattering at $Q^2 = 2 \text{ GeV}^2$ with (solid) and without (dashed) soft resummation in the coefficient function. We have set $\mu_F = \mu = Q$ . . . . .	104
4-3	As in Fig. 4-2, but for $Q^2 = 5 \text{ GeV}^2$ . . . . .	105
4-4	Results for $F_2^c(x, Q^2)$ for charm quark production in positron-proton scattering at HERA. for $Q^2 = 2 \text{ GeV}^2$ We have set $\mu_F = \mu = Q$ . In the inset figure, we show the same plots at large $x$ and on a linear scale. . . . .	106
4-5	As in Fig. 4-4, but for $Q^2 = 1000 \text{ GeV}^2$ . . . . .	106

4-6	Dependence of $F_2$ on the factorization scale for neutrino scattering at NuTeV. Solid lines include soft resummation in the coefficient function, dashed lines are fixed-order predictions	107
4-7	As in Fig. 4-6, but at HERA for $Q^2 = 300$ GeV $^2$ . In the inset figure, we plot the same curves at large $x$ and on a linear scale.	108
4-8	Comparison of massive (dashes) and massless (dots) fixed-order calculations with the resummed massive result (solid) for $Q^2 = 2$ GeV $^2$ and $\mu = \mu_F = Q$ . Plotted is the theoretical structure function $\mathcal{F}_2^c(\chi, Q^2)$ defined in Eq.(4.22).	109

# Chapter 1

## Introduction

For the three decades of its existence, the Standard Model (SM) of elementary particles has proved to be extremely successful. It has withstood all experimental tests and has become a well established theory. All predictions based on the SM have been experimentally verified and most of its parameters have been fixed. The only sector of the SM that has not been directly experimentally verified as of today is the Higgs sector and, in particular, the existence of a neutral massive spin-zero particle often simply referred to as Higgs. There is still no direct evidence for its existence and, despite the many constraints from precision electro-weak physics, the Higgs mass is not known. Not all of the parameters of the Higgs potential are determined, and its Yukawa couplings to the fermions are only implicitly tested through the measurements of the masses of the fermions (quarks and leptons). Experiments in the near future and most notably the Large Hadron Collider (LHC) and the Tevatron, will either confirm that particle's existence and fix the above mentioned parameters, or will significantly increase the limit on its mass.

The SM describes three of the four presently known interactions: Electromagnetic, Weak and Strong. The fourth one - Gravity - will not be considered in this

thesis. We will only point out that the orthodox viewpoint – that gravity becomes important only at scales of the order of the Plank one and is thus completely irrelevant for present day collider experiments – has been recently challenged. New ideas have emerged (Arkani-Hamed, Dimopoulos and Dvali [1], Randall and Sundrum [2]) suggesting that it may be possible for gravity to play an important role at energies as low as a TeV. However, at least at presently accessible energies, the experimental data do not favor any gravitational effects (usually through so-called Kaluza-Klein modes of gravity or other higher dimensional matter) and most of the models dealing with those effects typically assume that the lowest masses of the new particles are close to or above 1 TeV.

The SM is a gauge-field theoretical model based on the following non-abelian gauge group:

$$G_{SM} = SU(3)_C \times SU(2)_I \times U(1)_Y. \quad (1.1)$$

The gauge group is non-simple and involves three different dimensionless coupling constants corresponding to each of the three group factors above. The  $SU(2)_I \times U(1)_Y$  part corresponds to the Weinberg-Salam model [3] and provides a unified description <sup>1</sup> of the electromagnetic and weak interactions. There are four gauge bosons associated with that group: two neutral ones  $\gamma$  and  $Z$  and two charged ones  $W^\pm$ . The photon  $\gamma$  is exactly massless due to the unbroken  $U(1)$  subgroup that is identified with electro-magnetism. The other three are heavy, with masses approximately <sup>2</sup>  $m_Z = 91$  GeV and  $m_{W^\pm} = 80$  GeV; their masses arise as a result of electroweak symmetry breaking via the Higgs mechanism. The same mechanism also supplies the tree-level masses of the fermions through their

---

<sup>1</sup>Strictly speaking it is not truly unified since the group is not simple and we introduce *a priori* more than one dimensionless coupling.

<sup>2</sup>The values of the various constants used throughout this thesis are taken from the Particle Data Group [4].

Yukawa couplings to the Higgs doublet. The electroweak vector bosons couple to all fermions. The magnitude of those couplings is relatively small; the electromagnetic interactions are suppressed by powers of  $\alpha = e^2/4\pi \approx 1/137$ , while the effects of the weak interactions are typically proportional to powers of the Fermi constant  $G_F$ . For that reason the quantum corrections introduced by electro-weak interactions are much smaller than the ones due to strong interactions <sup>3</sup>.

The dependence of the dimensionless electroweak gauge couplings  $g$  and  $g'$  on energy is “intuitive” i.e. the strength of the electroweak interactions increase with the energy scale. For that reason the  $SU(2) \times U(1)$  theory of the electroweak interactions is a true perturbation theory formulated directly in terms of observable fields <sup>4</sup>. The situation changes dramatically when one considers the strong interactions described by the  $SU(3)_C$  factor in (1.1). First, the coupling constant is not small. Moreover, as is well known, a non-abelian gauge theory with such a gauge group and with sufficiently small number of active fermions (flavors) exhibits the “counter-intuitive” behavior known as asymptotic freedom: the dimensionless coupling constant associated with that group decreases with the increasing of the energy scale and effectively such a theory behaves as a free theory at high energies. However, at small energies the coupling grows and eventually diverges at some finite value of the energy scale. That scale, usually denoted as  $\Lambda_{QCD}$ , has a value of the order of 200–300 MeV and quantifies the borderline between the perturbative and non-perturbative regimes in such a theory. Although the detailed description of QCD will be spared for the next Chapter, from the above discussion it becomes clear that such a theory exhibits another remarkable property: confinement. The growing of the coupling at low energies (which corresponds to large distances)

---

<sup>3</sup>This is also the case in the applications considered in this thesis as will be detailed in the subsequent sections.

<sup>4</sup>With the exception of the quarks; see below.

indicates that the particles whose interaction is described by such a gauge theory may not be able to exist as free (asymptotic) states at all. Instead, they will form bound states. That expectation is confirmed by experiment: no free quarks have ever been observed experimentally. Unlike the quarks that carry an additional quantum number called color, the observable strongly interacting particles – the hadrons – are colorless objects and have the quantum numbers of two-particle (mesons) and three-particle (baryons) bound states of quarks. Strictly speaking, the property of confinement is an assumption based on the above mentioned behavior of the strong coupling constant and the non-observation of free colored particles. The derivation of the properties of the hadrons from the first principles (i.e. from QCD) is one of the fundamental problems in theoretical physics today.

It is a remarkable achievement that we are able to make precise predictions for the observed hadronic states in high energy experiments based on a theory formulated in terms of non-observable constituents - the quarks. One of the main ingredients of the theory that makes this possible is the so-called factorization theorem. In essence, it states that in hard scattering experiments with typical hard scale  $Q \gg \Lambda_{QCD}$  an observable (e.g. a cross-section) can be written as a product (more precisely - convolution) of perturbative and non-perturbative parts. The former part can be calculated in perturbation theory based on an expansion in the strong coupling constant  $\alpha_S(Q^2)$  while the latter part has to be extracted from the experiment. It is possible to extend the factorization theorem even to processes where other scales besides  $Q$  are present, e.g. when heavy quarks are involved. As will be clear from discussions throughout this thesis, there is no absolute notion of heavy quarks, i.e. whether a quark is considered heavy or light depends on the particular problem being studied. However, in general, light quarks are considered to be those with masses below  $\Lambda_{QCD}$  (i.e.  $u, d, s$ ) while the ones with masses above that scale are usually considered to be heavy ( $c, b, t$ ). The reason behind such a

separation is easy to understand: for a heavy quark with mass  $M$ ,  $\alpha_S(M^2) < 1$  and it is indeed sensible to apply perturbation theory. Studies of QCD involving processes with heavy quarks are at present an important internal test for QCD as well as for obtaining precision predictions that will be needed to distinguish signals from new physics (Supersymmetry, Extra Dimensions, etc.).

QCD has another peculiar feature: there are situations where the convergence of the perturbation series is spoiled because of the appearance of additional factors that multiply the coupling constant to any order in perturbation series. The presence of such terms effectively alters the expansion parameter to a larger value which in turn spoils the convergence of the series. To be able to obtain useful information in that case, one needs to resum classes of such terms to all orders in the coupling constant.

There are many examples of physical processes where the factorization theorem plays a decisive role in studies of processes involving heavy quarks and where often the application of the above mentioned resummations leads to serious improvement of the perturbative results. This thesis is devoted to the study of two such processes in perturbative QCD (pQCD) with detailed phenomenological applications: the spectrum of  $b$ -flavored hadrons in top quark decay and neutrino production of charm in Deep Inelastic Scattering (DIS).

In the SM, it is the mass of the top that uniquely distinguishes it from the other five flavors. The very large value of this parameter, however, is sufficient to draw particular attention to the top quark. Top's large mass is responsible for its small lifetime, the latter preventing the top from forming bound states (a process known as hadronization). For that reason, the top quark behaves like a real particle and one can safely describe its decay in perturbation theory. Since the only experimental information about the top is through its decay products, it is very important to have a precise prediction for the decay products of the top.

In this thesis we make a prediction for the spectrum of the hadrons resulting from the hadronization of the  $b$ -quark in top quark decay and resumming to all orders in  $\alpha_S$  and with next-to-leading logarithmic (NLL) accuracy two classes of large logs: quasi-collinear ones that are due to the large ratio of top-to-bottom mass and soft ones that are due to soft-gluon radiation and affect the distribution in particular kinematical regions. Such results will be very important after the near future high energy experiments supply enough data on top decay.

The second process studied in this thesis is Deep Inelastic Scattering (DIS), a process of scattering of a lepton off a hadronic target. Since the leptons do not interact strongly, that process can serve as a tool to study the structure of the hadrons by probing them with a virtual vector boson emitted from the lepton. DIS is perhaps the most studied high energy process; it was in this process in the late 1960's that Bjorken scaling was discovered, and which in turn served as a motivation for the introduction of the quark-parton model. Using the available next-to-leading (NLO) calculations for heavy quark production in charged-current (CC) DIS we calculate the corrections to the charm structure functions in the region of low momentum transfer and fully accounting for the mass of the charm quark. Such a result is important for the precise determination of the parton distribution functions in the target hadrons as well as the value of the charm mass.

This thesis is organized as follows: in the next Chapter we discuss some general features of QCD from the perspective of our applications. In Chapter 3 we present our original results on  $b$ -fragmentation in top decay. In Chapter 4, we discuss our original results for soft-gluon resummation in the coefficient function for heavy quark production in CC DIS, which we apply to study the effect of the threshold resummation on charm production at low energy transfer. In Chapter 5 are our conclusions. In the appendix we have listed some useful results.

# Chapter 2

## Preliminaries: Perturbative QCD

In the previous Chapter we made some general remarks about the relevance of QCD as a theory of the strong interactions as well as few of its peculiar features. In this Chapter we are going to systematically review that theory and derive many of its properties. The organization of the material in the present Chapter does not follow any particular review on QCD but is presented in a way that is suitable for our applications. There are many excellent reviews of QCD; some of those include [5, 6, 7, 8, 9].

### 2.1 QCD as a Fundamental Model for the Strong Interactions

The strong interactions govern the interactions of hadrons at a wide range of energies: from the highest energies accessible to the present day colliders down to energies typical for the nuclear physics. At the same time the behavior of the strong interaction is very different in the low and high energy regimes. At low energies, i.e. energies characterized by a scale  $\mu \ll \Lambda_{QCD}$ , the hadrons behave

as if they are fundamental particles. However, no successful field-theoretical description in terms of the observed hadrons was found that was able to describe the high energy regime and explain the proliferation of observed hadrons at high energy colliders. Contrary to the early expectations, the breakthrough towards the understanding of the strong interactions was made in the study of the high energy behavior of the hadrons.

### 2.1.1 Quark Hypothesis

In 1964 Gell-Mann and Zweig [10] introduced the idea of quarks: a few elementary particles that are the building blocks of all hadrons. There are six known types of quarks (quark flavors); they are spin 1/2 fermions with rational electric charges (in units of the charge of the electron):  $u, c, t$  have charge +2/3 while  $d, s, b$  have charge -1/3. The quark hypothesis assumes that the wave function of a hadron is constructed from the one-particle wave functions of quarks and/or antiquarks. The mesons have the quantum numbers of a quark-antiquark pair while the baryons are combinations of three (anti)quarks. Also, in order to avoid a problem with the spin-statistics theorem, it was necessary to introduce additional hidden quantum number - *color* [11]. From a comparison with experiment it was concluded that each quark flavor must have three different “copies” labelled by an additional color index. Since no colored particles have been observed it was postulated that the hadrons can only form “colorless” combinations of quarks, i.e. color was introduced as an exact global symmetry. It can be shown that the above observations plus the requirement that quarks and antiquarks transform under different (complex-conjugated) irreducible representations of the color symmetry group uniquely fixes the group to be  $SU(3)_C$ . The quarks transform under the fundamental representation **3** of that group, while the antiquarks transform under

its conjugated representation  $\overline{\mathbf{3}}$ .

### 2.1.2 Parton Model

The idea that the hadrons are built from elementary constituents - the partons [12] - was extremely successful not only in explaining the hadron spectroscopy but also in the description of the Bjorken scaling [13] observed in Deep Inelastic Scattering (DIS) experiments [14]. The experimental data showed that at large scales the structure functions of the nucleons are (approximately) independent of the value of the hard energy scale  $Q$  and depend only on the Bjorken variable  $x$  (for a detailed description of DIS we refer the reader to Section (4.1)). The parton model assumes that in high energy lepton-nucleon scattering, where the transferred momentum is large enough so the masses of the partons and their transverse motion inside the nucleon can be neglected, the virtual electroweak vector boson emitted from the initial lepton is scattered incoherently by a single free point-like parton  $a$ . The whole information about the structure of the hadron that is relevant to the high energy process is encoded in a scalar function  $f_a(\xi)$  called the parton distribution function (pdf) representing the probability distribution for finding the parton  $a$  inside the hadron and carrying a fraction  $\xi : 0 \leq \xi \leq 1$  of the momentum of the parent hadron. The philosophy of the parton model then suggests the following form of the hadronic interactions at high energy:

$$d\sigma(h, \dots) = \sum_a \int_0^1 d\xi \ f_a(\xi) \ d\hat{\sigma}(a, \dots) , \quad (2.1)$$

where  $d\sigma(h, \dots)$  is the cross-section for scattering of a hadron  $h$  and  $\dots$  stands for the other particles in the scattering process;  $d\hat{\sigma}(a, \dots)$  is a parton level cross-section with the hadron  $h$  replaced by a free parton  $a$ , and the partonic cross-section is weighted with the distribution function  $f_a(\xi)$ . Since the parton model is a free theory, to lowest order in the electroweak coupling the partonic cross-section is

very simple:  $d\hat{\sigma} \sim \delta(\xi - x)$ , so that the momentum fraction  $\xi$  is identified with the Bjorken variable  $x$  (cf. Section (4.1)). Therefore under the parton model assumption (2.1), the structure functions are simply proportional to the pdf  $f_a(x)$  and naturally independent of the hard transferred momentum  $Q$ .

The success of the parton model goes beyond the description of Bjorken scaling. It also makes a prediction about various relations involving the measurable structure functions  $F_1, F_2, \dots$  (that will be properly introduced in Section (4.1)), among which is the Callan-Gross relation [15]:

$$F_2(x) = xF_1(x) , \quad (2.2)$$

which is related to the fact that quarks have spin 1/2. The parton model can be generalized to other processes as well; one just needs to measure the pdfs for the various quarks in a specific process in order to predict a measurable quantity for another process. In that procedure, the following relations between the various parton distributions following from isospin invariance are often assumed:

$$f_u^{proton}(x) = f_d^{neutron}(x) ; \quad f_d^{proton}(x) = f_u^{neutron}(x). \quad (2.3)$$

### 2.1.3 QCD: the Dynamical Theory of Color

Although the parton model was quite successful in the description of many high energy processes, it was clear that it is at best a good hint towards a complete dynamical theory of the strong interactions. The complete theory would be able to explain one of the basic assumptions of the parton model - asymptotic freedom. Such a theory was constructed around 1973 after it was understood that the Yang-Mills theories do play an important role in high energy physics; at that time the renormalizeability of those theories was proved and methods for their quantization were developed [16]. It was also shown that the non-abelian theories were the only

theories which may exhibit asymptotic freedom, or technically, have negative first coefficient in the  $\beta$ -function (see next section). All these developments led to the construction of QCD as the dynamical theory of the strong interactions [17] as follows:

QCD is a non-abelian gauge theory with six quark flavors. The gauge group can be naturally obtained by gauging the exact global color symmetry group  $SU(3)_C$ . The quarks transform under the fundamental representation of  $SU(3)_C$ . Since  $\dim(SU(3)) = 8$ , there are eight gauge bosons called *gluons* that are electrically neutral, carry color charge and, as usual, are hermitian fields that transform under the adjoint representation of the gauge group  $SU(3)_C$ .

The lagrangian of QCD has the following form:

$$\mathcal{L}_{QCD} = -\frac{1}{4}F_{\mu\nu}^a F^{a,\mu\nu} + i \sum_q \overline{\psi^i}_q \gamma^\mu (D_\mu)_{ij} \psi_q^j - \sum_q m_q \overline{\psi^i}_q \psi_q^i, \quad (2.4)$$

where the index  $i = 1, 2, 3$  runs over the different quark colors and  $q$  over the quark flavors:  $q = u, b, s, c, b, t$ . The field-strengths are given by:

$$F_{\mu\nu}^a = \partial_\mu A_\nu^a - \partial_\nu A_\mu^a - g_S f^{abc} A_\mu^b A_\nu^c, \quad (2.5)$$

and the gauge-covariant derivative is:

$$(D_\mu)_{ij} = \delta_{ij} \partial_\mu + i g_S \sum_a t_{ij}^a A_\mu^a. \quad (2.6)$$

In the above equations,  $g_S$  is the strong coupling constant,  $f^{abc}$  are the structure constants of the gauge group and  $t^a$  are the generators of the fundamental representation of the gauge group. In general, the lagrangian (2.4) must be supplemented with gauge-fixing and ghost terms. The quarks have non-zero masses but their origin is outside QCD; in SM their masses result from the electroweak symmetry breaking. The only free parameters in QCD are the six quark masses and the single gauge coupling constant.

The gauge group has the following matrix structure which, for generality, we present for arbitrary group  $SU(N)$ : the fundamental representation has generators  $t^a$ ,  $a = 1, \dots, N^2 - 1$  that satisfy

$$\begin{aligned} \text{tr}(t^a t^b) &= \frac{1}{2} \delta^{ab} \\ \sum_a t_{ij}^a t_{jk}^a &= C_F \delta_{ik}, \quad i, j, k = 1, \dots, N. \end{aligned} \quad (2.7)$$

For the group  $SU(3)$ , the generators  $t^a$  are usually given by the Gell-Mann matrices  $\lambda^a$ :  $t^a = \lambda^a/2$ . Similarly, the adjoint representation has generators  $T^a$  that can be related to the structure constants  $f^{abc}$  through:

$$(T^a)_{bc} = f^{abc}, \quad (2.8)$$

and

$$\text{tr}(T^c T^d) = \sum_{a,b} f^{abc} f^{abd} = C_A \delta^{cd}. \quad (2.9)$$

Above,  $C_F$  and  $C_A$  are the values of the quadratic Casimir of the gauge algebra in the fundamental and adjoint representations respectively:

$$C_F = \frac{N^2 - 1}{2N}; \quad C_A = N, \quad (2.10)$$

and for the case of  $SU(3)$ :

$$C_F = \frac{4}{3}; \quad C_A = 3. \quad (2.11)$$

Once formulated, it must be shown that QCD indeed is capable of reproducing the success of the parton model as a first step. That in fact follows since from the very formulation of QCD it is clear that the parton model corresponds to the Born approximation of QCD. The real challenge however is to derive the asymptotic freedom from first principles and also to derive the corrections to the Bjorken scaling.

### 2.1.4 Strong Coupling Constant

The running of the renormalized strong coupling  $\alpha_S = g_S^2/4\pi$  is determined from the following equation:

$$\mu \frac{\partial \alpha_S}{\partial \mu} = 2\beta(\alpha_S). \quad (2.12)$$

The  $\beta$ -function  $\beta(\alpha_S)$ <sup>1</sup> has a series expansion in the coupling constant  $\alpha_S$ . It can be determined up to a fixed order in perturbation theory from explicit evaluation of the gauge coupling renormalization constant  $Z_g$ :

$$\beta(g) = \lim_{\epsilon \rightarrow 0} \left( -\epsilon g - \frac{\mu}{Z_g} \frac{dZ_g}{d\mu} g \right). \quad (2.13)$$

At present, the  $\beta$ -function of QCD is known to four loops in the  $\overline{\text{MS}}$  scheme [18]. However, since for all applications in this Thesis we need the evolution of the strong coupling to two loops, we will present only the two loop result:

$$\beta(\alpha_S) = -b_0 \alpha_S^2 - b_1 \alpha_S^3 - \dots, \quad (2.14)$$

with  $b_0$  and  $b_1$  given by

$$b_0 = \frac{33 - 2n_f}{12\pi}, \quad b_1 = \frac{153 - 19n_f}{24\pi^2}. \quad (2.15)$$

The first two coefficients of the  $\beta$ -function are independent of the renormalization scheme. However, that is no longer true for the higher order terms. In Eq.(2.15),  $n_f$  is the number of active massless flavors. In the presence of quark masses, its value becomes scale dependent. If one assumes strong ordering among the quark masses, then for scale  $\mu$ :  $m_n \ll \mu \ll m_{n+1}$  all flavors with masses below  $m_{n+1}$  are effectively massless while the rest of the flavors are heavy and can be integrated out. An example is the case of top decay considered in Chapter 3 where the scale

---

<sup>1</sup>In contrast to most of the standard presentations (e.g. [5]), we have introduced  $\beta(\alpha_S)$  through the relation:  $\beta(\alpha_S) = (g_S/4\pi)\beta(g)$ .

is running between the  $b$  and the  $t$  masses and because of their large difference we simply fix  $n_f = 5$ . However, in practical applications (especially with scales of the order of the  $b$  and the  $c$  quark) the strong ordering assumption is not always valid and therefore the choice of  $n_f$  is somehow ambiguous. The common practice is to change the value of  $n_f$  by one unit when the hard scale crosses the mass of the corresponding heavy quark. Such a change should be supplemented with an additional constraint that relates the values of the strong coupling evaluated in the two schemes at the switching point. In the  $\overline{\text{MS}}$  renormalization scheme, the strong coupling is continuous at the switching points [19] ( see also [4]), up to negligible corrections of order  $\mathcal{O}(\alpha_S^3)$ .

Now it is easy to show that indeed QCD enjoys the property of asymptotic freedom [20]. In a regime where the strong coupling is small, from (2.15) and (2.12), it is easy to see that the strong coupling is a decreasing function of the scale  $\mu$  if the number of flavors  $n_f < 33/2$ . That requirement is satisfied in QCD. The exact solution of Eq.(2.12) to NLO is given by:

$$\alpha_S(\mu^2) = \frac{1}{b_0 \ln(\mu^2/\Lambda^2)} \left\{ 1 - \frac{b_1 \ln [\ln(\mu^2/\Lambda^2)]}{b_0^2 \ln(\mu^2/\Lambda^2)} \right\}. \quad (2.16)$$

One can use this expression in order to relate the values of the strong coupling at two different scales with NLO accuracy [21]:

$$\begin{aligned} \alpha_S(k^2) &= \frac{\alpha_S(\mu^2)}{1 + b_0 \alpha_S(\mu^2) \ln(k^2/\mu^2)} \left( 1 - \frac{b_1}{b_0} \frac{\alpha_S(\mu^2)}{1 + b_0 \alpha_S(\mu^2) \ln(k^2/\mu^2)} \right. \\ &\quad \left. \times \ln(1 + b_0 \alpha_S(\mu^2) \ln(k^2/\mu^2)) + \mathcal{O}(\alpha_S^2(\mu^2) [\alpha_S(\mu^2) \ln(k^2/\mu^2)]^n) \right). \end{aligned} \quad (2.17)$$

The constant  $\Lambda$  contains all the information about the boundary condition to which Eq.(2.12) must be subjected. It is a low energy scale where the strong coupling diverges. As we mentioned in Chapter 1,  $\Lambda$  represents the border between the perturbative and non-perturbative regimes of QCD. In practice the value of  $\Lambda$

is not unambiguous. In high energy experiments one typically obtains information about the strong coupling constant at some large scale and only from there the value of  $\Lambda$  is inferred. It is obvious however, that in this way the determination of  $\Lambda$  “absorbs” all ambiguities such as the dependence on the order of  $\alpha_S$  (LO, NLO, etc.), the choice of the value of  $n_f$  and the choice of the renormalization scheme. In this Thesis we use the following value of the strong coupling at NLO [4]:

$$\alpha_S(M_Z^2) = 0.118 \quad (2.18)$$

It leads to  $\Lambda^{(5)} \approx 200$  MeV and  $\Lambda^{(4)} \approx 300$  MeV. The precise values used in our applications will be discussed in the next Chapters.

## 2.2 QCD Factorization Theorem

QCD is formulated in terms of quarks and gluons while the experimentally observed states are hadrons. Since at present we are not able to describe the non-perturbative regime of QCD, a fruitful application of QCD to the hadronic interactions requires a universal way of splitting the contributions from short- and long-distance physics.

Such a separation is possible. It is known as the (QCD) factorization theorem [22, 23] and states that for processes that have initial and/or observed final state hadrons the differential cross-section has the following form:

$$\begin{aligned} d\sigma(x, Q^2, m^2) &= \prod_{h,h'} \sum_{i,f} f_{i/h}(x, \mu^2) \otimes d\hat{\sigma}_{i \rightarrow f}(x, Q^2, m^2, \mu_r^2, \mu_F^2) \\ &\otimes D_{h'/f}(x, \mu^2) + \mathcal{O}(\Lambda/Q) \end{aligned} \quad (2.19)$$

The factor  $f_{i/h}$  stands for the parton distribution function of the parton  $i$  inside the hadron  $h$  present in the initial state, and  $Q$  and  $x$  represent the hard scale and some kinematical variable respectively. Unlike the simple parton model (2.1), the

parton distributions also depend on the factorization/renormalization scale  $\mu^2$ . That difference has important consequences since it incorporates the violations of Bjorken scaling. The second factor  $d\hat{\sigma}_{i \rightarrow f}$ , also known as the (Wilson) coefficient function, represents the partonic hard scattering cross section for the reaction  $i \rightarrow f$  that depends on the unphysical renormalization and factorization scales  $\mu_r^2$  and  $\mu_F^2$  and on the masses of the heavy quarks  $m^2$ . The last factor in (2.19) is the so called fragmentation function  $D$ . It contains the information for the hadronization of the hard parton  $f$  (that is produced in the hard process described by the partonic cross-section  $d\hat{\sigma}$ ) into an observed hadron  $h'$ . The integral convolution appearing in (2.19) is defined as:

$$(f \otimes g)(x) = \int_x^1 \frac{dz}{z} f(z) g(x/z), \quad (2.20)$$

where  $f$  and  $g$  are two functions with argument  $x : 0 \leq x \leq 1$ . The convolution has the property (2.40) which is important in practical applications.

The real power of the factorization theorem is in the fact that the distribution/fragmentation functions are universal: they depend only on the non-perturbative transition they describe and not on the hard scattering process. That is why once they are measured in one process, they can be applied to any other process. At the same time, the coefficient function contains all the information about the hard scattering process and is independent of the details of the non-perturbative transitions. Although the  $\otimes$ -product of coefficient function and distribution/fragmentation function is an observable and therefore free from any ambiguity, the distribution, fragmentation and the coefficient functions are separately ambiguous. In particular, they are scheme dependent; the origin of that scheme dependence is in the treatment of the IR divergences associated with their computation. Let us describe that in more detail:

The evaluation of the coefficient function proceeds in the following way: one

calculates the hadronic process  $d\sigma$  that is under study by formally replacing each initial hadron  $h$  with an *on-shell* parton  $a$ . To that end, and in accordance with the factorization theorem (2.19) we just described, one introduces (also formally) new parton distributions  $f_{i/a}$  which have the meaning of a distribution of a parton  $i$  inside a parton  $a$ ; we treat the fragmenting partons in a similar fashion. The main purpose of the fictitious distributions  $f_{i/a}$  is to absorb all the IR sensitive contributions from the calculated cross-section. As a next step, one simply discards the functions  $f_{i/a}$  and what is left is the needed coefficient function  $d\hat{\sigma}$ . The extraction of the partonic pdfs is physically equivalent to the absorption of the IR sensitive contributions into the pdfs  $f_{i/h}$  (see also Section (2.4.1)).

Clearly, such a procedure is very similar (and is in fact related) to the UV renormalization where one introduces appropriate counter-terms to absorb (and thus cancel) the UV divergences appearing in the Feynman diagrams. In the most often used  $\overline{\text{MS}}$  subtraction scheme the partonic pdfs read:

$$f_{i/a}(x) = \delta_{ia}\delta(1-x) + \frac{\alpha_S}{2\pi} \left( -\frac{1}{\epsilon} + \gamma_E - \ln(4\pi) \right) P_{ia}^{(0)}(x) + \mathcal{O}(\alpha_S^2), \quad (2.21)$$

where  $P_{ij}^{(0)}(x)$  are the leading order Altarelli-Parisi splitting functions that will be defined and thoroughly discussed in the next section, and  $\epsilon = (4 - D)/2$  (see the appendix for more details). The subtraction scheme for the IR divergences emerging in the limit  $\epsilon \rightarrow 0$  is related to the renormalization scheme used to remove the UV divergences appearing in the formal (operator) definition of the parton densities. Following the approach in [22], the quark distribution can be defined (in the light-cone gauge  $A^+ = 0$ ) as:

$$f_{q/h}(x) = \frac{1}{4\pi} \int dy^- e^{-ixP^+y^-} \langle h(P) | \bar{\psi}(0, y^-, 0_\perp) \gamma^+ \psi(0, 0, 0_\perp) | h(P) \rangle, \quad (2.22)$$

with similar results for the antiquark and gluon distributions. In Eq.(2.22)  $P$  is the momentum of the hadronic state  $h$ ,  $V^\pm = 1/\sqrt{2}(V^0 \pm V^3)$  is the light-cone

co-ordinate of a four-vector  $V$  and  $\psi$  is the operator of the quark field that carries momentum fraction  $x$ :  $p_q^+ = xP^+$ . For a partonic initial state, one can evaluate the partonic PDF in powers of  $\alpha_S$  by explicit calculation of the matrix element in (2.22). The result to order  $\alpha_S$  shows the following structure of the singularities:

$$f_{i/a}(x, \epsilon) = \delta_{ia}\delta(1-x) + \frac{\alpha_S}{2\pi} \left( \frac{1}{\epsilon_{UV}} - \frac{1}{\epsilon_{IR}} \right) P_{ia}^{(0)}(x) + \text{UV counterterm.} \quad (2.23)$$

Since by the UV renormalization the UV counterterm cancels the  $1/\epsilon_{UV}$  pole, we have a remaining IR divergence in the partonic PDF. The explicit form of that singularity obviously depends on the chosen UV renormalization scheme; for the  $\overline{\text{MS}}$  scheme the result is presented in (2.21). Similar considerations apply for the distribution functions as well; that is discussed e.g. in [24] and [25].

The factorization theorem in the presence of massive quarks is accurate up to terms  $\mathcal{O}(\Lambda/Q)$ ; see Eq.(2.19). The remainder in (2.19) contains terms that are power suppressed and are uniform in  $Q$  i.e. no terms with suppression  $\sim (m/Q)^n$  are present [23]. The proof of the factorization theorem presented in [23] uses a variable flavor number scheme (VFNS). The VFNS treats the light quarks  $u, d$  and  $s$  as massless and always includes them as active flavors in the running of the strong coupling  $\alpha_S$ . The treatment of the heavy flavors  $c, b$  and  $t$  is, however, process dependent. If the typical energy scale is below the corresponding quark mass then that quark is treated as heavy and is integrated out. In particular it does not contribute to the evolution of the strong coupling and does not have an associated parton density. The quarks with masses below the hard scale are treated in a different way: they contribute to the strong coupling as if they are exactly massless, and they have their own distribution functions <sup>2</sup> which are evolved with

---

<sup>2</sup>These are introduced in order to systematically resum large logs of collinear origin that appear to all orders in  $\alpha_S$ . Schemes without heavy quark densities exist and are called Fixed Flavor Number Schemes (FFNS). An example is the GRV 98 set of parton distributions [26].

the energy scale via evolution equations with massless kernels (see next section). Such a scheme corresponds to the renormalization scheme of Collins, Wilczek and Zee [27] and is also used (through the so-called Aivazis-Collins-Olness-Tung (ACOT) prescription [28]) in the evolution of the CTEQ parton densities [29].

The physical picture behind the factorization theorem is quite simple. One formally introduces a scale  $\mu_F$  which separates the short- from long-distance physics involved in the process. It is intuitively clear that such separation must indeed occur in the limit of large values of the hard scale  $Q$ . The time scale for the hard interaction is of the order of  $Q^{-1}$  and therefore quite small, while the typical time for the hadronization effects is not smaller than  $\Lambda_{QCD}^{-1} \gg Q^{-1}$ . As a result, in the limit  $Q \rightarrow \infty$ , short- and long-distance effects cannot interfere with each other and therefore factorize. More formally, the separation between small and large scales means that all contributing Feynman diagrams that have lines with small virtuality can be separated from the lines with large (of the order of the hard scale  $Q$ ) virtuality. The former diagrams constitute the distribution functions while the latter give the hard coefficient function. Such non-trivial factorization for the terms with leading power in  $1/Q^2$  (the so-called leading twist terms) was proved by Libby and Sterman [30]. If one works in a covariant gauge then there are present additional gluon lines that connect the small- and large-scale factors. However, those additional contributions cancel when summed up in a gauge invariant subset of diagrams. These contributions disappear, however, if one works in a physical gauge  $n \cdot A = 0$ , where  $n$  is some fixed four-vector. The physical gauge also has the important property that each diagram that contributes to the physical cross-section can be given a direct partonic interpretation [8].

## 2.3 Perturbative Evolution: DGLAP Equations

In this section we will devote our attention to the dependence of the various factors in Eq.(2.19) on the renormalization and factorization scales which incorporate the scaling-violation effects. To better illuminate our point, we are going to make the following two simplifications throughout this section: first, we will set  $\mu_r = \mu_F \equiv \mu$ . This is a standard choice in the studies of pQCD which, however, will not restrict the generality of our discussion. If needed, the separate dependence on both scales can be easily restored with the use of the running of the strong coupling (see Eq.(2.17)). The second simplification is that we will consider Eq.(2.19) as having a single fragmentation or distribution function multiplying the coefficient function  $d\hat{\sigma}$ . We will consider those two “representative” cases (only initial or final observed hadrons) of Eq.(2.19) separately.

We start with:

$$d\sigma(x, Q^2, m^2) = \sum_i f_{i/N}(x, \mu^2) \otimes d\hat{\sigma}_{i \rightarrow X}(x, Q^2, m^2, \mu^2), \quad (2.24)$$

which corresponds to the case of a single hadron (nucleon  $N$ ) in the initial state and no observed hadrons in the final state. A prominent example is the case of inclusive Neutral Current (NC) or Charged Current (CC) DIS:

$$\ell + N \rightarrow \ell' + X, \quad (2.25)$$

with  $\ell$  and  $\ell'$  being leptons,  $N$  a hadron (usually a nucleon) and  $X$  stands for any unobserved hadrons produced in the reaction (2.25). This case describes reactions with so-called space-like evolution.

As a representative for a reaction with a single fragmentation function we take:

$$d\sigma(x, Q^2, m^2) = \sum_f d\hat{\sigma}_{e^+e^- \rightarrow f}(x, Q^2, m^2, \mu^2) \otimes D_{h/f}(x, \mu^2), \quad (2.26)$$

which corresponds to the case of inclusive production of a single hadron  $h$  in a non-hadronic collision. These reactions are known as having time-like evolution. An example is the case of a single particle inclusive  $e^+e^-$  annihilation:



with  $h$  being an observed hadron and, as usual,  $X$  stands for any unobserved hadrons produced in the reaction (2.27). Also, for brevity, we have omitted the remainders in Eqns.(2.24) and (2.26).

### 2.3.1 The Case of Space-like Evolution

Let us concentrate on Eq.(2.24). Since the LHS is independent of  $\mu$  we can set that scale to any value we like. Among all the possible values, the choice  $\mu^2 = Q^2$  is particularly appealing as will become clear below.

From dimensional considerations the coefficient function can be written as

$$d\hat{\sigma}_{i \rightarrow X}(z, Q^2, \mu^2) = \sigma_B C \left( z, \frac{Q^2}{\mu^2}, \alpha_S(\mu^2) \right). \quad (2.28)$$

where for the time being we consider the case when no heavy quarks are present; we will generalize our considerations in the next section. In Eq.(2.28)  $\sigma_B$  is the Born cross-section for the partonic subprocess and the function  $C$  is a dimensionless function that has a power series decomposition in the strong coupling  $\alpha_S$ .

It is now obvious that upon setting  $\mu^2 = Q^2$  the coefficient function takes the form  $C(1, \alpha_S(Q^2))$  and depends only on the strong coupling and on no other large (or small) parameters. Since  $\alpha_S$  is evaluated at the large scale  $Q^2$  where the former is small, the coefficient function can be easily and efficiently calculated to some fixed order in perturbation theory. However, as a result of the choice of scale we have made, the distribution function has now become  $Q$ -dependent. That dependence is very important. It indicates that the universality of a distribution

function may be reduced since the PDF is specific to the experimental setup where it is extracted and therefore cannot be applied to processes with different hard scale.

Fortunately, there exists a way to relate distribution functions at different scales. The scale dependence of the fragmentation functions  $f_i$ ,  $i = q, \bar{q}, g$  is perturbatively controlled and is given as a solution to a system of integro-differential equations known as Dokshitzer-Gribov-Lipatov-Altarelli-Parisi (DGLAP) equations [31, 32]. That way the universality of the distribution function is retained; we only need to extract from experiment the distribution functions at one given scale  $Q_0$ . Then that input can be used as the initial condition for the DGLAP equations and the PDF at any other scale can be predicted. In practice that procedure works in the following way: at some low scale  $Q_0 \sim 1$  GeV one writes down a function of  $z$ , that contains small number of free parameters. Then one evolves that initial condition via the DGLAP equations to different scales where experimental data exist, and one tries to fit those data by adjusting the parameters of the initial condition.

The DGLAP equations are:

$$\frac{d}{d \ln \mu^2} f_i(z, \mu) = \sum_j \int_z^1 \frac{d\xi}{\xi} P_{ij} \left( \frac{z}{\xi}, \alpha_S(\mu) \right) f_j(\xi, \mu), \quad (2.29)$$

and describe in general a system of  $2n_f + 1$  equations for the distribution functions of all flavors of quarks, antiquarks and the gluon. The kernels  $P_{ij}$  have perturbative expansions in powers of the strong coupling:

$$P_{ij}(z, \alpha_S(\mu)) = \frac{\alpha_S(\mu)}{2\pi} P_{ij}^{(0)}(z) + \left( \frac{\alpha_S(\mu)}{2\pi} \right)^2 P_{ij}^{(1)}(z) + \mathcal{O}(\alpha_S^3). \quad (2.30)$$

$P_{ij}^{(0)}(z)$  are the Altarelli-Parisi splitting functions [31] that also appeared in Eq.(2.21).

Because color and flavor commute, those functions are independent of the quark

flavor i.e.  $P_{q_i q_j}^{(0)}(z) = \delta_{ij} P_{qq}^{(0)}(z)$ . They also satisfy other relations as a result of probability conservation:

$$\int_0^1 dz P_{qq}^{(0)}(z) = 0, \quad (2.31)$$

and momentum conservation:

$$\begin{aligned} \int_0^1 dz z \left( P_{qq}^{(0)}(z) + P_{gq}^{(0)}(z) \right) &= 0, \\ \int_0^1 dz z \left( 2n_f P_{qg}^{(0)}(z) + P_{gg}^{(0)}(z) \right) &= 0. \end{aligned} \quad (2.32)$$

Note that because of the property (2.31), the functions  $P_{qq}^{(0)}(z)$  are not positive definite. They are distributions instead. The kernels  $P_{ij}$  satisfy also the following important relations as a result of charge invariance and the  $SU(n_f)$  flavor symmetry:

$$\begin{aligned} P_{q_i q_j} &= P_{\bar{q}_i \bar{q}_j} \quad ; \quad P_{q_i \bar{q}_j} = P_{\bar{q}_i q_j} \\ P_{q_i g} &= P_{\bar{q}_i g} = P_{qg} \quad ; \quad P_{gq_i} = P_{g\bar{q}_i} = P_{gq}. \end{aligned} \quad (2.33)$$

The explicit expressions for the four independent leading order splitting functions are:

$$\begin{aligned} P_{qq}^{(0)}(z) &= C_F \left( \frac{1+z^2}{(1-z)_+} + \frac{3}{2} \delta(1-z) \right), \\ P_{qg}^{(0)}(z) &= \frac{1}{2} \left( z^2 + (1-z)^2 \right), \\ P_{gq}^{(0)}(z) &= C_F \left( \frac{1+(1-z)^2}{z} \right), \\ P_{gg}^{(0)}(z) &= 2C_A \left( \frac{z}{(1-z)_+} + \frac{1-z}{z} + z(1-z) \right) \\ &+ \frac{11C_A - 2n_f}{6} \delta(1-z). \end{aligned} \quad (2.34)$$

The distribution  $(F(z))_+$  is defined as  $\int_0^1 (F(z))_+ H(z) dz = \int_0^1 F(z) (H(z) - H(1)) dz$ , and its properties are discussed in the appendix.

One can substantially simplify the study of the DGLAP equations if one takes advantage of the flavor symmetry. As we mentioned earlier, the DGLAP equations describe the evolution of  $2n_f + 1$  partons that are all massless (see also the discussion following Eq.(2.23)). From the form of the QCD lagrangian with  $n_f$  massless quarks (2.4), it is evident that the theory has an additional global  $SU(n_f)$  flavor symmetry. Since the gluons are flavor-neutral, they transform as singlets under the flavor group. The quarks in general transform nontrivially under that group. One can split the  $2n_f$  (anti)quark fields into one singlet:

$$\Sigma(x, \mu) = \sum_i^{n_f} (f_{q_i}(x, \mu) + f_{\bar{q}_i}(x, \mu)),$$

and  $2n_f - 1$  non-singlet (NS) combinations.  $n_f$  of the NS fields can be taken as the differences  $M_i^- = f_{q_i}(x, \mu) - f_{\bar{q}_i}(x, \mu)$ . The other  $n_f - 1$  combinations, which we denote by  $M_j^+$ , depend on the value of  $n_f$  and can be found in [6]. Clearly, the NS combinations do not mix with the singlet; in particular they do not mix with the gluon. To LO, all NS fields also split from each other so we have a separate equation for each NS field:

$$\frac{d}{d \ln \mu^2} f^{NS}(z, \mu) = \frac{\alpha_S(\mu)}{2\pi} \int_z^1 \frac{d\xi}{\xi} P_{qq}^{(0)} \left( \frac{z}{\xi} \right) f^{NS}(\xi, \mu), \quad (2.35)$$

with  $P_{qq}^{(0)}(z)$  given in Eq.(2.34). Beyond the leading order, however, the evolution kernels are no longer flavor diagonal. One can still write the evolution equations in diagonal form that is similar to the LO case Eq.(2.35), but the kernels  $P_{NS}^{(1)+}$  and  $P_{NS}^{(1)-}$  corresponding to the fields  $M^+$  and  $M^-$  are now different. Their explicit expressions can be found in [6] as well.

In the singlet sector, there is non-trivial mixing between the gluon density  $g$  and the quark singlet state  $\Sigma$ . The kernels of the evolution equations for the

“two-vector”  $(\Sigma(z, \mu), g(z, \mu))$  form a  $2 \times 2$  matrix:

$$\begin{pmatrix} P_{qq}(z, \alpha_S(\mu^2)) & 2n_f P_{qg}(z, \alpha_S(\mu^2)) \\ P_{gq}(z, \alpha_S(\mu^2)) & P_{gg}(z, \alpha_S(\mu^2)) \end{pmatrix}.$$

The NLO kernels in the singlet sector can be found in [6]. Similarly to the NS case, we do not present them here because of their length. The original derivations are presented in [25, 33]. For future reference we will only present the large  $z$  behavior of the  $\overline{\text{MS}}$  splitting functions at NLO:

$$\begin{aligned} \lim_{z \rightarrow 1} P_{qq} &= C_F \frac{\alpha_S}{\pi} \left( 1 + K \frac{\alpha_S}{2\pi} + \mathcal{O}(\alpha_S^2) \right) \frac{1}{(1-z)_+} \\ \lim_{z \rightarrow 1} P_{gg} &= C_A \frac{\alpha_S}{\pi} \left( 1 + K \frac{\alpha_S}{2\pi} + \mathcal{O}(\alpha_S^2) \right) \frac{1}{(1-z)_+} \end{aligned} \quad (2.36)$$

where:

$$K = C_A \left( \frac{67}{18} - \frac{\pi^2}{6} \right) - \frac{5}{9} n_f. \quad (2.37)$$

The origin of the DGLAP equations is in renormalization group invariance. That invariance is manifested as independence of physical quantities (for example a cross-section) of the renormalization scale  $\mu_r$  that is introduced as a result of the renormalization procedure. Eq.(2.24) is a typical example. Before we exploit the fact that the LHS is independent of  $\mu$ , let us take the Mellin transform of Eq.(2.24) (with all masses omitted for now):

$$d\sigma(N, Q^2) = \sum_i f_i(N, \mu^2) d\hat{\sigma}_{i \rightarrow X}(N, Q^2, \mu^2), \quad (2.38)$$

where the Mellin transform  $F(N)$  of a function  $F(z)$  is defined as

$$F(N) = \int_0^1 dz z^{N-1} F(z). \quad (2.39)$$

To derive Eq.(2.38) we used the following important property: the Mellin transform of a convolution of two functions is the ordinary product of the Mellin transforms of those functions, i.e.

$$\int_0^1 dz z^{N-1} (F \otimes G)(z) = F(N)G(N). \quad (2.40)$$

Taking  $\mu$ -derivatives of both sides of Eq.(2.38) and omitting the summation over the partons (as in the NS case for example), one has:

$$\mu \frac{d}{d\mu} \ln f(N, \mu^2) = -\mu \frac{d}{d\mu} \ln C \left( N, \frac{Q^2}{\mu^2}, \alpha_S(\mu^2) \right) = 2\gamma(N, \alpha_S(\mu^2)). \quad (2.41)$$

In Eq.(2.41) we have also used Eq.(2.28). From the derivation of Eq.(2.41) it is clear that the function  $\gamma(N, \alpha_S(\mu^2))$  plays the role of a “separation constant” that depends on the common variables of the functions  $f$  and  $C$ . Therefore, that equation is of importance only if the function  $\gamma$  is known. Let us assume for the moment that this is the case; then with simple integration one can obtain the scale dependence of the moments of the distribution function  $f$ :

$$f(N, \mu^2) = f(N, \mu_0^2) \exp \left( \int_{\mu_0^2}^{\mu^2} \frac{dk^2}{k^2} \gamma(N, \alpha_S(k^2)) \right), \quad (2.42)$$

if the value of the fragmentation function at some initial scale  $\mu_0$  is known. Combining this result with Eq.(2.24) and after setting  $\mu = Q$  we can finally complete the factorization program discussed in the previous section. To calculate a physical observable we only need the PDF at some initial scale and the coefficient function for the hard process which is computable in perturbation theory since it does not contain any large parameters:

$$d\sigma(N, Q) = \sigma_B f(N, \mu_0^2) C(N, 1, \alpha_S(Q^2)) \exp \left( \int_{\mu_0^2}^{Q^2} \frac{dk^2}{k^2} \gamma(N, \alpha_S(k^2)) \right). \quad (2.43)$$

Of course, in practical applications one needs to carefully account for the mixing between the various distribution functions that would appear in the relation (2.43).

To make contact with the DGLAP equations, we need only notice that by setting

$$\gamma_{ij}(N, \alpha_S(\mu^2)) = \int_0^1 dz z^{N-1} P_{ij}(z, \alpha_S(\mu^2)), \quad (2.44)$$

and applying a Mellin transformation to both sides of the DGLAP equation we get exactly the equation (2.41) for the fragmentation function  $f$ . That way we

conclude that the functions  $\gamma_{ij}$  are the Mellin moments of the evolution kernels  $P_{ij}$ .

The functions  $\gamma_{ij}$  indeed have a deep physical meaning which is not hard to understand. For that purpose let us rewrite schematically Eq.(2.41) for  $f$ :

$$\left( \mu \frac{\partial}{\partial \mu} + \beta(g_S) \frac{\partial}{\partial g_S} - 2\gamma(g_S) \right) \ln f = 0 \quad (2.45)$$

Eq.(2.45) resembles the renormalization-group equation of a matrix element of an operator in a massless theory with anomalous dimension  $\gamma$ . The functions  $\gamma_{ij}(N, \alpha_S(\mu^2))$  are indeed anomalous dimensions but of local operators of spin- $N$  and twist-two that appear in the light-cone operator product expansion (OPE) of two currents. The derivation of this result is rather lengthy and can be found in [34, 35]; for a more pedagogical discussion see [5]. Here we shall only mark the main steps in the example of DIS. The DIS cross-section is of the form  $L^{\mu\nu}W_{\mu\nu}$  where  $L$  is a tensor constructed from the lepton's four-momentum and  $W$  has the form:

$$W_{\mu\nu} \sim \int d^4y e^{iq \cdot y} \langle P | [J_\mu(y), J_\nu(0)] | P \rangle. \quad (2.46)$$

The non-local product of the two electromagnetic currents  $J_\mu(y)J_\nu(0)$  is sandwiched between the hadronic state  $|h(P)\rangle$  and its conjugate. This operator product can be expanded in a series over local operators  $O_n$ :

$$J(y)J(0) = \sum_{n,i} C_n^i(y^2) O_{n,i}^{\nu_1 \dots \nu_n} y_{\nu_1} \dots y_{\nu_n}. \quad (2.47)$$

Sandwiching the current product in the hadronic states:

$$\langle P | O_{n,i}^{\nu_1 \dots \nu_n} | P \rangle = A_{n,i}(\mu^2) P^{\nu_1} \dots P^{\nu_n}, \quad (2.48)$$

results in the following expression:

$$F(n, Q^2) = A_{n,i}(\mu^2) C_n^i(Q^2/\mu^2, \alpha_S). \quad (2.49)$$

Above,  $F$  is the  $n$ -th Mellin moment of any of the structure functions. Eq.(2.47) implies that the coefficient function  $C$  satisfies the renormalization group equation with anomalous dimension  $2\gamma_J - \gamma_O$ . Since the current  $J$  is conserved its anomalous dimension vanishes. The anomalous dimension corresponding to an operator  $O$  can be computed in perturbation theory from the relation:

$$\gamma_O = \frac{\mu}{2} \frac{\partial}{\partial \mu} \ln Z_O, \quad (2.50)$$

where  $Z_O$  is the renormalization constant for the operator  $O$ .

Collecting the results above, we see that after setting  $\mu = Q$  we obtain Eq.(2.43) for the DIS structure functions, and the anomalous dimension  $\gamma(N)$  presented there corresponds to the local operators  $O_N$ .

Let us make few more brief comments on the DGLAP equations. First, the DGLAP equations in the form that we discussed were first introduced by Altarelli and Parisi in [31]. There the authors were following a more or less reversed approach: starting from the OPE results we discussed above, they introduced the AP splitting functions through the relations (2.44). The important result is that not only are the  $z$ -space evolution equations equivalent to the renormalization group ones, but the former offer new way of deriving the splitting functions based on their partonic interpretation. Second, similarly to the beta-function, the one-loop splitting functions  $P_{ij}^{(0)}(z)$  are renormalization scheme independent. However, that is not true for the higher order functions which are renormalization scheme dependent. The most common choice is to work in  $\overline{\text{MS}}$  scheme.

### 2.3.2 The Case of Time-like Evolution

All the considerations that were made for the case of Eq.(2.24) can also be made for the fragmentation case (2.26). There are, however, a few differences between those two cases and we will discuss them now.

The fragmentation functions  $D$  have an interpretation different from that of the parton distribution functions. The function  $D_{i/h}(z, \mu^2)$  represents the probability density that a parton  $i$  produced at scale  $\mu^2$  will fragment to an observed (and therefore on-mass-shell) hadron  $h$ . Similarly to the distribution functions, the evolution of the fragmentation functions is also described by the DGLAP equations. The one-loop splitting functions  $P_{time-like, ij}^{(0)}(x)$  coincide with those in the space-like case (2.34). However the time-like and the space-like evolution kernels differ beyond the leading order. The NLO time-like functions can be found in [25, 33]. The large  $z$  behavior of the NLO time-like evolution kernels is the same as for the space-like kernels, Eq.(2.36).

## 2.4 Infrared Effects

In our previous discussion we neglected the presence of masses of the quarks. However for a theory which is sensitive to the IR such as QCD, a detailed account for those effects is needed.

It is well known that in a gauge theory with massless matter fields, in addition to the usual UV divergences, there is another type of divergences that occurs in the evaluation of the Feynman diagrams. These are known as infrared (IR) divergences and as shown by Sterman for QCD in [36] can be divided into two types: collinear and soft.

The collinear divergences are due to the vanishing mass of the radiating particle (usually the quarks). When a quark radiates a gluon that is almost collinear to it, the corresponding real or virtual emission diagrams diverge. One can regulate such a divergence by introducing a small quark mass or by working in  $D = (4 - \epsilon)/2$  space-time dimensions. Then a collinear divergence shows up as logarithmic singularity  $\sim \ln(m^2)$  or as  $1/\epsilon$  pole respectively. In principle, since

quarks have non-vanishing masses, the quantities calculated should be finite and free of IR collinear singularities. That is not the case, however. In the perturbative regime it is not the absolute value of the quark that is important but its value with respect to some typical scale. If that typical scale - usually the hard scale  $Q$  - is much larger than the quark mass, then in a perturbative calculation there appear large logs  $\ln(m^2/Q^2)$ . Although these logs are finite, they appear to any order in perturbation theory and systematically multiply the strong coupling constant. Thus, the effective perturbation parameter is not  $\alpha_S$  anymore but  $\alpha_S \times (\text{a power of } \ln m^2/Q^2)$ . The latter can be quite large and can even invalidate the perturbation series. In effect, small but non-zero quark mass leaves the result finite but unphysical; one should sum up to all orders terms of this type in order to be able to make definite perturbative predictions. Such large logs are called quasi-collinear logs and are classified in the following way: a term at order  $\alpha_S^n$  has the form

$$\alpha_S^n \sum_{k=0}^n c_k \ln^k \left( \frac{m^2}{Q^2} \right). \quad (2.51)$$

Terms with  $k = n$  are known as leading logarithmic (LL) terms, the ones with  $k = n - 1$  are the next-to-leading logarithms (NLL) etc. It is a peculiar feature of QCD that due to its non-abelian gauge group not only quarks but also gluons can radiate collinear gluons. Unlike the quarks however the gluons are exactly massless due to the gauge symmetry.

The origin of the soft divergences is in the vanishing mass of the gauge fields (the gluon). These divergences manifest themselves as singularities in the loop integrals over gauge boson lines in the kinematical region where the energy  $\omega_q$  of the gluon vanishes or in the real emission diagrams where gluons with vanishing energy are emitted. The most convenient way to regularize those divergences is to work with dimensional regularization since it preserves both Poincare and gauge

invariance (unlike gluon-mass regularization).

It was understood long ago [37] that the problem of IR divergences is rooted in the way the physical observables are defined. It is intuitively clear that a state containing a hard parton cannot be distinguished from a state containing in addition arbitrary number of soft (or collinear) gluons. In those singular limits the particle nature of the real soft (or collinear) gluon is not well defined and as a result we need to deal with degenerate states. The conditions for cancellation of the IR divergences are stated in the following theorem:

**Kinoshita-Lee-Nauenberg Theorem** [38]: In a theory with massless fields, transition rates are free of IR divergences if a summation over the initial and final degenerate states is carried out.

The proof of the theorem can be found in [5]. Its content is however clear: a physical state is one that contains arbitrary number of soft (collinear) gluons. When applied to perturbative calculations, the KLN theorem means that to some fixed order in the coupling constant one should take into account the contributions from virtual and real emission diagrams with arbitrary numbers of radiated gluons. Only their sum will be IR finite. That way we arrive at the idea of an inclusive observable: a calculated cross-section will be IR finite if it does not distinguish a state with one particle from a state with a number of soft (collinear) gluons. We will see examples in the next Chapter when we discuss the decay of the top quark.

In terms of Feynman diagrams (to all orders), the IR divergences are generated only from real or virtual emission lines connected exclusively to external (hard) lines in the diagram. The reason is that the internal lines are typically highly off-shell and thus regulate any possible divergence. That observation is important for constructing an explicit proof of cancellation of the soft divergences and was used first by Weinberg [39] in the context of QED. Let us also mention that in fact that property leads in the context of QCD to the factorization of the IR singularities

in the hard diagrams. This is a very important property that we will make use of in the next section. For an excellent discussion see [40].

### 2.4.1 Heavy Quark Masses

Let us return to Eq.(2.24) or (2.26) and now take into account the masses of the quarks that we neglected in the discussion in the previous section. For example, Eq.(2.28) now generalizes to:

$$d\hat{\sigma}_{i \rightarrow X}(x, Q^2, m^2, \mu^2) = \sigma_B C \left( x, \frac{Q^2}{\mu^2}, \frac{m^2}{\mu^2}, \alpha_S(\mu^2) \right). \quad (2.52)$$

It is clear that whatever choice we make for the scale  $\mu$ , we cannot set equal to one both mass ratios that appear in the RHS of Eq.(2.52). Just for the sake of being less abstract, let us set as before  $\mu^2 = Q^2$ . Then (2.52) takes the form:

$$d\hat{\sigma}_{i \rightarrow X}(x, Q^2, m^2, \mu^2 = Q^2) = \sigma_B C \left( x, 1, \frac{m^2}{Q^2}, \alpha_S(Q^2) \right). \quad (2.53)$$

Since the ratio  $m^2/Q^2$  can take any non-negative real value, we anticipate a strong dependence on the value of the quark mass. The case when  $m^2 \gg Q^2$  was already discussed in Section (2.2): one can simply integrate out the heavy quark and work in an effective theory where that flavor is omitted. As a result, the definition of the coupling constant becomes dependent on the number of flavors lighter than  $Q$  and satisfies non-trivial conditions at the switching points. To understand the dependence on  $m^2$  in the case when  $m^2$  is not (much) larger than  $Q^2$ , we first need to know if the cross-section  $d\hat{\sigma}$  is IR safe, i.e. if it is finite in the limit  $m^2 \rightarrow 0$ . If it is collinearly safe, we can represent it as:

$$C \left( x, 1, \frac{m^2}{Q^2}, \alpha_S(Q^2) \right) = C \left( x, 1, 0, \alpha_S(Q^2) \right) + \mathcal{O} \left( \frac{m^2}{Q^2} \right). \quad (2.54)$$

Such cross-sections are well behaved and can be obtained by explicit calculation to any order in perturbation theory. A typical example is the case when  $d\hat{\sigma}$  is a total partonic cross-section, e.g. for the process  $e^+e^- \rightarrow \text{hadrons}$ .

The case when  $d\hat{\sigma}$  is not IR safe is more complicated and at the same time perhaps more common. In this case the limit  $m \rightarrow 0$  is singular, i.e.  $d\hat{\sigma}$  diverges. Examples are the cases where  $d\hat{\sigma}$  is an inclusive differential cross-section for production of a parton, or a process which is initiated by a single parton (the generalization to multiple partons is straightforward). According to (2.19), the hadron level result is a convolution of the partonic cross-section with distribution/fragmentation function. However in the presence of IR divergences we should first understand how to make sense of such divergent results.

Let us first consider the case when the parton in consideration is light i.e. we take  $m^2 \approx 0$ . The first thing to note is that since it is experimentally measurable, the physical process of creation of a hadron or the process that is initiated by a single hadron is not IR divergent. Such a process undergoes complicated stages that are controlled by long-distance physics. However, our present ignorance about confinement makes us simplify the calculation by assuming that the produced hadron has been created from a single parton, which later non-perturbatively hadronizes (the latter process being described by the fragmentation function  $D$ ). Such a description is typical for production of light hadrons (i.e. hadrons that are constructed out of light quarks). Thus in simplifying the process we necessarily introduce mass singularities. The understanding of their origin suggests the method to cure them: one calculates the partonic cross-section in perturbation theory that is (usually) regulated in dimensional regularization. As we discussed in Section (2.2) those divergences factorize and can be subtracted in a particular scheme (usually  $\overline{\text{MS}}$ ). Then the subtracted partonic cross-section is convoluted with a non-perturbative fragmentation function which is process independent but subtraction scheme dependent. The same considerations apply for a process with space-like evolution. The justification for such a procedure is that the subtraction is physically equivalent to the absorption of the effects sensitive to long-distance

physics into the distribution/fragmentation functions.

After the subtraction of the mass singularities and defining the corresponding distribution/fragmentation functions we are in the situation described by Eq.(2.43):

$$d\sigma(N, Q) = \sigma_B C(N, 1, \alpha_S(Q^2)) \exp \left( \int_{\mu_0^2}^{Q^2} \frac{dk^2}{k^2} \gamma(N, \alpha_S(k^2)) \right) D(N, \mu_0^2) \quad (2.55)$$

where we again consider the non-singlet case for simplicity. The function  $C$  here describes the  $(\overline{\text{MS}})$  subtracted partonic cross-section while  $D$  is an initial condition for the fragmentation function that is extracted from experiment where light hadrons are measured at some low scale  $\mu_0$ .

### 2.4.2 Perturbative Fragmentation Function Formalism

Let us turn our attention to the case of collinearly-sensitive processes that involve heavy quarks and typical hard scale  $Q$  somewhat larger than the quark mass. As usual, by heavy we mean  $c, b$  or  $t$  quarks. Although the partonic cross-section for such processes is divergent in the zero-mass limit, we cannot really set the masses of the heavy quarks to zero since they are not that small. We are then in a situation that we previously described: the results are formally finite but in practice perturbation theory cannot be applied in a straightforward way since, as shown in Eq.(2.51), potentially large logs  $\ln(m^2/Q^2)$  appear to all orders in  $\alpha_S$ . There are two physically different cases where such a situation can occur.

The first is the case of partonic processes that are initiated by quarks with non-zero mass. Although this is an interesting problem, it is outside the scope of this Thesis since it mostly concerns the non-trivial treatment of heavy flavors in the nucleons. We will only indicate that in such situations one typically would subtract the divergent part of the coefficient function and then convolute it with the usual massless parton density. An example is the case of [41] where the strange

quark was treated as having non-zero mass and after the subtraction of the quasi-collinear logs the effect of the (finite) power corrections of the mass of the strange quark was studied.

The second case is the one where a heavy quark (usually  $c$  or  $b$ ) is created in a hard collision with a typical scale  $Q$ . Such processes contribute to the creation of  $c$ - or  $b$ -flavored hadrons and can be described within the formalism of the perturbative fragmentation function (PFF) [42]. This approach has been extensively used for  $e^+e^-$  annihilation [43, 44, 45, 46, 47], hadron collisions [48, 49] and photoproduction [50, 45]. In the next Chapter we describe its application for bottom quark production in top quark decay  $t \rightarrow bW$  [51].

According to the factorization theorem (2.19), we can write the cross-section for creating a heavy-flavored hadron  $H$  in the following way:

$$\frac{1}{\sigma_0} \frac{d\sigma^H}{dz}(z, Q, m) = \frac{1}{\sigma_0} \int_z^1 \frac{d\xi}{\xi} \frac{d\sigma^q}{d\xi}(\xi, Q, m) D_{np}^H\left(\frac{z}{\xi}\right), \quad (2.56)$$

where  $\sigma^H$  ( $\sigma^q$ ) is the cross-section for production of hadron  $H$  (heavy quark  $q$ ) and  $D_{np}$  is a non-perturbative function that describes the transition  $q \rightarrow H$  at the scale set by the mass  $m$  of the heavy quark  $q$ . That function is to be obtained from a comparison with experiment. The kinematical variable  $z$  describes the parameter(s) of the observed final state and typically is an appropriately normalized energy fraction. The normalization of the cross-sections is chosen in such a way that the Born term equals exactly  $\delta(1 - z)$ .

The partonic cross-section  $\sigma^q$  can be calculated in perturbation theory. It is finite because of the finite mass  $m$  but is not IR safe since the process is not completely inclusive. It contains large quasi-collinear logs to all orders in  $\alpha_S$  that must be resummed as we previously discussed. The resummation of those logs is

done in complete analogy with Eq.(2.55). One writes:

$$\frac{1}{\sigma_0} \frac{d\sigma^q}{dz}(z, Q, m) = \frac{1}{\sigma_0} \sum_i \int_z^1 \frac{d\xi}{\xi} \frac{d\hat{\sigma}_i}{d\xi} \left( \frac{z}{\xi}, Q, \mu \right) D_i(\xi, \mu, m), \quad (2.57)$$

where  $\hat{\sigma}$  is the cross-section for production of massless parton  $i$  with the collinear singularity subtracted in the  $\overline{\text{MS}}$  scheme. The function  $D_i(z, \mu, m)$  is the PFF and it describes the transition of a massless parton  $i$  to a massive quark  $q$ .

The ansatz (2.57) has the following physical interpretation: in a hard collision set by the large scale  $Q$  a massive parton is produced at large transverse momentum. For that reason it behaves like a massless parton. The replacement of a massive parton with a massless one after the collinear divergence is subtracted is justified up to powers of  $m^2/Q^2$ . The formalism of the PFF is applicable when such power corrections are small and can be neglected. For that reason, the cross-section  $\hat{\sigma}$  is insensitive to low energy (i.e. at the order of  $m$ ) physics and depends only on  $Q$  but not on  $m$ . The scale  $\mu$  is the factorization scale that, as usual, separates the low from the high energy regimes. Similarly, the function  $D_i(z, \mu, m)$  depends only on the mass and the factorization scale, but is insensitive to the high energy part of the process. In particular, the perturbative fragmentation function is universal, *i.e.* independent of the process.

The PFF satisfy the DGLAP equations (2.29). The latter can be solved with NLL accuracy. To completely specify the solution however, one needs to specify at some scale  $\mu_0$  an initial condition  $D_i^{ini}(z, \mu_0, m)$  that is also valid to NLL accuracy. Clearly, such a condition is also universal and can be obtained from a perturbative calculation [42]. To that end one first needs to observe that if the scale  $\mu_0$  is chosen of the order of the mass  $m$  then no large logs will be present in the initial condition. Therefore, the initial condition can be simply calculated in perturbation theory:

$$D_i^{ini}(z, \mu_0, m) = d_i^{(0)}(z) + \frac{\alpha_S(\mu_0)}{2\pi} d_i^{(1)}(z, \mu_0, m) + \mathcal{O}(\alpha_S^2). \quad (2.58)$$

To obtain the above functions one needs to independently compute to order  $\alpha_S$  both  $\sigma^q$  and  $\hat{\sigma}$  for some process and then plug the results into Eq.(2.57). Comparing the terms order by order in  $\alpha_S$  one gets in the  $\overline{\text{MS}}$  scheme [42]:

$$\begin{aligned} d_i^{(0)}(z) &= \delta_{iq}\delta(1-z), \\ d_{i=q}^{(1)}(z, \mu_0, m) &= C_F \left[ \frac{1+z^2}{1-z} \left( \ln \frac{\mu_0^2}{m^2} - 2\ln(1-z) - 1 \right) \right]_+, \\ d_{i=g}^{(1)}(z, \mu_0, m) &= \frac{1}{2} \left( z^2 + (1-z)^2 \right) \ln \left( \frac{\mu_0^2}{m^2} \right), \\ d_{i \neq q, g}^{(1)}(z, \mu_0, m) &= 0. \end{aligned} \quad (2.59)$$

Process independent derivations of these initial conditions also exist [43, 52].

The most convenient way to solve the DGLAP equations is to work with the Mellin moments of the fragmentation functions. Then the evolution equations take the following form:

$$\frac{d}{d \ln \mu^2} D_i(N, \mu, m) = \sum_j \gamma_{ij}(N, \alpha_S(\mu)) D_j(N, \mu, m), \quad (2.60)$$

where we have introduced  $D_i(N)$  through Eq.(2.39) and the anomalous dimensions are defined in Eq.(2.44). Also, one can conveniently factorize the dependence on the initial conditions:

$$D_i(N, \mu, m) = \sum_j E_{ij}(N, \mu, \mu_0) D_j^{ini}(N, \mu_0, m), \quad (2.61)$$

where the functions  $E_{ij}(N, \mu, \mu_0)$  are universal solutions to the DGLAP equation (2.60) subject to the initial condition  $E_{ij}(N, \mu_0, \mu_0) = \delta_{ij}$ . From the factorization property (2.40) it follows that the  $z$ -space counterpart of this condition is  $E_{ij}(z, \mu_0, \mu_0) = \delta_{ij}\delta(1-z)$ .

The DGLAP equations (2.60) couple all flavors that potentially participate in the process thus making the system hard to solve in general. An often made approximation is to neglect the mixing of the heavy flavor  $q$  with the light flavors

and the gluon. Such an approximation is justified in situations where the probability to create a heavy quark from a secondary gluon is small. The approximation amounts to considering only the non-singlet contributions to the evolution kernels. We will consider only this case hereinafter. In this approximation it is very easy to solve Eq.(2.60) with NLL accuracy:

$$E_q(N, \mu, \mu_0) = \exp \left\{ P_N^{(0)} t + \frac{1}{4\pi^2 b_0} [\alpha_S(\mu_0) - \alpha_S(\mu)] \left[ P_N^{(1)} - \frac{2\pi b_1}{b_0} P_N^{(0)} \right] \right\}, \quad (2.62)$$

where we have introduced the variable  $t$  as

$$t = \frac{1}{2\pi b_0} \ln \frac{\alpha_S(\mu_0)}{\alpha_S(\mu)}. \quad (2.63)$$

The coefficients  $b_{0,1}$  are defined in (2.15) and the functions  $P_N^{(0,1)}$  are the Mellin transforms of the LO and NLO coefficients in (2.30). Their explicit form as well as  $N$ -moments of the initial conditions (2.59) are given in the appendix. Collecting the results in Eqns.(2.56), (2.57), (2.61), (2.62) and (A.27), we can write the differential cross-section for production of a heavy-flavored hadron as:

$$\frac{1}{\sigma_0} \frac{d\sigma^H}{dz}(z, Q, m) = \mathcal{M}^{-1} \left[ C(N, Q, \mu) E_q(N, \mu, \mu_0) D_q^{ini}(N, \mu_0, m) D_{np}^H(N) \right] (z). \quad (2.64)$$

With  $\mathcal{M}^{-1}$  we denote the inverse Mellin transform:

$$f(z) = \mathcal{M}^{-1}[f(N)](z) = \frac{1}{2\pi i} \int_{C-i\infty}^{C+i\infty} dN z^{-N} f(N), \quad (2.65)$$

which is typically performed numerically. We will give more details in the next Chapters where we discuss our applications. In Eq.(2.64) we have also introduced the  $N$ -space coefficient function:

$$C(N, Q, \mu) = \frac{1}{\sigma_0} \int_0^1 dz z^{N-1} \frac{d\sigma^q}{dz}(z, Q, \mu), \quad (2.66)$$

and the non-perturbative fragmentation function  $D_{np}(N)$ . The latter is extracted from fits to experimental data. We will present details for how that procedure works in the next Chapter where we consider the case of top decay.

Eq.(2.64) is the improved cross-section for production of a hadron  $H$  carrying longitudinal momentum fraction  $z$ , and with all quasi-collinear logs  $\ln(m^2/Q^2)$  resummed with NLL accuracy. As we will also see in the next Chapter in the example of top quark decay, the application of the resummation via the perturbative fragmentation function represents a serious improvement over the fixed order perturbative calculation.

### 2.4.3 Soft-gluon Threshold Resummation

Before we move to the discussion of our processes of interest, let us describe another, more subtle source of large logarithmic corrections that arise to all orders in perturbation theory and also need to be resummed. Those logs appear in processes containing massless and/or massive particles and are also of IR origin.

Let us go back to Eq.(2.43). Since no masses were present there, we concluded that such a renormalization group improved cross-section does not contain any large parameters and therefore can be unambiguously computed. We did not consider however its behavior as a function of the dimensionless parameter  $N$ , the Mellin conjugate of  $z$ . This parameter can be large since the limit of large  $z$  (i.e.  $z \rightarrow 1$ ) corresponds through the Mellin transform (2.39) to  $N \rightarrow \infty$ . Therefore in the kinematical limit of large  $z$  one may expect terms  $\sim \ln(N)$  to appear in the conjugate space and to spoil the perturbative expansion in  $\alpha_S$ . Indeed, a typical perturbative calculation of a hard cross-section shows terms like

$$\alpha_S^n \sum_{m=0}^{2n} c_m \ln^m(N). \quad (2.67)$$

The terms with  $n < m \leq 2n$  are called leading logs (LL), the ones with  $m = n$  are next-to-leading (NLL) logs and so on <sup>3</sup>. An example is the large  $N$  behavior

---

<sup>3</sup>We will give more convenient characterization of these logs below; see Eq.(2.80).

of both space- and time-like anomalous dimensions shown in Eq.(2.36) where the latter are as singular as a single power of  $\ln(N)$ . Relations between the large  $z$  and large  $N$  behavior of various relevant functions are given in the appendix.

The physical origin of the above mentioned (soft) logs is in the soft gluon radiation near the boundary of phase space. As we discussed in Section (2.4), the soft divergences cancel when all the contributions from real and virtual radiation are taken into account. However, this cancellation is incomplete near the boundary of the phase space  $z \rightarrow 1$  for semi-inclusive cross-sections, and as a result large terms  $\sim \ln^k(1-z)/(1-z)$  are present in the perturbative calculation.

The all order resummation of classes of such soft logs is performed in terms of the Mellin moments because in Mellin space the factorization properties of the amplitudes are explicit. We will consider cross-sections of the type (2.64), where  $D$  can be a general fragmentation or distribution function. The form of Eq.(2.64) suggests the following approach for the resummation procedure: one can obtain separate resummed expressions for each of the factors appearing in the RHS of (2.64) that require such resummation. This way, one explicitly separates the process-dependent from the universal factors which makes the resummation procedure more universal. Of course, this is not the only possibility; one can solve directly for the whole cross-section. An example is the large- $z$  resummation performed in [42].

In what follows, we will describe the method of Catani and Trentadue [53] originally applied to Drell-Yan and DIS. We will apply their method in the next two chapters for the calculation of the resummed expressions for the coefficient functions for top-quark decay and inclusive CC DIS. The equivalence of their result with the Sterman's [54] was shown in [55].

The coefficient function represents the normalized cross-section for production of a massless quark after the corresponding collinear singularities are subtracted.

Up to non-singular terms in the limit  $z \rightarrow 1$ , it is approximated by the eikonal cross-section [53]:

$$d\sigma = \sigma_B \overline{\sum_{n=0}} \int d\phi^{(n)} \langle n | \hat{S} | 0 \rangle |^2, \quad (2.68)$$

where  $\int d\phi^{(n)}$  is the (partially integrated) phase space for  $n$ -soft gluons,  $|n\rangle$  is a state with  $n$  real soft gluons and  $\hat{S}$  is the (nonlocal) eikonal operator:

$$\hat{S} = TP \exp \left[ -ig_S \int_C dx^\mu A_\mu \right]. \quad (2.69)$$

The contour  $C$  is the classical path of the radiating hard partons and  $A$  is the gluon field in the Heisenberg picture.  $T$  is a time-ordering operation for the operators  $A$  and  $P$  denotes path-ordering for the color matrices along to contour  $C$ . From the unitarity property <sup>4</sup> of the eikonal operators [56], it follows that the total eikonal cross-section equals exactly the leading order cross-section, *i.e.* the higher order contributions vanish (in particular that also implies cancellation of the soft-gluon divergences). For example at order  $\alpha_S$ :

$$\omega^{(0)} + \omega^{(1)} = 0, \quad (2.70)$$

where  $\omega^{(i)}$ ,  $i = 0, 1$  is the total probability for virtual ( $i = 0$ ) and real ( $i = 1$ ) soft gluon emission.

One can evaluate the eikonal cross-section to some fixed order in  $\alpha_S$  by working in the eikonal approximation. In this approximation, the emission of a soft gluon with momentum  $q$  from a hard quark with momentum  $p$  is described by vertex  $2p_\mu$  and with eikonal propagator  $1/2p.q$ . An important property of the eikonal approximation is that real gluon emission factorizes [40]. To order  $\alpha_S$  the amplitude for a real soft-gluon emission in a process involving  $k$  hard particles is

---

<sup>4</sup>For the applications we consider in this Thesis it is satisfied, since the unitarity of the eikonal operators is explicit in the case when every two points of the contour  $C$  are separated by a time-like interval, *i.e.* the contour is time-ordered; see [56].

proportional to the  $k$ -particle hard amplitude. In general however, there are color correlations involved. In the case  $k = 2, 3$  one can show that the correlations are absent since the product of color matrices can be expressed completely in terms of the Casimir (2.10) [40]. For the purposes of our applications we will only need the result for the case of two hard partons (quarks):

$$d\omega^{(1)} = -g_S^2 \frac{d^3 q}{(2\pi)^3 2q_0} C_F |J(q)|^2, \quad (2.71)$$

where  $J^\mu$  is the eikonal current:

$$J^\mu = \frac{p_1^\mu}{p_1 \cdot q} - \frac{p_2^\mu}{p_2 \cdot q}, \quad (2.72)$$

and  $p_{1,2}$  are the momenta of the two hard quarks that constitute the path  $C$  in Eq.(2.69). In case the hard partons are gluons the color factor in Eq.(2.71) should be replaced with  $C_A$ .

Collecting the results above, one can easily obtain the eikonal coefficient function to order  $\alpha_S$ :

$$C^{soft}(z) = \frac{1}{\sigma_B} \frac{d\sigma}{dz} = (1 + \omega^{(0)}) \delta(1 - z) + \int d\omega^{(1)} \delta\left(1 - z - \frac{q_0}{p_0}\right) + \mathcal{O}(\alpha_S^2), \quad (2.73)$$

where  $q_0$  is the energy of the soft gluon and  $p_0$  is the c.m. energy of the hard parton. To obtain the all-order result valid up to NLL accuracy one has to take the Mellin moment of Eq.(2.73) and then to exponentiate the  $\alpha_S$  term. The resulting integral typically takes the following form:

$$\begin{aligned} \ln C^{soft}(N) &= \frac{C_F}{\pi} \int_0^1 dz \frac{z^{N-1} - 1}{1 - z} \left\{ \int_{\mu_F^2}^{(1-z)^a Q^2} \frac{dq^2}{q^2} \alpha_S(q^2) \right. \\ &\quad \left. + J \left[ \alpha_S((1-z)^a Q^2) \right] \right\}. \end{aligned} \quad (2.74)$$

To put Eq.(2.74) in its present form, we have introduced the variable  $z = 1 - q_0/p_0$  (as follows from the argument of the  $\delta$ -function in (2.73)) and have worked in

spherical co-ordinates conveniently determined by the hard momenta. Two of the integrations over the phase-space of the radiated gluon are trivial. The one remaining integration is over the azimuthal angle which in turn can be related to the transverse momentum of the radiated gluon. The latter is known to set the scale of the running coupling in the soft region [57], [7] and is an important leading order effect. More details on these relations will be presented when we consider our applications. The origin of the  $-1$  term in Eq.(2.74) is in the virtual emission term  $\omega^{(0)}$  after (2.70) is used. The number  $a$  is process dependent; typically  $a = 1, 2$ . The kinematical constraints imply that the lower limit of the  $q^2$  integration is zero. It is convenient to regularize the low- $q^2$  collinear divergence by introducing a cut-off. The (singular) dependence on the cut-off is later absorbed into the partonic distribution/fragmentation function as was discussed in Section (2.4.1). As a result, in the  $\overline{\text{MS}}$  factorization scheme the lower limit is set by the factorization scale  $\mu_F^2$  [43], [58].

The function  $J$  is process dependent and has a perturbative expansion in  $\alpha_S$ . To NLL accuracy, only the  $\mathcal{O}(\alpha_S)$  term participates. That function receives two contributions: the first one is from the collinearly non-enhanced term of the square of the eikonal current, after the  $q^2$  integration has been explicitly performed. Up to NLL accuracy one can use the following result:

$$\frac{1}{Q^2(1-z)^a} \int_0^{Q^2(1-z)^a} dq^2 \alpha_S(q^2) = \alpha_S(Q^2(1-z)^a), \quad a = 1, 2. \quad (2.75)$$

To show Eq.(2.75), one needs to use the running of the strong coupling (see Eq.(2.17)) and then to carefully identify and collect the NLL contributions. Both in (2.75) and (2.74),  $Q$  stands for some process-dependent hard scale.

To specify the second contribution to the function  $J$ , we need to first explain the physical origin of the various enhanced contributions in the soft limit. From kinematical considerations it is clear that in the limit  $z \rightarrow 1$ , typically, the initial

partons can emit only soft gluons. The hard partons in the final state however may or may not be subject to that constraint. In the case of inclusive DIS for example, the hard parton in the final state is completely free to fragment with the only restriction being on the virtuality of the final jet. If however the final parton is observed (and considered as massless as is appropriate for a coefficient function) it can only radiate soft gluons. Since the eikonal approximation handles only the contribution from soft gluon radiation (that itself can be collinear), one needs to specify in addition to the eikonal cross-section the contribution from the fragmentation region. Such a contribution was evaluated in [53] after the soft-gluon radiation was completely decoupled from the final massless quark (with appropriate choice of the vector specifying the physical gauge). The jet function that incorporates the effect of the collinear radiation in the fragmenting jet was obtained from a modified evolution equation. We will return to that point later when we consider our applications.

Finally, the results to NLL order can be completed by introducing an additional  $\mathcal{O}(\alpha_S^2)$  contribution to the RHS of Eq.(2.74). One needs to make the replacement:

$$\frac{C_F}{\pi} \frac{\alpha_S(q^2)}{q^2} \rightarrow \frac{A[\alpha_S(q^2)]}{q^2}, \quad (2.76)$$

where the function  $A(\alpha_S)$  can be expanded as follows:

$$A(\alpha_S) = \sum_{n=1}^{\infty} \left( \frac{\alpha_S}{\pi} \right)^n A^{(n)}. \quad (2.77)$$

The first two coefficients are needed at NLL level and are given by [53, 59]:

$$A^{(1)} = C_F, \quad (2.78)$$

$$A^{(2)} = \frac{1}{2} C_F \left[ C_A \left( \frac{67}{18} - \frac{\pi^2}{6} \right) - \frac{5}{9} n_f \right]. \quad (2.79)$$

A numerical estimate for  $A^{(3)}$  is known too [60] (see also [61]). The function  $A$  represents the coefficient of the singular term of the anomalous dimension (2.36).

After the replacement (2.76), Eq.(2.74) contains all NLL contributions. Its explicit evaluation would, however, contain subleading terms as well. One can evaluate explicitly the integrals and extract only the LL and NLL terms. After that is performed, the eikonal cross-section takes the form:

$$C^{soft}(N, Q, \alpha_S(\mu^2), \mu, \mu_F) = \exp \left[ \ln N g^{(1)}(\lambda) + g^{(2)}(\lambda, Q, \mu, \mu_F) \right] \quad (2.80)$$

where we have specified all arguments, restored the separate dependence on the renormalization and factorization scales, and introduced:

$$\lambda = b_0 \alpha_S(\mu^2) \ln N. \quad (2.81)$$

The functions  $g^{(1)}$  and  $g^{(2)}$  contain all LL ( $\ln(N)(\alpha_S \ln(N))^n$ ) and NLL ( $(\alpha_S \ln(N))^n$ ) contributions respectively. The results at NNLL order and beyond can be also written in terms of functions  $\alpha_S^k(N)g^{(k+2)}(\lambda)$ ,  $k = 1, \dots$  (see e.g. [62]). To evaluate the integrals in (2.74) with NLL accuracy, one makes use of the running coupling Eq.(2.17) and the following identity, valid to NLL [53]:

$$z^{N-1} - 1 \rightarrow -\Theta \left( 1 - \frac{e^{-\gamma_E}}{N} - z \right). \quad (2.82)$$

We would like to emphasize the fact that the use of the replacement (2.82) makes it possible to evaluate the integral in (2.74). It is clear that the integrals in (2.74) are divergent for any value of  $N$  simply because of the presence of the Landau pole in the running coupling  $\alpha_S$ ; see Eq.(2.16). The role of the replacement (2.82) is that it extracts finite values from the integrals in (2.74) up to NLL accuracy, while neglecting subleading terms that are formally divergent. Consistency is however, preserved because of the neglecting of similar subleading terms in the derivation of (2.74). A detailed description can be found in [63] and [64].

So far we discussed only the evaluation with NLL accuracy of the coefficient function. However, the  $\mathcal{O}(\alpha_S)$  expression for the initial condition of the quark

initiated perturbative fragmentation function (2.59) also shows enhancement in the limit  $z \rightarrow 1$ . The resummation of the soft-gluon contribution to the (universal) initial condition for the PFF was performed in [43] with NLL accuracy. We shall only present the final result here:

$$\begin{aligned} \ln D_q^{ini}(N, \mu_0^2, \mu_{0F}^2, m^2, \alpha_S(\mu_0^2)) &= \int_0^1 dz \frac{z^{N-1} - 1}{1-z} \left\{ \int_{(1-z)^2 m^2}^{\mu_{0F}^2} \frac{dq^2}{q^2} A[\alpha_S(q^2)] \right. \\ &\quad \left. + H[\alpha_S((1-z)^2 m^2)] \right\}. \end{aligned} \quad (2.83)$$

Here  $m$  is the mass of the heavy quark and the function  $H$  also has a perturbative expansion in  $\alpha_S$ :

$$H(\alpha_S) = \sum_{n=1}^{\infty} \left( \frac{\alpha_S}{\pi} \right)^n H^{(n)}. \quad (2.84)$$

At NLL level, we are just interested in the first term of the above expansion:

$$H^{(1)} = -C_F. \quad (2.85)$$

The explicit evaluation of the initial condition (2.83) to order NLL gives:

$$D_q^{ini} = \exp \left[ \ln N g_{ini}^{(1)}(\lambda_0) + g_{ini}^{(2)}(\lambda_0) \right] \quad (2.86)$$

where we have suppressed the arguments for brevity, and  $\lambda_0$  is given in (2.81) with the replacement  $\mu^2 \rightarrow \mu_0^2$ . The functions  $g_{ini}^{(1,2)}$  are:

$$g_{ini}^{(1)}(\lambda_0) = -\frac{A^{(1)}}{2\pi b_0 \lambda_0} [2\lambda_0 + (1-2\lambda_0) \ln(1-2\lambda_0)], \quad (2.87)$$

$$\begin{aligned} g_{ini}^{(2)}(\lambda_0) &= \frac{A^{(1)}}{2\pi b_0} \left[ \ln \frac{\mu_{0F}^2}{m^2} + 2\gamma_E \right] \ln(1-2\lambda_0) \\ &\quad - \frac{A^{(1)} b_1}{4\pi b_0^3} [4\lambda_0 + 2 \ln(1-2\lambda_0) + \ln^2(1-2\lambda_0)] \\ &\quad + \frac{1}{2\pi b_0} [2\lambda_0 + \ln(1-2\lambda_0)] \left( \frac{A^{(2)}}{\pi b_0} + A^{(1)} \ln \frac{\mu_0^2}{\mu_{0F}^2} \right) \\ &\quad + \frac{H^{(1)}}{2\pi b_0} \ln(1-2\lambda_0). \end{aligned} \quad (2.88)$$

So far we discussed how one can evaluate the approximate expressions for the coefficient function and the initial condition of the PFF in the limit  $z \rightarrow 1$ . However, to obtain a result equally applicable for all  $z$ , one needs to give a matching prescription for the fixed order result and its approximation in the soft limit. In this Thesis we will use the following matching procedure: one adds the fixed order result and the result valid in the soft limit together, and then subtracts what they have in common. Note that for consistency, the decomposition of the result valid in the soft limit in powers of  $\alpha_S$  should coincide with the soft limit of the fixed order result. We will give details for that procedure in the next Chapters.

# Chapter 3

## ***b*-quark Fragmentation in *t*-quark Decay**

In this Chapter we present our original results for *b*-fragmentation in top decay. In their derivation we apply several techniques within perturbative QCD such as the fixed order calculation and resummation of large quasi-collinear and soft logs. Those techniques were discussed in the previous Chapter. We also extract the non-perturbative fragmentation function from fits to  $e^+e^-$  data and thus make a prediction for the spectrum of *b*-flavored hadrons in top decay. This Chapter is based on the papers [51] and [65].

### **3.1 Motivation: Top Physics**

The existence of the top quark is a prediction of the Standard Model. It was discovered at the Fermilab Tevatron [66] and its mass was measured [67] to be  $174.3 \pm 5.1$  GeV. This large mass applies, among other things, a large coupling to the Higgs boson (the top-Yukawa coupling  $g_{t\bar{t}H} \sim 1$ ). Unlike the other five

quarks, top's CKM matrix elements are dominated by a single element –  $V_{tb}$  – which is very close to one. As a result top decays almost exclusively to a real  $W$  boson and a  $b$ -quark. Its electric charge (as predicted by the SM) is  $+(2/3)e$  but is not yet measured directly [68]. The present status of these and other top-quark properties can be found in the extensive recent review [69].

At present, and for the foreseeable future, the study of processes involving the top quark is of great interest. On the experimental side, because of its very large mass, the top is still a challenge to present experimental facilities. The CDF and DØ collaborations in Run I at the Fermilab Tevatron produced a small but sufficient number of top events to directly prove its existence in 1995 [66] and to pinpoint its mass. Since then the Tevatron has been upgraded and Run II is presently collecting data. The expectations are that during Run II more detailed measurements of the top quark properties will be possible. In the near future (around 2007-8) the LHC proton-proton collider is expected to start operation. Due to its much larger energy of operation it is expected to produce vast numbers of top quarks with a corresponding improvement in top studies [70]. There is another high-energy machine – the electron-positron Linear Collider [71] – the prospects of building which are being studied at present. Such a machine will not produce as many top events as LHC, but will have the potential for precise measurements of the top quark parameters.

On the theoretical side, the large mass of the top quark makes it decay very fast to a  $b$ -quark and a  $W^+$  boson. That implies a very large top decay width, the NLO value being  $\Gamma_{top} \approx 1.4$  GeV. The corresponding life-time is about an order of magnitude shorter than the typical hadronization times set by the scale  $\Lambda_{QCD}$ . An immediate consequence is that the top quark cannot form  $t$ -flavored hadrons; it simply decays before it is able to hadronize [72]. For that reason the top behaves much like a free particle. That property of the top as well as the very

small ratio of its width to its mass suggest that it is reasonable for most purposes to assume that top production and top decay factorize to a good approximation.

It is not only the study of the SM that draws attention to the top quark. As we mentioned, the top has very large Yukawa coupling, i.e. its coupling to the Higgs sector is largest among all known particles. For that reason it is reasonable to expect that new physics that may be related to the mechanism of electroweak symmetry breaking may first show up in the top sector. For a more detailed account of such models see [69].

Clearly, a precise knowledge of the properties of the top quark is necessary not only in order to verify experimentally the SM predictions but also to be able to discriminate non-SM effects should they be discovered in forthcoming experiments. However, because the top has such a small life-time, the only way one can get any information about the top itself is through its decay products. Clearly, this requires – among other observables – a reliable description of the fragmentation of the *b*-quark in top-quark decay.

As shown in [73], *b*-fragmentation is indeed one of the sources of uncertainty in the measurement of the top mass at the Tevatron. At the LHC, recent studies [74] have suggested that final states with leptons and a  $J/\psi$ , with the  $J/\psi$  coming from the decay of a *b*-flavored hadron and the isolated lepton from the *W* decay, will be a promising channel to reconstruct the top mass. In [74], the expected experimental error, including statistics and systematics, has been estimated to be  $\Delta m_t \simeq 1$  GeV and the *b* fragmentation is the largest source of uncertainty, accounting for about 0.6 GeV.

In this Chapter we will study the *b*-spectrum in top decay in the following framework: neglecting the interference effects between top production and decay,

one has

$$\frac{1}{\sigma} \frac{d\sigma}{dx_b} = \frac{1}{\Gamma} \frac{d\Gamma}{dx_b}. \quad (3.1)$$

In the above equation,  $(1/\sigma)d\sigma/dx_b$  is the normalized differential cross section for the process of production of a  $b$  quark with energy fraction  $x_b$  (defined in Eq.(3.5)) via top quarks for any production mechanism. Similarly,  $(1/\Gamma)d\Gamma/dx_b$  is the normalized differential distribution of  $b$ -quark in the decay of a real top quark. Our purpose in this Chapter is to give a precise prediction for the distribution on the RHS of Eq.(3.1); through the relation (3.1) our results will then be applicable to top quarks produced in  $p\bar{p}$  (Tevatron),  $pp$  (LHC) or  $e^+e^-$  (Linear Collider) collisions.

We start by first calculating in Section (3.2) the differential top width with respect to the  $b$ -energy fraction in NLO QCD taking full account of the mass of the  $b$  quark. Then in Section (3.3) we resum with NLL accuracy the large quasi-collinear logs  $\ln(m_b^2/m_t^2)$ . Applying soft-gluon resummation techniques in Section (3.4) we improve the prediction for the  $b$ -energy spectrum at large  $x_b \rightarrow 1$ . Then we discuss the improvement to the fixed order calculation due to the various resummations. Finally, in Section (3.5) we extract the non-perturbative fragmentation function using  $e^+e^-$  data to make predictions for the energy spectrum of  $b$ -flavored hadrons in top decay.

## 3.2 $t \rightarrow bW$ in NLO QCD

In this section we present our results for the NLO QCD calculation of the differential width:

$$\frac{1}{\Gamma_0} \frac{d\Gamma_b}{dx_b}, \quad (3.2)$$

for the Standard Model top-quark decay:

$$t(q, m_t) \rightarrow b(p_b, m_b) W(p_W, m_W) (g(p_g, 0)), \quad (3.3)$$

of an on-shell top quark at next-to-leading order in  $\alpha_S$ , with respect to the energy fraction of the produced *b*-quark (defined below). We assume that the decay process (3.3) is the only decay mode of the top quark. That assumption is consistent with recent measurements of the CDF Collaboration of the ratio  $R = B(t \rightarrow Wb)/B(t \rightarrow Wq)$ , where  $q$  is a *d*, *s* or *b* quark, and the subsequent extraction of the Cabibbo–Kobayashi–Maskawa matrix element  $V_{tb}$  [75]. We present the results from two independent calculations: when the exact dependence on the bottom mass is kept, thus regulating the collinear divergences, and when the bottom mass is set to zero from the outset. In the latter case additional collinear divergences occur. In all our calculations we use dimensional regularization to regulate the UV and all IR divergences, that is, we perform the calculations in  $D = 4 - 2\epsilon$  space-time dimensions (see appendix). We use the on-shell renormalization scheme to remove the UV divergences. Let us note that in principle one does not need to calculate Eq.(3.2) both in the  $m_b = 0$  and  $m_b \neq 0$  cases; one can infer the massless result for the normalized distribution (3.2) (with the collinear singularity subtracted in the  $\overline{\text{MS}}$  scheme) from the massive one, using the initial conditions for the PFF, Eq.(2.59). In fact with our independent calculation of those two cases we were able to reproduce those initial conditions in the case of top-quark decay.

### 3.2.1 Calculation with $m_b \neq 0$

In this section we will present in more detail the calculation in the case when the full dependence on the  $b$ -mass is kept. Let us first introduce our notation:

$$\begin{aligned}
b &= \frac{m_b^2}{m_t^2}, \\
w &= \frac{m_W^2}{m_t^2}, \\
s &= \frac{1}{2}(1 + b - w), \\
\beta &= \frac{\sqrt{b}}{s}, \\
Q &= s\sqrt{1 - \beta^2}, \\
G_0 &= \frac{1}{2} \left[ 1 + b - 2w + \frac{(1 - b)^2}{w} \right], \\
\Phi(x_b) &= s \left[ \sqrt{x_b^2 - \beta^2} - \operatorname{arcth} \left( \frac{\sqrt{x_b^2 - \beta^2}}{x_b} \right) \right], \tag{3.4}
\end{aligned}$$

where:

$$x_b = \frac{x_E}{x_{E,\max}} = \frac{p_b \cdot p_t}{m_t^2 s} \quad , \quad \beta \leq x_b \leq 1. \tag{3.5}$$

It is obvious that  $x_b$  is an invariant, which in the top rest frame coincides with the energy of the  $b$ -quark, normalized with respect to its maximum value. The LO width  $\Gamma_0$  is:

$$\Gamma_0 = \frac{\alpha m_t |V_{tb}|^2}{16 \sin^2 \theta_W} 4QG_0, \tag{3.6}$$

where  $\alpha$  is the electromagnetic coupling constant and  $\theta_W$  is the Weinberg angle.

Next we proceed with the details of the calculation. At order  $\mathcal{O}(\alpha_S)$  one has to calculate the contributions from the diagrams in Figures (3-1), (3-2) and (3-3).

To obtain the contribution from the real emission diagrams – Fig.(3-3) – one has to add the two matrix elements and square them. After averaging/summing over spins and colors (all the needed details can be found in the appendix) one gets

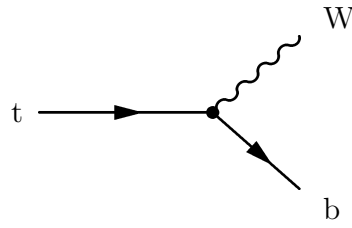


Figure 3-1: Tree level (Born) diagram.

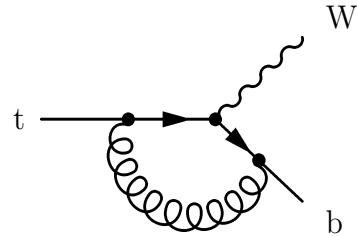
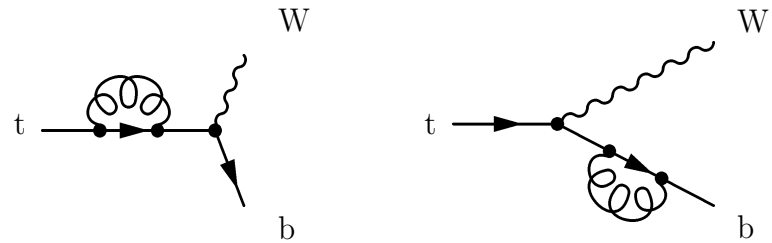


Figure 3-2: Contributing virtual emission diagrams.

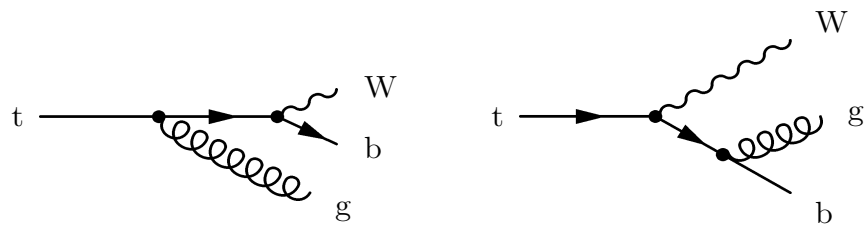


Figure 3-3: Contributing real emission diagrams.

the following expression for the square of the matrix element:

$$\overline{|M_{real}|^2} = \frac{2}{3} g^2 g_S^2 |V_{tb}|^2 \left[ \frac{m_t^4}{(p_t \cdot p_g)(p_b \cdot p_g)} (2sG_0 - \epsilon 4s^2) \right]$$

$$\begin{aligned}
& + \frac{1}{(p_t \cdot p_g)^2} \left( -\frac{1+b}{w} (p_t \cdot p_g)^2 + \left( 2 + \frac{1+b}{w} \right) (p_t \cdot p_g) (p_b \cdot p_g) \right. \\
& + 2(p_t \cdot p_g) m_t^2 G_0 + m_t^4 (-G_0 + \epsilon 2s) \Big) \\
& + \frac{1}{(p_b \cdot p_g)^2} \left( -\frac{1+b}{w} (p_b \cdot p_g)^2 + \left( 2 + \frac{1+b}{w} \right) (p_t \cdot p_g) (p_b \cdot p_g) \right. \\
& \left. \left. - 2(p_b \cdot p_g) m_t^2 G_0 + m_t^4 (-bG_0 + \epsilon 2bs) \right) \right], \tag{3.7}
\end{aligned}$$

in terms of the scalar products of the four vectors. We have kept those terms linear in  $\epsilon$  that will give finite contributions after the singular integration over the phase space is performed. The next step is to integrate the matrix element (3.7) over the three-body phase space. More details about that procedure are relegated to the appendix. As a result, we obtain the following contribution from the real emission diagrams to the differential width (3.2) at order  $\alpha_S$ :

$$\begin{aligned}
\frac{1}{\Gamma_0} \frac{d\Gamma_{real}^{(\alpha_S)}}{dx_b} = & \frac{C_F \alpha_S(\mu)}{\pi Q} \left\{ \left[ \Phi(x_b = 1) \left( \frac{1}{\epsilon} - 2\gamma_E + 2 - \ln \left( \frac{Q^2 m_t^2}{4\pi^2 \mu^2} \right) \right) \right. \right. \\
& + s \left( \text{Li}_2 \left( \frac{2Q}{1-s+Q} \right) - \text{Li}_2 \left( \frac{2Q}{s-b+Q} \right) \right. \\
& - \ln \left( \frac{s+Q}{\sqrt{b}} \right) \left( \ln \left( \frac{s+Q}{\sqrt{b}} \right) + 2 \ln \left( \frac{1-s+Q}{2s(1-\beta)} \right) \right) \\
& + \ln \left( \frac{s+Q}{\sqrt{b}} \right) \left( s-b+2 \frac{s^2}{G_0} \right) + \ln \left( \frac{1-s+Q}{\sqrt{w}} \right) (1-b) \\
& \left. \left. + 2Q \left( \ln \left( \frac{\sqrt{w}}{2s(1-\beta)} \right) - \frac{s}{G_0} \right) \right] \delta(1-x_b) \right. \\
& - 2 \Phi(x_b) \left[ \frac{1}{(1-x_b)_+} + \frac{s}{G_0} \left( 1 + \frac{1+b}{2w} \right) (1-x_b) - 1 \right] \\
& \left. + 2s\sqrt{x_b^2 - \beta^2} \left[ 2 \frac{s^2}{G_0} \left( \frac{1-x_b}{1-2sx_b+b} \right) + \frac{s}{G_0} \left( 1 + \frac{1+b}{2w} \right) (1-x_b) - 1 \right] \right\} \tag{3.8}
\end{aligned}$$

As expected, the real emission contribution to the differential distribution contains an explicit soft divergence  $\sim 1/\epsilon$ . The latter will be cancelled after we add the contribution from the virtual diagrams. Let us explain their evaluation.

The diagrams with virtual gluon emission that contribute to order  $\alpha_S$  are shown in Fig.(3-2). They represent the same physical process as the leading order (Born) diagram in Fig.(3-1). Because the virtual diagrams contain loop integrals, they are UV divergent. We regularize these divergences by working in  $D$  space-time dimensions. The cancellation of the UV divergences requires an appropriate introduction of counterterms. The counterterms are determined from the on-shell condition:

$$\Sigma(\not{p} = m) = 0, \quad \frac{\partial \Sigma(\not{p} = m)}{\partial \not{p}} = 0, \quad (3.9)$$

where  $\Sigma$  is the quark self-energy for quark  $q$  with mass  $m$ . From the second condition in (3.9), one can derive the quark wave function renormalization constant (it coincides with the one in [76]):

$$Z_2^{(q)} = 1 - \frac{\alpha_S}{3\pi} \left( \frac{1}{\epsilon_{UV}} + \frac{2}{\epsilon_{IR}} + 4 - 3\gamma_E - 3 \ln \left( \frac{m^2}{4\pi\mu^2} \right) \right). \quad (3.10)$$

This then determines the vertex renormalization constant:

$$Z^{(\Lambda)} = 1 - \frac{\alpha_S}{3\pi} \left( \frac{1}{\epsilon_{UV}} + \frac{2}{\epsilon_{IR}} + 4 - 3\gamma_E - \frac{3}{2} \ln \left( \frac{m_t^2}{4\pi\mu^2} \right) - \frac{3}{2} \ln \left( \frac{m_b^2}{4\pi\mu^2} \right) \right). \quad (3.11)$$

The renormalized vertex thus becomes:

$$\Lambda_\mu^{reg} = \Lambda_\mu - i \left( Z^{(\Lambda)} - 1 \right) \gamma_\mu. \quad (3.12)$$

The function  $\Lambda_\mu$  contains the higher order contributions to the vertex amplitude, and is defined through the relation:  $M = g/\sqrt{8}V_{tb}\bar{u}\Lambda_\mu(1 - \gamma^5)u\epsilon^\mu$ .

Let us make a remark on the evaluation of the second term in Eq.(3.9). The function  $\Sigma(p)$  is UV divergent and its finite part is a regular function of the momentum  $p$  for  $p^2 \leq m^2$ . The point  $p = m$  is a (finite) logarithmic branching point, i.e. there  $\Sigma$  contains terms behaving as:

$$\lim_{y \rightarrow 0} \Sigma \sim y \ln(y) + \text{regular terms.}$$

For that reason, although  $\Sigma$  is finite for  $p = m$ , its derivative with respect to  $p$  diverges at that point. This is an IR divergence which we have regulated and distinctly parameterized in Eq.(3.10).

The evaluation of the vertex correction and of the self energy diagrams can be done by applying the Passarino-Veltman method [77] for reduction of tensor integrals. As a result, after some extensive algebra, one can reduce the calculation to the evaluation of the three scalar integrals  $A_0$ ,  $B_0$  and  $C_0$ . The latter are defined as the integration in  $D$  space-time dimensions of a product of one, two and three scalar propagators with, generally, different masses. For their evaluation we use standard techniques and Feynman parametrization. In the present case of one-to-two particle decay, the phase space is very simple (see the appendix). To obtain the differential cross-section one does not need to perform any nontrivial integrations. The resulting expression is:

$$\begin{aligned} \frac{1}{\Gamma_0} \frac{d\Gamma_{virt}^{(\alpha_S)}}{dx_b} = & \frac{C_F \alpha_S(\mu)}{\pi Q} \left\{ -\Phi(x_b = 1) \left( \frac{1}{\epsilon} - 2\gamma_E + 2 - \ln \left( \frac{Q^2 m_t^2}{4\pi^2 \mu^2} \right) \right) \right. \\ & + s \left[ \text{Li}_2 \left( \frac{2Q}{1-s+Q} \right) - \text{Li}_2 \left( \frac{2Q}{s-b+Q} \right) \right. \\ & - 2 \ln(s+Q) \ln \left( \frac{1-s+Q}{\sqrt{w}} \right) - \ln \left( \frac{s+Q}{\sqrt{b}} \right) \ln \left( (s+Q)\sqrt{b} \right) \left. \right] \\ & + \frac{3Q^2 - 2s^2}{G_0} \ln \left( \frac{s+Q}{\sqrt{b}} \right) + 2Q \left( \frac{s}{G_0} - 1 \right) \\ & \left. - \frac{Q}{4wG_0} (1 + 4b + bw - 5b^2 - 5w + 4w^2) \ln(\sqrt{b}) \right\} \delta(1-x_b) \quad (3.13) \end{aligned}$$

To get the needed distribution we need to only add the contributions (3.13) and (3.8). After also adding the LO contribution, the result reads:

$$\begin{aligned} \frac{1}{\Gamma_0} \frac{d\Gamma}{dx_b} = & \delta(1-x_b) + \frac{C_F \alpha_S(\mu)}{\pi Q} \left\{ \left\{ 2s \left[ \text{Li}_2 \left( \frac{2Q}{1-s+Q} \right) - \text{Li}_2 \left( \frac{2Q}{s-b+Q} \right) \right. \right. \right. \\ & \left. \left. \left. - \ln(s+Q) \left( \ln \left( \frac{1-s+Q}{\sqrt{w}} \right) + \ln \left( \frac{s-b+Q}{2s(1-\beta)} \right) \right) \right] \right\} \right. \end{aligned}$$

$$\begin{aligned}
& + \frac{1}{2} \ln(b) \ln \left( \frac{s-b+Q}{2s(1-\beta)} \right) \left] + \left( 3 \frac{Q^2}{G_0} + s-b \right) \ln \left( \frac{s+Q}{\sqrt{b}} \right) \right. \\
& + (1-b) \ln \left( \frac{1-s+Q}{\sqrt{w}} \right) + Q \left[ \left( 6 \frac{(w-b)(s-b)}{wG_0} - 1 \right) \frac{\ln(b)}{4} \right. \\
& - 2 \left. \ln \left( \frac{2s(1-\beta)}{\sqrt{w}} \right) - 2 \right] \left. \right\} \delta(1-x_b) \\
& - 2 \Phi(x_b) \left[ \frac{1}{(1-x_b)_+} + \frac{s}{G_0} \left( 1 + \frac{1+b}{2w} \right) (1-x_b) - 1 \right] \\
& + 2s\sqrt{x_b^2 - \beta^2} \left[ 2 \frac{s^2}{G_0} \left( \frac{1-x_b}{1-2sx_b+b} \right) + \frac{s}{G_0} \left( 1 + \frac{1+b}{2w} \right) (1-x_b) - 1 \right] \left. \right\}. \tag{3.14}
\end{aligned}$$

Separately, the contributions from the virtual and from the real emission are IR divergent but those divergences cancel in the sum. In the derivation of the above result, we have extensively made use of various relations between the dilogarithms (Spence functions); see the appendix for details. Finally, one can verify that the integral of the differential distribution (3.14) coincides with the total top-decay width to order  $\alpha_S$  evaluated in [76]. As expected from the KLN theorem (see Section (1.4)), all IR sensitive contributions disappear. Let us also note that the top width is known at present to order  $\alpha_S^2$  [78].

Let us also present here the result (3.14) in the limit  $m_b \rightarrow 0$ , where all power corrections of the type  $m_b/m_t$  can be neglected. The result reads:

$$\frac{1}{\Gamma_0} \frac{d\Gamma}{dx_b} = \delta(1-x_b) + \frac{\alpha_S(\mu)}{2\pi} A_1(x_b), \tag{3.15}$$

with

$$\begin{aligned}
A_1(x_b) & = C_F \left\{ \left[ \frac{1+x_b^2}{(1-x_b)_+} + \frac{3}{2} \delta(1-x_b) \right] \ln \frac{m_t^2}{m_b^2} \right. \\
& + 2 \frac{1+x_b^2}{(1-x_b)_+} \ln[(1-w)x_b] - \frac{4x_b}{(1-x_b)_+} + \frac{4w(1-w)}{1+2w} \frac{x_b(1-x_b)}{1-(1-w)x_b} \\
& + \delta(1-x_b) \left[ 4\text{Li}_2(1-w) + 2 \ln w \ln(1-w) - \frac{2\pi^2}{3} \right. \\
& \left. \left. - \frac{2(1-w)}{1+2w} \ln(1-w) - \frac{2w}{1-w} \ln w - 4 \right] \right\}. \tag{3.16}
\end{aligned}$$

The origin of the plus-prescription appearing in the above results as well as some its properties are discussed in the appendix.

### 3.2.2 Calculation with $m_b=0$

In a similar fashion to the above derivation one can also obtain the massless results with the bottom mass set to zero from the outset. In this calculation we proceeded in the same way as in the  $m_b \neq 0$  case. The integrals to be evaluated simplify significantly in this case. We use the same renormalization scheme as in the case  $m_b \neq 0$ . The essential difference is that in the massless case, the contributions to the differential width from real and virtual gluon emission, after the UV renormalization is performed, contain IR divergent terms up to  $1/\epsilon^2$ . An extra power of  $1/\epsilon$  appears because the  $b$ -mass no longer prevents collinear divergences. For that reason, in general, one need to keep terms to order  $\mathcal{O}(\epsilon^2)$ . Similarly to the case  $m_b \neq 0$ , in the sum of the real and virtual contributions to the differential width the leading IR divergences  $\sim 1/\epsilon^2$  cancel. The resulting expression contains a singularity  $\sim 1/\epsilon$  which is in one-to-one correspondence with the quasi-collinear  $\log(m_b/m_t)$  present in the massive result (3.16). Finally, the massless result reads:

$$\begin{aligned} \frac{1}{\Gamma_0} \frac{d\hat{\Gamma}_b}{dx_b} &= \delta(1-x_b) + \frac{\alpha_S(\mu)}{2\pi} \left\{ C_F \left[ \frac{1+x_b^2}{(1-x_b)_+} + \frac{3}{2}\delta(1-x_b) \right] \right. \\ &\quad \times \left. \left( -\frac{1}{\epsilon} + \gamma_E - \ln 4\pi \right) + \hat{A}_1(x_b) \right\}, \end{aligned} \quad (3.17)$$

with  $\hat{A}_1(x_b)$  defined as:

$$\begin{aligned} \hat{A}_1(z) &= C_F \left\{ \left[ \frac{1+z^2}{(1-z)_+} + \frac{3}{2}\delta(1-z) \right] \left[ \ln \frac{m_t^2}{\mu_F^2} + 2\frac{1+w}{1+2w} - 2\ln(1-w) \right] \right. \\ &\quad \left. + \frac{1+z^2}{(1-z)_+} \left[ 4\ln[(1-w)z] - \frac{1}{1+2w} \right] \right\} \end{aligned}$$

$$\begin{aligned}
& - \frac{4z}{(1-z)_+} \left[ 1 - \frac{w(1-w)(1-z)^2}{(1+2w)(1-(1-w)z)} \right] \\
& + 2(1+z^2) \left[ \left( \frac{1}{1-z} \ln(1-z) \right)_+ - \frac{1}{1-z} \ln z \right] \\
& + \delta(1-z) \left[ 4\text{Li}_2(1-w) + 2\ln(1-w) \ln w - \frac{2\pi^2}{3} + \frac{1+8w}{1+2w} \ln(1-w) \right. \\
& \left. - \frac{2w}{1-w} \ln w + \frac{3w}{1+2w} - 9 \right] \}.
\end{aligned} \tag{3.18}$$

In order to get the correct finite term in the normalized differential width, the Born width  $\Gamma_0$  (see Eq.(3.6)) will have to be evaluated in dimensional regularization to order  $\mathcal{O}(\epsilon)$ . We find:

$$\begin{aligned}
\Gamma_0 & = \frac{\alpha m_t |V_{tb}|^2}{16 \sin^2 \theta_W} \frac{(1-w)^2(1+2w)}{w} \{ 1 + \epsilon \\
& \times \left[ -\gamma_E + \ln 4\pi - 2\ln(1-w) + 2\frac{1+w}{1+2w} \right] \}.
\end{aligned} \tag{3.19}$$

One can easily verify that the difference  $A_1(x_b) - \hat{A}_1(x_b)$  exactly reproduces the (heavy quark initiated) initial condition for the perturbative fragmentation function, Eq.(2.59). We also checked that the integral of Eq. (3.17) agrees with the result of [79], where the  $\mathcal{O}(\alpha_S)$  corrections to the top width have been evaluated in the approximation of a massless  $b$  quark. Of course, it also coincides with the massless limit of the total width obtained from our calculation with non-zero bottom mass. It is worth noting that in the total width the IR divergences disappear together with the dependence on the unphysical factorization scale  $\mu_F$ . Technically that is obvious since the terms that depend on  $\mu_F$  are multiplied in (3.17) by the LO Altarelli-Parisi splitting function (2.34) whose integral vanishes (see Eq.(2.31)).

### 3.3 NLL Resummation of logs $\ln(m_b^2/m_t^2)$

In principle the perturbative result Eq.(3.14) gives a finite prediction for the *b*-spectrum in top decay. However, that quantity is not IR safe (in the sense of Section (2.4)) since it diverges in the limit  $m_b \rightarrow 0$ . As follows from our general discussions in the previous Chapter, to obtain a reliable perturbative prediction one needs to resum the quasi-collinear logs  $\ln(m_b^2/m_t^2)$  to all orders<sup>1</sup> in the strong coupling. We will show later in this section that the numerical difference between the two expressions for the *b*-spectrum – Eqns.(3.14) and (3.15) – is totally negligible. Since the two expressions differ by power corrections  $\sim (m_b/m_t)^n$  which are small since  $m_b/m_t = \mathcal{O}(10^{-2})$ , one can conclude that the power corrections can indeed be safely neglected. Let us recall that this is precisely the condition for validity of the method of the perturbative fragmentation function described in detail in Section (2.4.2). Therefore, in the following we will present the application of this method for resummation of the above mentioned quasi-collinear logs in top-quark decay with NLL accuracy.

Following the general discussion in Section (2.4.2), the differential width for the production of a massive *b* quark in top decay can be expressed via the following convolution:

$$\frac{1}{\Gamma_0} \frac{d\Gamma}{dx_b}(x_b, m_t, m_W, m_b) = \frac{1}{\Gamma_0} \int_{x_b}^1 \frac{dz}{z} \frac{d\hat{\Gamma}}{dz}(z, m_t, m_W, \mu, \mu_F) D\left(\frac{x_b}{z}, \mu_F, m_b\right), \quad (3.20)$$

where we have restricted the above result to the flavor non-singlet case, i.e. to the perturbative fragmentation of a massless *b* into a massive *b*. In doing so, we have ignored the strongly suppressed mixing of the *b*-quark with the gluon and the other flavors through DGLAP evolution. In Eq. (3.20)  $\mu$  and  $\mu_F$  are the

---

<sup>1</sup>There is another mass parameter in our problem - the *W* mass  $m_W$ . However, we will treat it as not small with respect to  $m_t$ , and therefore will not resum terms like  $\ln(m_W^2/m_t^2)$ .

renormalization and factorization scales respectively, the former associated with the renormalization of the strong coupling constant. In principle, one can use two different values for the factorization and renormalization scales; however, a choice often made consists of setting  $\mu = \mu_F$  and we shall adopt this convention for most of the results which we shall show.

The NLO,  $\overline{\text{MS}}$ -subtracted coefficient function is:

$$\frac{1}{\Gamma_0} \frac{d\hat{\Gamma}_b}{dz}^{\overline{\text{MS}}} = \delta(1-z) + \frac{\alpha_S(\mu)}{2\pi} \hat{A}_1(z), \quad (3.21)$$

with  $\hat{A}_1$  given in Eq.(3.18). The consistent NLO plus NLL (as defined in Eq.(2.51)) evaluation of the *b*-production rate requires that  $\alpha_S$  is the NLO strong coupling constant (2.16) with  $n_f = 5$  for the number of active flavors. The initial condition for the perturbative fragmentation function must be evaluated to order  $\alpha_S$  as well. The initial condition is presented in (2.59) with  $m$  being the bottom mass  $m_b$  and, in order to avoid large logs there, we need to take the initial scale  $\mu_{0F}$  of the order of  $m_b$ .

As follows from our discussion of Eq.(2.64), we will work in analytical form in terms of the Mellin moments  $N$ ; the Mellin transformation is defined in (2.39). The Mellin transform of Eq. (3.20) is:

$$\Gamma_N(m_t, m_W, m_b) = \hat{\Gamma}_N(m_t, m_W, \mu, \mu_F) D_{b,N}(\mu_F, m_b), \quad (3.22)$$

with

$$\Gamma_N(m_t, m_W, m_b) = \frac{1}{\Gamma_0} \int_0^1 dx_b x_b^{N-1} \frac{d\Gamma}{dx_b}(x_b, m_t, m_W, m_b). \quad (3.23)$$

The fragmentation function  $D_{b,N}$  is a product of the solution of the DGLAP equations Eq.(2.62) with the initial condition Eq.(A.27). The explicit  $N$ -space expression for the coefficient function  $\hat{\Gamma}_N$  can also be found in the appendix.

For our numerical study, we shall assume  $m_t = 175$  GeV,  $m_W = 80$  GeV,  $m_b = 5$  GeV and  $\Lambda = 200$  MeV.

The  $b$ -quark energy distribution in  $x_b$ -space will finally be obtained by inverting the  $N$ -space result (3.22) numerically, by a contour integral in the complex  $N$ -plane. We will use the so-called minimal prescription introduced in [63], where the integration contour is deformed with respect to the one in Eq.(2.65). We will discuss that point in more detail in the next section.

We already have all the ingredients needed to obtain the expression for the  $b$ -quark spectrum in top-quark decay with collinear logs  $\sim \ln(m_b/m_t)$  resummed with NLL accuracy. We normalize our plots to the total NLO width  $\Gamma$ , obtained by neglecting powers  $\sim (m_b/m_t)^p$ . Its expression can be found in [79]. In fact, that normalization is not affected by the factorization on the right-hand side of Eq. (3.20), the DGLAP evolution of the relevant factors, or the resummation of soft logarithms in the initial condition of the perturbative fragmentation function and the coefficient function.

We first present our results for the  $x_b$  spectrum in Fig. 3-4. We plot the  $x_b$  distribution according to the perturbative fragmentation approach. For the sake of comparison, we also show the exact  $\mathcal{O}(\alpha_S)$  result for a massive  $b$  quark, Eq.(3.14). We set  $\mu = \mu_F = m_t$  and  $\mu_0 = \mu_{0F} = m_b$ . As an illustration, the effect of NLL soft-gluon resummation only in the initial condition of the perturbative fragmentation function is also presented; it will be systematically discussed in the next section. Clearly, the use of perturbative fragmentation functions has a strong impact on the  $x_b$  distribution. The fixed-order result lies well below the perturbative fragmentation results for about  $0.1 \lesssim x_b \lesssim 0.9$  and diverges once  $x_b \rightarrow 1$ , due to a behavior  $\sim 1/(1 - x_b)_+$ . Moreover, as we previously noted, the full inclusion of powers of  $m_b/m_t$  has a negligible effect on the  $x_b$  spectrum; the dot-dashed and dotted lines in Fig. 3-4 are in fact almost indistinguishable. As for the perturbative fragmentation results, the distribution shows a very sharp peak, though finite, once  $x_b$  approaches unity. This behavior will be smoothed

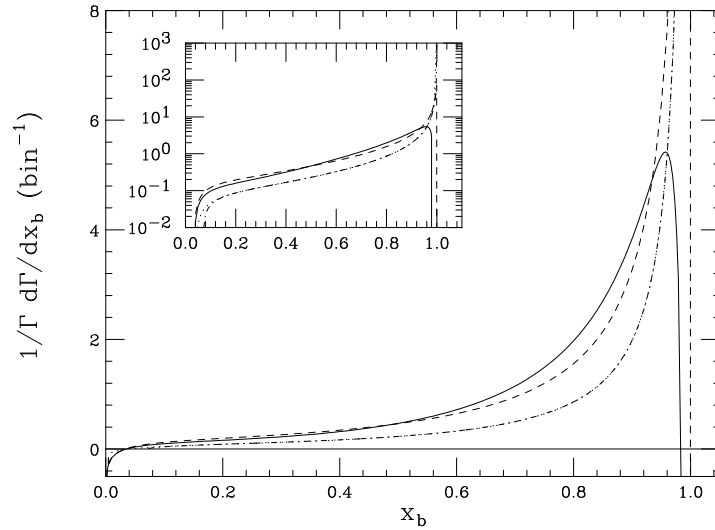


Figure 3-4:  $b$ -quark energy distribution in top decay according to the perturbative fragmentation approach, with (solid line) and without (dashes) NLL soft-gluon resummation in the initial condition of the perturbative fragmentation function, and according to the exact NLO calculation, with (dot-dashes) and without (dots) inclusion of powers of  $m_b/m_t$ . In the inset figure, we show the same curves on a logarithmic scale.

out after we resum the soft NLL logarithms appearing in the initial condition of the perturbative fragmentation function and the coefficient function; an indication is the behavior of the distribution after the soft-resummation (Eq.(2.86)) in the initial condition (2.59) is performed. Both perturbative fragmentation distributions become negative for  $x_b \rightarrow 0$  and  $x_b \rightarrow 1$ , which is a known result, already found for heavy-quark production in  $e^+e^-$  annihilation [43],[46]. For  $x_b \rightarrow 0$ , the coefficient function (3.21) contains large logarithms  $\sim \alpha_S(\mu) \ln x_b$  which have not been resummed yet. Likewise, in the soft limit  $x_b \rightarrow 1$ , Eq. (3.18) contains contributions  $\sim \alpha_S(\mu)/(1-x_b)_+$  and  $\sim \alpha_S(\mu)[\ln(1-x_b)/(1-x_b)]_+$  whose resummation is discussed in the next section. As stated in [43], once  $x_b$  gets closer to unity, non-perturbative contributions also become important and should be taken into account. The region of reliability of the perturbative calculation at large  $x_b$  may

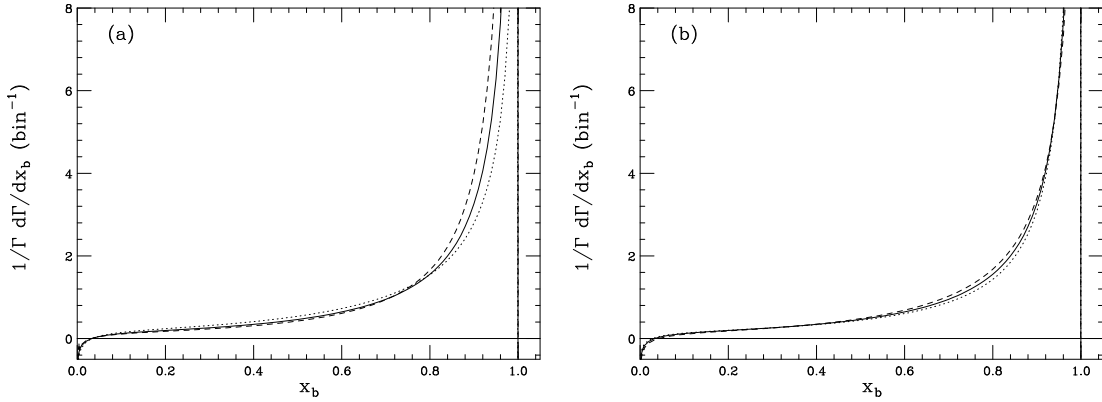


Figure 3-5: (a):  $x_b$  spectrum for  $\mu_F = m_t$  and  $\mu_{0F} = m_b/2$  (dots),  $\mu_{0F} = m_b$  (solid) and  $\mu_{0F} = 2m_b$  (dashes); (b):  $\mu_{0F} = m_b$  and  $\mu_F = m_t/2$  (dots),  $\mu_F = m_t$  (solid) and  $\mu_F = 2m_t$  (dashes). The renormalization scales are kept at  $\mu = m_t$  and  $\mu_0 = m_b$ . Though not visible, all distributions show a finite, sharp peak once  $x_b$  is close to 1.

be related to the Landau pole in the expression for the strong coupling constant (2.16), and is estimated to be  $x_b \lesssim 1 - \Lambda/m_b$ . Fig. 3-5 shows the dependence of the perturbative fragmentation  $x_b$  distributions on the factorization scales  $\mu_{0F}$  (a) and  $\mu_F$  (b). It is obvious that the results exhibit non-trivial dependence on the choice of those non-physical scales. Still, this dependence is concentrated close to the region of the Sudakov peak and is relatively mild far from it. Since the presence of scale dependence indicates the importance of higher order terms that are unaccounted for, we expect that after we resum large soft-logs the result will be less sensitive to the choice of those scales. That will be discussed in the next section. As a check of our results we have verified that for  $\mu_F$  approaching  $\mu_{0F}$ , the distribution gets closer to the fixed-order, unevolved one shown in Fig. 3-4.

### 3.4 NLL Threshold Resummation

The  $\overline{\text{MS}}$  coefficient function (3.21) and the initial condition of the perturbative fragmentation function (2.59) contain terms behaving like  $1/(1 - x_b)_+$  or  $[\ln(1 - x_b)/(1 - x_b)]_+$ , which become arbitrarily large when  $x_b$  approaches one. This is equivalent to contributions proportional to  $\ln N$  and  $\ln^2 N$  in moment space, as can be seen by writing the  $\overline{\text{MS}}$  coefficient function in the large- $N$  limit <sup>2</sup>:

$$\begin{aligned}\hat{\Gamma}_N(m_t, m_W, \mu_F) &= 1 + \frac{\alpha_S C_F}{2\pi} \left\{ 2 \ln^2 N + \left[ 4\gamma_E + 2 - 4 \ln(1 - w) - 2 \ln \frac{m_t^2}{\mu_F^2} \right] \ln N \right. \\ &\quad \left. + K(m_t, m_W, \mu_F) + \mathcal{O}\left(\frac{1}{N}\right) \right\}\end{aligned}\quad (3.24)$$

In Eq.(3.24) we have introduced the function  $K(m_t, m_W, \mu_F)$ , which contains terms which are constant with respect to  $N$ ; more details for the extraction of the terms which  $\sim \text{const}$  when  $N \rightarrow \infty$  can be found in the appendix. The function  $K$  reads:

$$\begin{aligned}K(m_t, m_W, \mu_F) &= \left( \frac{3}{2} - 2\gamma_E \right) \ln \frac{m_t^2}{\mu_F^2} + 2\gamma_E^2 + 2\gamma_E [1 - 2 \ln(1 - w)] \\ &\quad + 2 \ln w \ln(1 - w) - 2 \frac{1 - w}{1 + 2w} \ln(1 - w) - \frac{2w}{1 - w} \ln w \\ &\quad + 4\text{Li}_2(1 - w) - 6 - \frac{\pi^2}{3}.\end{aligned}\quad (3.25)$$

The  $x_b \rightarrow 1$  ( $N \rightarrow \infty$ ) limit corresponds to soft-gluon radiation in top decay. These soft logarithms need to be resummed to all orders in  $\alpha_S$  [53], [54] to improve our prediction.

We can perform the soft-gluon (threshold) resummation for the coefficient function following the general procedure described in Section (1.4.3). We treat the *b*-quark as exactly massless and therefore the result is collinearly divergent.

---

<sup>2</sup>Following [62], we note that, by defining  $n = N \exp(\gamma_E)$ , we could rewrite this expression in terms of  $\ln(n)$  rather than  $\ln N$ , with no  $\gamma_E$  terms explicitly appearing.

That divergence is subtracted in the  $\overline{\text{MS}}$  scheme. The eikonal current reads:

$$|J(p_t, p_b, p_g)|^2 = \left| \frac{m_t^2}{(p_t \cdot p_g)^2} - 2 \frac{(p_t \cdot p_b)}{(p_t \cdot p_g)(p_b \cdot p_g)} \right|. \quad (3.26)$$

We express the  $\mathcal{O}(\alpha_S)$  width in the soft approximation as an integral over the variables  $q^2 = (p_b + p_g)^2 x_g$  and  $z = 1 - x_g$ , with  $0 \leq q^2 \leq m_t^2(1-w)^2(1-z)^2$  and  $0 \leq z \leq 1$ . The limits  $z \rightarrow 1$  and  $q^2 \rightarrow 0$  correspond to soft and collinear emission respectively. In the soft approximation,  $z \simeq x_b$ ;  $x_g$  is the gluon energy fraction that is defined similarly to  $x_b$  (3.5). In the  $m_b = 0$  case which we consider here:

$$x_b = \frac{1}{1-w} \frac{2p_b \cdot p_t}{m_t^2}, \quad x_g = \frac{1}{1-w} \frac{2p_g \cdot p_t}{m_t^2}, \quad 0 \leq x_{b,g} \leq 1. \quad (3.27)$$

We point out that our definition of the integration variable  $q^2$  is analogous to the quantity  $(1-z)k^2$  to which the authors of Ref. [53] set the scale for  $\alpha_S$  for soft-gluon resummation in Drell–Yan and Deep-Inelastic-Scattering processes. For small-angle radiation,  $q^2 \simeq q_T^2$ , the gluon transverse momentum with respect to the  $b$ -quark line. The variable  $z$  is analogous to  $z = 1 - E_g/E_q$  of Ref. [53].

Performing the operations discussed in Section (1.4.3) we obtain:

$$\begin{aligned} \hat{\Gamma}_N(m_t, m_W, \mu_F) &= \frac{C_F}{\pi} \int_0^1 dz \frac{z^{N-1} - 1}{1-z} \left[ \int_{\mu_F^2}^{m_t^2(1-w)^2(1-z)^2} \frac{dq^2}{q^2} \alpha_S \right. \\ &\quad \left. - \frac{1}{m_t^2(1-w)^2(1-z)^2} \int_0^{m_t^2(1-w)^2(1-z)^2} dq^2 \alpha_S \right]. \end{aligned} \quad (3.28)$$

We note that it corresponds to Eq.(2.74) with  $a = 2$  and  $Q^2 = m_t^2(1-w)^2$ . The origin of the second term in (3.28) is in the collinearly non-enhanced term in the squared eikonal current (3.26).

In order to include all NLL contributions we only need to perform the replacement (2.76) and use the property (2.75). No additional contribution from collinear radiation from the final state is presented here because of the character of the cross-section that our coefficient function represents; the final  $b$ -quark is

“observed” and has its virtuality fixed by the on-shell condition  $p_b^2 = 0$ . Exponentiating the result we obtain the following form-factor that describes the soft limit of the corresponding production rate:

$$\begin{aligned} \ln \Delta_N &= \int_0^1 dz \frac{z^{N-1} - 1}{1-z} \left\{ \int_{\mu_F^2}^{m_t^2(1-w)^2(1-z)^2} \frac{dq^2}{q^2} A \left[ \alpha_S(q^2) \right] \right. \\ &\quad \left. + S \left[ \alpha_S \left( m_t^2(1-w)^2(1-z)^2 \right) \right] \right\}. \end{aligned} \quad (3.29)$$

The function  $S(\alpha_S)$  can be expanded according to:

$$S(\alpha_S) = \sum_{n=1}^{\infty} \left( \frac{\alpha_S}{\pi} \right)^n S^{(n)}. \quad (3.30)$$

At NLL level, we are just interested in the first term of the above expansion:

$$S^{(1)} = -C_F. \quad (3.31)$$

The integral in Eq.(3.29) can be performed, up to NLL accuracy, according to the methods described in Section (1.4.3). This leads to the following result:

$$\Delta_N(m_t, m_W, \alpha_S(\mu^2), \mu, \mu_F) = \exp \left[ \ln N g^{(1)}(\lambda) + g^{(2)}(\lambda, \mu, \mu_F) \right], \quad (3.32)$$

with  $\lambda$  defined in (2.81) and the functions  $g^{(1)}$  and  $g^{(2)}$  given by:

$$\begin{aligned} g^{(1)}(\lambda) &= \frac{A^{(1)}}{2\pi b_0 \lambda} [2\lambda + (1-2\lambda) \ln(1-2\lambda)], \\ g^{(2)}(\lambda, \mu, \mu_F) &= \frac{A^{(1)}}{2\pi b_0} \left[ \ln \frac{m_t^2(1-w)^2}{\mu_F^2} - 2\gamma_E \right] \ln(1-2\lambda) \\ &\quad + \frac{A^{(1)} b_1}{4\pi b_0^3} [4\lambda + 2\ln(1-2\lambda) + \ln^2(1-2\lambda)] \\ &\quad - \frac{1}{2\pi b_0} [2\lambda + \ln(1-2\lambda)] \left( \frac{A^{(2)}}{\pi b_0} + A^{(1)} \ln \frac{\mu^2}{\mu_F^2} \right) \\ &\quad + \frac{S^{(1)}}{2\pi b_0} \ln(1-2\lambda). \end{aligned} \quad (3.34)$$

In Eq.(3.32) the term  $\ln N g^{(1)}(\lambda)$  accounts for the resummation of leading logarithms  $\alpha_S^n \ln^{n+1} N$  in the Sudakov exponent, while the function  $g^{(2)}(\lambda, \mu, \mu_F)$  resums NLL terms  $\alpha_S^n \ln^n N$ .

Furthermore, we follow Ref. [43] and in our final Sudakov-resummed coefficient function we also include the constant terms of Eq.(3.25):

$$\begin{aligned}\hat{\Gamma}_N^S(m_t, m_W, \alpha_S(\mu^2), \mu, \mu_F) &= \left[ 1 + \frac{\alpha_S(\mu^2) C_F}{2\pi} K(m_t, m_W, \mu_F) \right] \\ &\times \exp \left[ \ln N g^{(1)}(\lambda) + g^{(2)}(\lambda, \mu, \mu_F) \right].\end{aligned}\quad (3.35)$$

One can check that the  $\mathcal{O}(\alpha_S)$  expansion of Eq.(3.35) yields Eq.(3.24) as it must for consistency. Next we match the resummed coefficient function to the exact first-order result, so that also  $1/N$  suppressed terms, which are important in the region  $x_b < 1$ , are taken into account. We adopt the same matching prescription as in [43]: we add the resummed result to the exact coefficient function and, in order to avoid double counting, we subtract what they have in common, i.e. the up-to- $\mathcal{O}(\alpha_S)$  terms in the expansion of Eq.(3.35). Our final result for the resummed coefficient function reads:

$$\begin{aligned}\hat{\Gamma}_N^{\text{res}}(m_t, m_W, \alpha_S(\mu^2), \mu, \mu_F) &= \hat{\Gamma}_N^S(m_t, m_W, \alpha_S(\mu^2), \mu, \mu_F) \\ &- \left[ \hat{\Gamma}_N^S(m_t, m_W, \alpha_S(\mu^2), \mu, \mu_F) \right]_{\alpha_S} \\ &+ \left[ \hat{\Gamma}_N(m_t, m_W, \alpha_S(\mu^2), \mu, \mu_F) \right]_{\alpha_S},\end{aligned}\quad (3.36)$$

where  $[\hat{\Gamma}_N^S]_{\alpha_S}$  and  $[\hat{\Gamma}_N]_{\alpha_S}$  are respectively the expansion of Eq.(3.35) up to  $\mathcal{O}(\alpha_S)$  and the full fixed-order top-decay coefficient function at  $\mathcal{O}(\alpha_S)$ , presented in the appendix.

We would like to compare our resummed expression with other similar results obtained in heavy quark decay processes [80, 81, 82, 62]. Besides the obvious replacement of a bottom quark with a top in the initial state, our work presents other essential differences. We have resummed large collinear logarithms  $\alpha_S \ln(m_t^2/m_b^2)$ , while Refs. [80, 81, 82, 62] just address the decay of heavy quarks into massless quarks. Moreover, this work still differs in a critical issue. Those papers are concerned with observing the lepton produced by the  $W$  decay or the photon in the

$b \rightarrow X_s \gamma$  process, while we wish instead to observe the outgoing  $b$  quark. This is immediately clear from the choice of the  $z$  variable whose  $z \rightarrow 1$  endpoint leads to the Sudakov logarithms. In our case it is the normalized energy fraction of the outgoing bottom quark; in [80, 81, 82, 62] it is instead related to the energy of either the lepton or the radiated photon.

The most evident effect of this different perspective is that an additional scale, namely the invariant mass of the recoiling hadronic jet, enters the results [80, 81, 82, 62], but as we noted above, is absent in our case. An additional function (called  $\gamma(\alpha_S)$  in [80, 81],  $C(\alpha_S)$  in [82],  $B(\alpha_S)$  in [62]) appears in those papers. The argument of  $\alpha_S$  in this function is related to the invariant mass of the unobserved final state jet constituted by the outgoing quark and the gluon(s). It is worth noting that an identical function, called  $B[\alpha_S(Q^2(1-z))]$ , also appears in the  $e^+e^-$  [43] and DIS [53] massless coefficient functions, where it is again associated with the invariant mass of the unobserved jet. We also observe that to order  $\alpha_s$  the coefficient  $S^{(1)}$  coincides with the corresponding  $H^{(1)}$  of the function  $H[\alpha_S(m_b^2(1-z)^2)]$  (see Eq.(2.83)), which resums soft terms in the initial condition of the perturbative fragmentation function. It will be very interesting to compare the functions  $S(\alpha_S)$  and  $H(\alpha_S)$  at higher orders as well.

One final comment we wish to make is that, as expected, in our final result, Eq.(3.22), which accounts for NLL soft resummation in both the coefficient function and the initial condition of the perturbative fragmentation function,  $\alpha_S^n \ln^{n+1} N$  terms do not appear, since they are due to soft *and* collinear radiation. Both the quarks being heavy, only the former leads to a logarithmic enhancement. Double logarithms are generated by a mismatch in the lower and upper  $q^2$  integration limits over the  $A[\alpha_S(q^2)]$  function in the exponent of the resummation expression. In our case both of them have the same functional dependence with respect to  $z$ , i.e.  $(1-z)^2$  in Eq.(3.29) and Eq.(2.83) (corresponding to  $a = 2$  in

(2.74)). The cancellation of the  $\alpha_S^n \ln^{n+1} N$  term can be explicitly seen at order  $\alpha_S$  by comparing the large- $N$  limit for the coefficient function, Eq. (3.24), and the initial condition (Eq.(A.27)): the  $\ln^2 N$  terms have identical coefficients and opposite signs.

As follows from Eq.(3.22), to obtain the resummed differential distribution in  $x_b$ -space, one needs to perform the inverse Mellin transformation (2.65). As we previously emphasized, we perform that inversion numerically, using the so-called Minimal Prescription [63]: the integration contour in the complex  $N$  plane crosses the real line at a value  $C_{MP}$  such that  $2 < C_{MP} < N_L$ . That way all singularities of the integrand are to the left of the contour with the exception of the Landau pole  $N_L = \exp(1/(2\alpha_S(\mu)b_0))$ . The origin of  $N_L$  is in the Landau pole associated with the integration over the running strong coupling in the Sudakov exponent (3.29), when combined with the relations (2.82), (3.32) and (2.81).

Next we present the results for the  $b$ -quark energy distribution in top decay including the soft-gluon resummation in the initial condition of the perturbative fragmentation function and the coefficient function. The rest of the settings are the same as the ones we discussed in the end of the previous section.

In Fig. 3-6 we present the  $x_b$  distribution according to the approach of perturbative fragmentation, with and without NLL soft-gluon resummation. For the scales we have set  $\mu_F = \mu = m_t$  and  $\mu_0 = \mu_{0F} = m_b$ . We note that the two distributions agree for  $x_b \lesssim 0.8$ , while for larger  $x_b$  values the resummation of large terms  $x_b \rightarrow 1$  smoothes out the distribution, which exhibits the Sudakov peak. Both distributions become negative for  $x_b \rightarrow 0$  and  $x_b \rightarrow 1$ . The negative behavior at small  $x_b$  can be related to the presence of unresummed  $\alpha_S \ln x_b$  terms in the coefficient function. At large  $x_b$ , we approach instead the non-perturbative region, and resumming leading and next-to-leading logarithms is still not sufficient to correctly describe the spectrum for  $x_b$  close to 1. In fact, the range of reliability of the

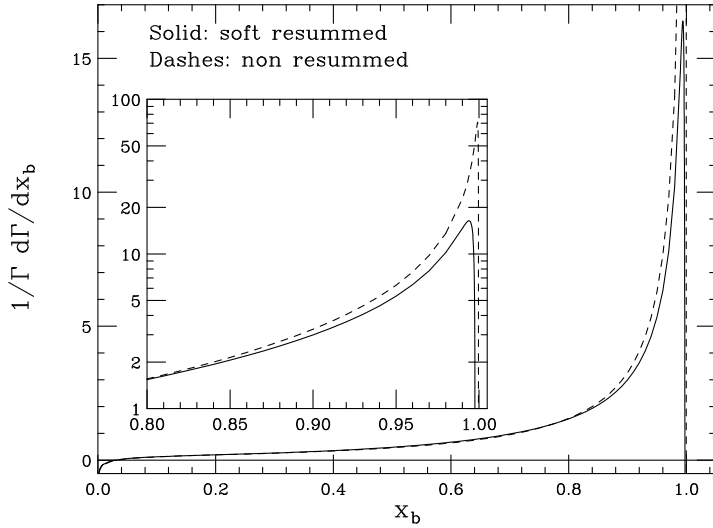


Figure 3-6:  $b$ -quark energy distribution in top decay according to the perturbative fragmentation approach, with (solid line) and without (dashes) NLL soft-gluon resummation. In the inset figure, we show the same curves on a logarithmic scale, for  $x_b > 0.8$ . We have set  $\mu_F = \mu = m_t$  and  $\mu_{0F} = \mu_0 = m_b$ .

perturbative calculation has been estimated to be  $x_b \lesssim 1 - \Lambda/m_b \simeq 0.95$  [43]. It is interesting to investigate the dependence of phenomenological distributions on the renormalization and factorization scales which enter the coefficient function ( $\mu$  and  $\mu_F$ ) and the initial condition of the perturbative fragmentation function ( $\mu_0$  and  $\mu_{0F}$ ). In particular, it is worth comparing the  $b$ -energy spectra with and without soft resummation. For the scales  $\mu$  and  $\mu_F$  we consider the values  $m_t/2$ ,  $m_t$  and  $2m_t$ ; for  $\mu_{0F}$  and  $\mu_0$  the choices are  $m_b/2$ ,  $m_b$  and  $2m_b$ . Figs. 3-7 and 3-8 show the dependence of the  $x_b$  spectrum on the factorization scales  $\mu_F$  and  $\mu_{0F}$ ; the dependence on the renormalization scales  $\mu$  and  $\mu_0$  is exhibited in Figs. 3-9 and 3-10.

We note that all distributions which include soft-gluon resummation exhibit a reduced dependence on the factorization and renormalization scales.

Fig. 3-7 shows that curves obtained using different values of  $\mu_F$  are almost

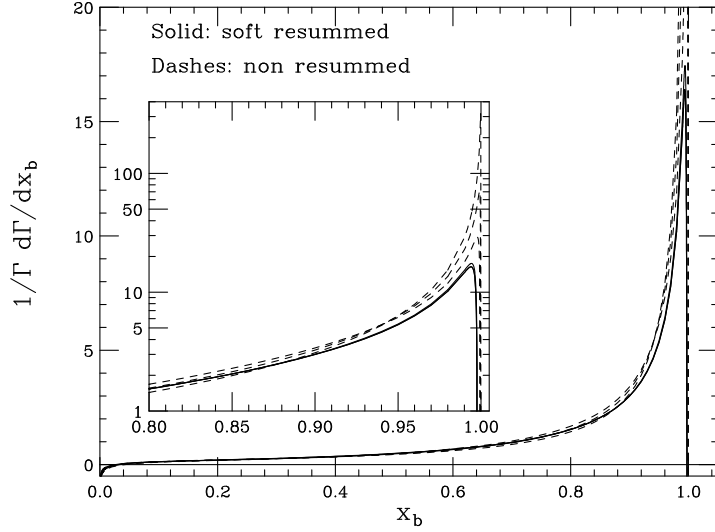


Figure 3-7:  $b$ -quark energy spectrum for different values of the factorization scale  $\mu_F$ , with (solid) and without (dashes) NLL soft-gluon resummation. The other scales are fixed at  $\mu = m_t$ ,  $\mu_0 = \mu_{0F} = m_b$ . As in Fig. 1, in the inset figure, we present the same plots for large values of  $x_b$ , on a logarithmic scale.

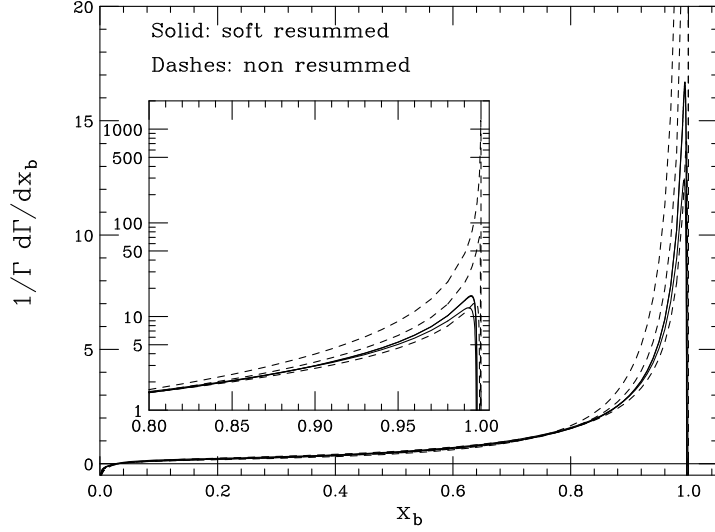


Figure 3-8: As in Fig. 3-7, but for different values of  $\mu_{0F}$ . The other scales are fixed at  $\mu = \mu_F = m_t$ ,  $\mu_0 = m_b$ .

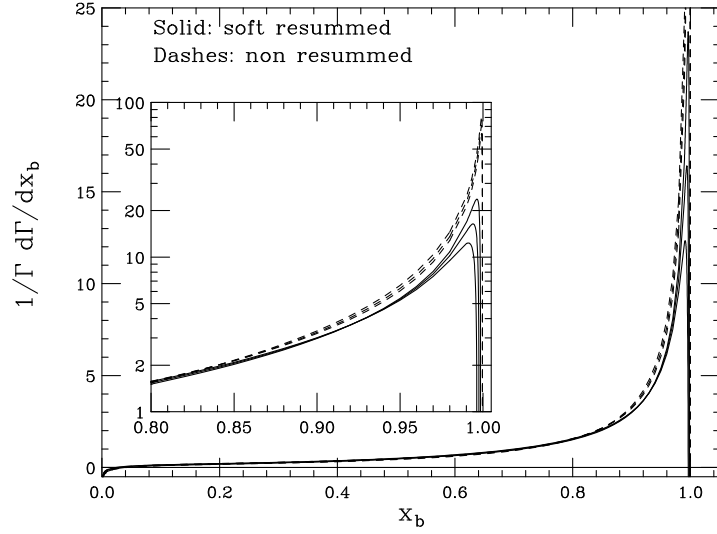


Figure 3-9: As in Fig. 3-7, but for different values of the renormalization scale  $\mu$ . The other scales are fixed at  $\mu_F = m_t$ ,  $\mu_0 = \mu_{0F} = m_b$ .

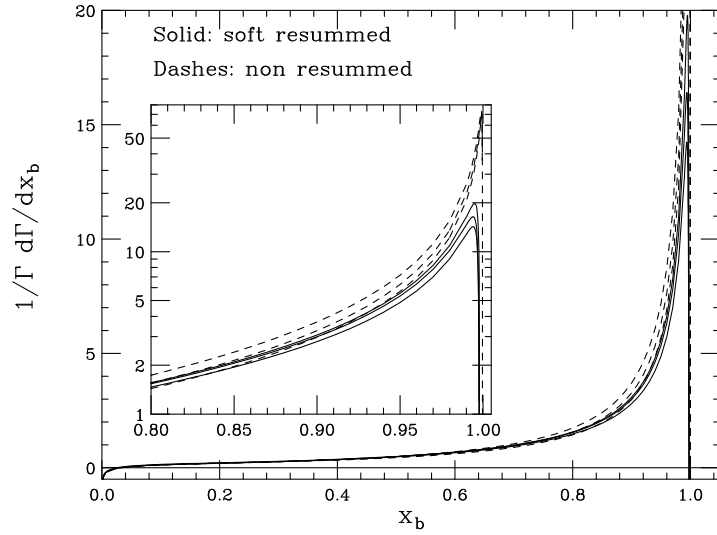


Figure 3-10: As in Fig. 3-7, but for different values of the renormalization scale  $\mu_0$ . The other scales are fixed at  $\mu = \mu_F = m_t$ ,  $\mu_{0F} = m_b$ .

indistinguishable once soft resummation is included; the unresummed plots exhibit a stronger effect of the chosen value for  $\mu_F$ . A similar result also holds for the scale  $\mu_{0F}$ : the dependence of the plots on its actual value for  $x_b > 0.8$  is small if soft logarithms are resummed and quite strong if the prediction is unresummed (Fig. 3-8).

The choice of the value for the renormalization scale  $\mu$  appearing in Eq. (3.24) affects only the neighborhood of the Sudakov peak of the resummed predictions, at  $x_b$ -values very close to one (Fig. 3-9), where, as we have pointed out, our perturbative approach is anyway unreliable. The effect of the choice of the renormalization scale  $\mu_0$  on the soft-resummed spectra is slightly larger than the effect of  $\mu$  and visible at  $x_b < 1$  as well (Fig. 3-10). As for the non-soft-resummed predictions, although all dashed curves in Figs. 3-9 and 3-10 seem to converge to the same point for  $x_b \rightarrow 1$ , the overall dependence on  $\mu$  and  $\mu_0$  for  $x_b < 1$  is stronger than for the resummed predictions.

As a whole, one can say that the implementation of NLL soft-gluon resummation, along with the NLL DGLAP evolution for the perturbative fragmentation function, yields a remarkable improvement of our phenomenological results, since the reduced dependence on the choice of factorization and renormalization scales in the region where the perturbative approach is reliable corresponds to a reduction of the theoretical uncertainty.

### 3.5 Energy Spectrum of *b*-flavored Hadrons in Top Decay

In this section we consider the inclusion of a non-perturbative component in addition to the perturbative result, so as to make predictions for observable *b*-flavored

hadrons (like *B* mesons) in top decay. At the same time, we also account for the inclusion of NLL soft and collinear resummation.

We write the normalized rate for the production of *b*-hadrons *B* as in Eq.(2.64), i.e. as a convolution of the rate for the production of *b* quarks in top decay, given by Eq.(3.22) and a non perturbative fragmentation function  $D^{np}(x)$ :

$$\frac{1}{\Gamma} \frac{d\Gamma^B}{dx_B}(x_B, m_t, m_W, m_b) = \frac{1}{\Gamma} \int_{x_B}^1 \frac{dz}{z} \frac{d\Gamma^b}{dz}(z, m_t, m_W, m_b) D^{np}\left(\frac{x_B}{z}\right), \quad (3.37)$$

where  $x_B$  is the *B* normalized energy fraction:

$$x_B = \frac{1}{1-w} \frac{2p_B \cdot p_t}{m_t^2}, \quad (3.38)$$

$p_B$  being the *B* four-momentum. Since  $D^{np}(x)$  contains non-perturbative information, it cannot - for the time being - be calculated from first principles in QCD, but can only be extracted from data.

We shall assume a universality property for such a function, i.e. that it does not depend on the process but only on the non-perturbative transition it describes, and extract it from fits to *B*-production data collected at LEP in  $e^+e^-$  collisions. In particular, we can choose different functional forms for  $D^{np}(x)$ , and tune these hadronization models to the available data. We shall consider three models: a power law with two tunable parameters:

$$D^{np}(x; \alpha, \beta) = \frac{1}{B(\beta + 1, \alpha + 1)} (1-x)^\alpha x^\beta, \quad (3.39)$$

the model of Kartvelishvili et al. [83]:

$$D^{np}(x; \delta) = (1+\delta)(2+\delta)(1-x)x^\delta, \quad (3.40)$$

and the Peterson et al. model [84]:

$$D^{np}(x; \epsilon) = \frac{A}{x[1 - 1/x - \epsilon/(1-x)]^2}. \quad (3.41)$$

In Eq.(3.39),  $B(x, y)$  is the Euler Beta function; in (3.41)  $A$  is a normalization constant for which an explicit expression can be found in [45].

In order for our extraction procedure to be self-consistent, we employ the same underlying perturbative description in both the  $e^+e^- \rightarrow b\bar{b}$  process (where the non-perturbative contribution is fitted) and  $t \rightarrow bW$  (where it is used). This will be ensured by using in both cases NLO,  $\overline{\text{MS}}$  coefficient functions, along with a fully NLL soft-gluon resummed description, with the large collinear logarithms resummed to NLL accuracy by DGLAP evolution. For the coefficient functions in  $e^+e^-$  annihilation we shall refer to [85].

Fits to data points can be performed either in  $x_B$ -space, or, as recently advocated [47], in the conjugated moment space. When fitting in  $x_B$  space we discard data points close to  $x_B = 0$  and  $x_B = 1$  and consider ALEPH [86] data in the range  $0.18 \lesssim x_B \lesssim 0.94$ . Good-quality data are also available from SLD [87] on  $b$ -flavored mesons and baryons. Recently, the OPAL [88] and DELPHI [89] Collaborations also published new results, which are fully compatible with the ones from ALEPH. The results of our fits are shown in Table 3.1.

The models in Eqs. (3.39) and (3.40) yield very good fits to the data, while the model (3.41) is marginally consistent. We have also fitted the SLD data and found qualitatively similar results. However, the values for the parameters which best fit the SLD data are different from the ones obtained for ALEPH and quoted in Table 3.1. Using the results in Table 3.1 we can give predictions for the spectrum of  $b$ -flavored hadrons in top decay. To account for the errors on the best-fit parameters, we shall plot bands which correspond to predictions at one-standard-deviation confidence level. In Fig. 3-11 we show our predictions for the  $x_B$  distribution using the three models fitted to the ALEPH data. At one-standard-deviation confidence level, the three predictions are different, with the Peterson model yielding a distribution which lies quite far from the other two

$\alpha$	$0.51 \pm 0.15$
$\beta$	$13.35 \pm 1.46$
$\chi^2(\alpha, \beta)/\text{dof}$	$2.56/14$
$\delta$	$17.76 \pm 0.62$
$\chi^2(\delta)/\text{dof}$	$10.54/15$
$\epsilon$	$(1.77 \pm 0.16) \times 10^{-3}$
$\chi^2(\epsilon)/\text{dof}$	$29.83/15$

Table 3.1: Results of fits to  $e^+e^- \rightarrow b\bar{b}$  ALEPH data, using matched coefficient function and initial condition, with NLL DGLAP evolution and NLL soft-gluon resummation. We set  $\Lambda^{(5)} = 200$  MeV,  $\mu_{0F} = \mu_0 = m_b = 5$  GeV and  $\mu_F = \mu = \sqrt{s} = 91.2$  GeV.  $\alpha$  and  $\beta$  are the parameters in the power law (3.39),  $\delta$  refers to (3.40),  $\epsilon$  to (3.41). The fits have been performed neglecting the correlations between the data points.

and peaked at larger  $x_B$ -values. Within two standard deviations, the predictions obtained using the models (3.39) and (3.40) are nonetheless in agreement.

We would like to emphasize that the differences between the various models mainly originate from the varying quality of the fits to  $e^+e^-$  data where, as the  $\chi^2$  values in Table 3.1 seem to suggest, a given model is sometimes not really able to describe the data properly, due to its too restrictive functional form.

An alternative, and probably better, way of determining and including non-perturbative information makes use of moment space perturbative predictions and data [47]. The full hadron-level result can be written in  $N$ -space as the product of a perturbative and a non-perturbative contribution,  $\Gamma_N^B = \Gamma_N^b D_N^{np}$ . For each value of  $N$  one can then extract the corresponding  $D_N^{np}$  value from  $e^+e^-$  data, with no reference whatsoever to a specific hadronization model, and use it to predict the same moment in top decay. The DELPHI Collaboration [89] has

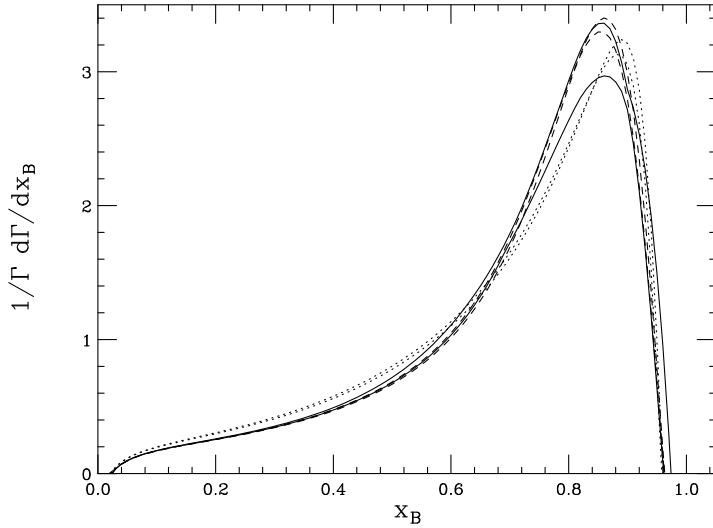


Figure 3-11:  $x_B$  spectrum in top decay, with the hadronization modelled according to a power law (solid lines), the Kartvelishvili et al. (dashes) and the Peterson (dots) model, with the relevant parameters fitted to the ALEPH data. The plotted curves are the edges of bands at one-standard-deviation confidence level. NLL soft-gluon resummation is included. We set  $\mu_F = \mu = m_t$  and  $\mu_{0F} = \mu_0 = m_b$ .

recently published preliminary results for the moments of  $B$ -meson fragmentation in  $e^+e^-$  collisions up to  $N = 5$ . From these data, and using the moments of the  $e^+e^-$  perturbative contributions [43], one can extract  $D_N^{np}$ . The corresponding  $\Gamma_N^B$  values can then be calculated making use of the results for  $\Gamma_N^b$  obtained in [65] and given by Eqns.(3.22) and (3.36). Calling  $\sigma_N^B$  and  $\sigma_N^b$  the moments for the production rate of  $B$  mesons (measured) and  $b$  quarks (calculated in perturbative QCD) in  $e^+e^-$  annihilation, we have  $\sigma_N^B = \sigma_N^b D_N^{np}$  and hence

$$\Gamma_N^B = \Gamma_N^b D_N^{np} = \Gamma_N^b \frac{\sigma_N^B}{\sigma_N^b} . \quad (3.42)$$

Table 3.2 shows a practical implementation of this procedure. Predictions for the moments  $\Gamma_N^B$  of  $B$ -meson spectra in top decay are given, making use of the DELPHI experimental data. Two sets of perturbative results ([A] and [B]) are

	$\langle x \rangle$	$\langle x^2 \rangle$	$\langle x^3 \rangle$	$\langle x^4 \rangle$
$e^+e^-$ data $\sigma_N^B$	$0.7153 \pm 0.0052$	$0.5401 \pm 0.0064$	$0.4236 \pm 0.0065$	$0.3406 \pm 0.0064$
$e^+e^-$ NLL $\sigma_N^b$ [A]	0.7666	0.6239	0.5246	0.4502
$e^+e^-$ NLL $\sigma_N^b$ [B]	0.7801	0.6436	0.5479	0.4755
$D_N^{np}$ [A]	0.9331	0.8657	0.8075	0.7566
$D_N^{np}$ [B]	0.9169	0.8392	0.7731	0.7163
$t$ -decay NLL $\Gamma_N^b$ [A]	0.7750	0.6417	0.5498	0.4807
$t$ -decay NLL $\Gamma_N^b$ [B]	0.7884	0.6617	0.5737	0.5072
$t$ -decay $\Gamma_N^B$ [A]	0.7231	0.5555	0.4440	0.3637
$t$ -decay $\Gamma_N^B$ [B]	0.7228	0.5553	0.4435	0.3633

Table 3.2: Experimental data for the moments  $\sigma_N^B$  from DELPHI [89], the resummed  $e^+e^-$  perturbative calculations for  $\sigma_N^b$  [43], the extracted non-perturbative contribution  $D_N^{np}$ . Using the perturbative results  $\Gamma_N^b$ , a prediction for the physical observable moments  $\Gamma_N^B$  is given. Set [A]:  $\Lambda^{(5)} = 0.226$  GeV and  $m_b = 4.75$  GeV, set [B]:  $\Lambda^{(5)} = 0.2$  GeV and  $m_b = 5$  GeV. The experimental error should of course be propagated to the final prediction.

shown, the first using  $\Lambda^{(5)} = 0.226$  GeV and  $m_b = 4.75$  GeV, the second one using our default parameters introduced in Section (3.3). As expected, the perturbative calculations and the corresponding non-perturbative components differ, but the final predictions for the physical results  $\Gamma_N^B$  are to a large extent identical.

# Chapter 4

## Charged–Current Deep Inelastic Scattering

In this Chapter we present our result for the threshold resummation of the coefficient function for heavy quark production in Charged-Current Deep Inelastic Scattering (CC DIS) at low transferred momentum  $Q$  (i.e. when  $Q$  is of the order of the mass of the heavy quark) and with next-to-leading logarithmic (NLL) accuracy. We then apply our result to the case of charm-quark production in CC DIS processes with the masses of the charm quark and the target taken fully into account. The presentation in this Chapter is based on the paper [90].

### 4.1 CC DIS: Notation and Overview

DIS is a process of scattering of a lepton and a hadron (usually nucleon) that produces another lepton and final hadronic state  $X$ :

$$\ell_{in}(p_{\ell_{in}}) + N(P) \rightarrow \ell_{out}(p_{\ell_{out}}) + X. \quad (4.1)$$

In general, the leptons  $\ell_{in}$  and  $\ell_{out}$  can be of the same type (neutral-current

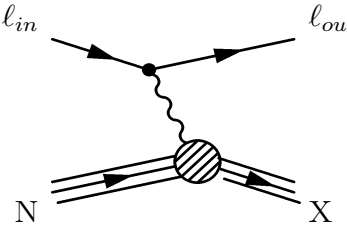


Figure 4-1: Deep Inelastic Scattering.

scattering) or be different (charged current scattering). To lowest order in the electroweak coupling, the DIS interaction has the structure shown in Fig.(4-1). It represents the interaction of a leptonic current  $j^\mu$  with a hadronic current  $J^\mu$  through the exchange of a virtual vector boson. The vector boson is a combination of a virtual photon  $\gamma$  and  $Z^0$  in the NC case and a virtual charged boson  $W^\pm$  in the CC case.

Let us introduce the following notation: as usual, we will denote by  $q$  the momentum of the transferred boson (of any type). The momentum is space-like, and  $Q^2 \equiv -q^2 > 0$ . The momentum of the incoming nucleon is  $P$  with  $P^2 = M^2$ ,  $M$  being the mass of the nucleon. We will consider two types of targets: one, where  $N$  is a proton and the other an isoscalar target, where  $N$  is a “half-sum” of a proton and a neutron. In the latter case, the partonic content of  $N$  is determined by assuming isospin invariance (2.3). We will not distinguish between the masses of the two target types. Numerically, in our applications we set  $M = 1$  GeV. A very important parameter is the Bjorken variable:

$$x = \frac{Q^2}{2P \cdot q}, \quad (4.2)$$

which is directly measured in the experiment. That variable has the nice property that in the parton model it coincides with the momentum fraction carried by the initial state parton, as was discussed in Section (2.1.2). Another common variable

is:

$$\nu = \frac{P \cdot q}{M}, \quad (4.3)$$

as well as the inelasticity  $y$ :

$$y = \frac{P \cdot q}{P \cdot p_{\ell_{in}}}. \quad (4.4)$$

From the discussion following Eq.(4.1) it becomes clear that the cross section for DIS process factorizes into leptonic and hadronic parts [91]:

$$d\sigma \sim L^{\mu\nu} W_{\mu\nu}, \quad (4.5)$$

where:

$$L_{\mu\nu} = \frac{1}{Q^2} \overline{\sum} \langle \ell_{in} | j_\nu^\dagger | \ell_{out} \rangle \langle \ell_{out} | j_\mu | \ell_{in} \rangle, \quad (4.6)$$

is a tensor containing the leptonic current and

$$W_{\mu\nu} = \frac{1}{4\pi} \overline{\sum} (2\pi)^4 \delta^4(P + q - P_X) \langle P | J_\mu | P_X \rangle \langle P_X | J_\nu^\dagger | P \rangle, \quad (4.7)$$

is the tensor containing all the hadronic contributions.

It is obvious that unlike  $L_{\mu\nu}$ , its hadronic counterpart  $W_{\mu\nu}$  cannot be simply calculated, since the latter contains non-perturbative information incorporated in the hadronic states present in Eq.(4.7). It is customary to parameterize the hadronic tensor in the following way:

$$W_{\mu\nu} = -g_{\mu\nu} W_1 + \frac{P_\mu P_\nu}{M^2} W_2 - i \frac{\epsilon_{\mu\nu\sigma\rho} P^\sigma q^\rho}{2M^2} W_3 + \dots, \quad (4.8)$$

where the functions  $W_{1,2,3}$  are scalar form-factors, and “ $\dots$ ” stands for other contributions that do not contribute in the limit when the lepton masses<sup>1</sup> are neglected. It is however more common to work in terms of the re-scaled form-factors:

$$\underline{F_1} = W_1$$

---

<sup>1</sup>For more details on the treatment of lepton masses see [91] and especially [92].

$$\begin{aligned} F_2 &= \frac{\nu}{M} W_2 \\ F_3 &= \frac{\nu}{M} W_3. \end{aligned} \quad (4.9)$$

One can then write the cross-section in Eq.(4.5) for the case of neutrino-nucleon scattering (which is what we need for our applications) in the following form:

$$\frac{d^2\sigma^{\nu(\bar{\nu})}}{dxdy} = \frac{G_F^2 M E_\nu}{\pi(1+Q^2/M_W^2)^2} \left[ y^2 x F_1 + \left( 1 - \left( 1 + \frac{Mx}{2E_\nu} \right) y \right) F_2 \pm y \left( 1 - \frac{y}{2} \right) x F_3 \right], \quad (4.10)$$

where  $E_\nu$  is the neutrino energy in the nucleon rest frame and  $y$  is given by (4.4). Similar results exist for the NC case. The functions  $F_{1,2,3}$  are known as structure functions. The knowledge of these is equivalent to the knowledge of the DIS cross-section. Since the structure functions are observables they are free from ambiguity. In the following we turn our attention to their evaluation.

Following [91], and in accordance with our discussion in Section (2.2) of the factorization theorem, one can write the DIS cross-section as a convolution of a parton distribution and a partonic cross-section:

$$W_{\mu\nu}(q, P) = \sum_a \int \frac{d\xi}{\xi} f_{a/N}(\xi, \mu) w_{\mu\nu}^a(q, p, \alpha_S(\mu)). \quad (4.11)$$

We prefer to work in terms of the tensor  $W_{\mu\nu}$  rather than  $d\sigma$  since the former already contains all the relevant information for the hadronic part of the reaction.

The partonic tensor  $w_{\mu\nu}$  is defined in complete analogy with  $W_{\mu\nu}$  (cf. Eq.(4.7)), but with the hadron target replaced by a partonic one. A parametrization similar to Eq.(4.8) holds for  $w_{\mu\nu}$  as well. One just needs to replace in (4.8) the hadron momentum  $P$  with the momentum  $p$  of the incoming parton  $a$ , and the factors containing  $W_{2,3}$  are normalized with respect to  $Q^2$  instead of  $M^2$ . The dependence of the partonic tensor  $w_{\mu\nu}$  on the convolution parameter  $\xi$  (which is the energy fraction carried by the parton  $a$ ) is through the relation  $p^+ = \xi P^+$  between the

plus light-cone components of the partonic and hadron momenta (see also the discussion following Eq.(2.22)). We will discuss that point in more detail below.

As follows from our general discussion in Section (2.2) and Section (2.4.1), the partonic tensor  $w_{\mu\nu}$  can be calculated in perturbation theory to any order in the strong coupling. As it was explained there, in the case of massless initial-state partons <sup>2</sup> the tensor  $w_{\mu\nu}$  contains a collinear divergence. That divergence must be subtracted (i.e. effectively absorbed into the parton distribution functions), and one usually does that in the  $\overline{\text{MS}}$  scheme. This is also the subtraction scheme that we use in our applications. The partonic tensor  $w_{\mu\nu}$  depends on the parton momentum  $p$  through the partonic analogue  $\hat{x}$  of the Bjorken variable.  $\hat{x}$  is defined by Eq.(4.2) but with the momentum  $P$  replaced by  $p$ .

In fact it is easy to see from the kinematics of the partonic scattering process for production at NLO of quark with mass  $m$

$$q_1(p)W^*(q) \rightarrow q_2(p_2)(+X), \quad (4.12)$$

that the partonic cross-section can be evaluated in terms of the following variable:

$$z = \frac{\hat{x}}{\lambda} = \frac{Q^2 + m^2}{2p \cdot q}, \quad 0 \leq z \leq 1. \quad (4.13)$$

In Eq.(4.13) we have also introduced the following parameter:

$$\lambda = \frac{Q^2}{Q^2 + m^2} \leq 1. \quad (4.14)$$

Although the tensors  $W_{\mu\nu}$  and  $w_{\mu\nu}$  have the same tensor structure, they are not simply proportional to each other because of their dependence on different momenta ( $P$  and  $p$  respectively). Therefore the relation between the invariant hadronic and partonic form-factors  $W_i$  and  $w_i$  depends on the relation between

---

<sup>2</sup>In our discussions we will only consider the case of massless incoming partons. Results for the case  $p^2 > 0$  can be found in [91]; see also [41].

the momenta  $P$  and  $p$ . One can parameterize the momentum  $p$  of the parton  $a$  in the following way [91]:

$$p^\mu = c_P P^\mu + c_q q^\mu, \quad (4.15)$$

where the coefficients  $c_P$  and  $c_q$  read:

$$\begin{aligned} c_P &= \frac{Q^2}{Q^2 + M^2\eta^2} \xi, \\ c_q &= -\frac{M^2\eta}{Q^2 + M^2\eta^2} \xi. \end{aligned} \quad (4.16)$$

In Eq.(4.16)  $\xi$  is the momentum fraction carried by the incoming parton and  $\eta$  is the Nachtmann variable [93], that corrects the Bjorken variable  $x$  for non-zero target mass  $M$ :

$$\frac{1}{\eta} = \frac{1}{2x} + \sqrt{\frac{1}{4x^2} + \frac{M^2}{Q^2}}, \quad \text{or:} \quad \frac{1}{x} = \frac{1}{\eta} - \frac{M^2}{Q^2} \eta. \quad (4.17)$$

It is now obvious that the whole dependence of the partonic cross-section  $w_{\mu\nu}(z)$  on the momentum fraction  $\xi$  (that is also the convolution variable) enters implicitly through the relation (4.15). One can make this dependence explicit by combining (4.15) with the other relations above. After some algebra one can show that:

$$z = \frac{\chi}{\xi}, \quad (4.18)$$

where, as is common in the DIS literature, we have introduced the following parameter:

$$\chi = \frac{\eta}{\lambda}. \quad (4.19)$$

The implication of the relation (4.18) is clear: one can calculate the partonic tensor in perturbation theory as a function of the variable  $z$  (as defined in Eq.(4.13)), and then use the relation (4.18) to show that indeed the product of the two terms in the integrand of Eq.(4.11) is of the general form (2.20). From simple kinematical considerations (i.e. using that  $s_{\text{partonic}} \geq m^2$ ) one can also show that

$\chi \leq \xi \leq 1$ . Clearly, that way the hadronic tensor  $W_{\mu\nu}$  in essence becomes a function of the variable  $\chi$ . In the limit of vanishing quark and target masses, that variable coincides with the usual Bjorken variable  $x$ :  $\chi \rightarrow x$ .

It will be, however, more convenient for us to work in terms of the structure functions because the  $w_{\mu\nu}$  depends on  $\xi$  not only through the arguments of the scalar form-factors  $w_{1,2,3}$ , but also through the partonic momenta defining the tensor structure of  $w_{\mu\nu}$  (cf. Eq.(4.8)). In the following, in order to relate the hadron level structure functions with their parton level counterparts, we follow the notation in [94] and [92]. First one defines the “theoretical” structure functions  $\mathcal{F}_i$  which are related to the  $F_i$ ’s of Eq.(4.9) and (4.10) via the following relations:

$$F_1 = \mathcal{F}_1 \quad (4.20)$$

$$F_2 = \frac{2x}{\lambda\rho^2} \mathcal{F}_2 \quad (4.21)$$

$$F_3 = \frac{2}{\rho} \mathcal{F}_3, \quad (4.22)$$

with:

$$\rho = \sqrt{1 + \left(\frac{2Mx}{Q}\right)^2}. \quad (4.23)$$

The introduction of the structure functions  $\mathcal{F}_i$  is convenient since they can be straightforwardly expressed as a convolution of parton distribution functions and  $\overline{\text{MS}}$  coefficient functions:

$$\begin{aligned} \mathcal{F}_i(x, Q^2) &= \int_x^1 \frac{d\xi}{\xi} \left[ C_i^q \left( \frac{\chi}{\xi}, \mu^2, \mu_F^2, \lambda \right) q_1 \left( \xi, \mu_F^2 \right) \right. \\ &\quad \left. + C_i^g \left( \frac{\chi}{\xi}, \mu^2, \mu_F^2, \lambda \right) g \left( \xi, \mu_F^2 \right) \right], \quad i = 1, 2, 3. \end{aligned} \quad (4.24)$$

In Eq.(4.24), we have explicitly shown the relevant arguments of the structure functions, although it is clear that the dependence on  $x$  comes through the variable  $\chi$  in the following way:

$$x = \frac{\lambda\chi}{1 - M^2\lambda^2\chi^2/Q^2}. \quad (4.25)$$

That relation follows from Eqns.(4.17) and (4.19). Bjorken  $x$  is constrained to be in the range:

$$0 < x \leq \frac{\lambda}{1 - M^2 \lambda^2 / Q^2}. \quad (4.26)$$

As usual, in Eq.(4.24)  $\mu$  and  $\mu_F$  are the renormalization and factorization scales;  $C^q$  and  $C^g$  are correspondingly the coefficient functions for the quark-scattering subprocess

$$q_1(p)W^*(q) \rightarrow q_2(p_2) (g(p_g)), \quad (4.27)$$

and for the gluon-fusion sub-process

$$g(p_g)W^*(q) \rightarrow \bar{q}_1(p)q_2(p_2). \quad (4.28)$$

In Eq.(4.24), by  $q_1(x, \mu_F^2)$  and  $g(x, \mu_F^2)$  we have denoted the parton distribution functions of the initial-state light quark and the gluon. For consistency, one has to use  $\overline{\text{MS}}$  parton distribution functions.

## 4.2 Behavior of the Coefficient Function in the Soft Limit

In our applications, we would like to consider  $\mathcal{O}(\alpha_S)$  corrections to CC DIS. The coefficient functions can be evaluated perturbatively and to  $\mathcal{O}(\alpha_S)$  they read:

$$C_i^q(z, \mu^2, \lambda) = \delta(1 - z) + \frac{\alpha_S(\mu^2)}{2\pi} H_i^q(z, \mu_F^2, \lambda) \quad (4.29)$$

$$C_i^g(z, \mu^2, \mu_F^2, \lambda) = \frac{\alpha_S(\mu^2)}{2\pi} H_i^g(z, \mu_F^2, \lambda). \quad (4.30)$$

The explicit expressions for the functions  $H_{1,2,3}^{q,g}$ , with the collinear divergences subtracted in the  $\overline{\text{MS}}$  factorization scheme, have been obtained in [95] and [94]. For our applications, we use the results for  $H_{1,2,3}^{q,g}$  as reported in [92].

As we are inclusive with respect to the final-state heavy quark  $q_2$  the quark-scattering coefficient functions are free from logarithms  $\ln(m^2/Q^2)$ . However, the functions  $H_i^q$  contain terms which behave like  $\sim 1/(1-z)_+$  or  $[\ln(1-z)/(1-z)]_+$  [94] and are therefore enhanced once the quark energy fraction approaches one. The  $z \rightarrow 1$  limit corresponds to soft-gluon emission. In Mellin moment space, such a behavior corresponds to contributions  $\sim \ln N$  or  $\sim \ln N^2$  in the limit  $N \rightarrow \infty$ ; see the appendix for more details.

The gluon-initiated coefficient functions  $H_i^g$  are not enhanced in the limit  $z \rightarrow 1$ , since the splitting  $g \rightarrow q\bar{q}$  is not soft divergent. Instead, they contain terms  $\sim \ln^k(1-z)$  of collinear origin but such terms are suppressed in Mellin space by an inverse power of  $N$  and are therefore neglected at our NLL level of accuracy. The gluon-fusion coefficients  $H_i^g$  also contain collinear logs  $\ln(m^2/Q^2)$  originating in collinear gluon splitting. The treatment of those terms is related to the choice of the parton distribution. We will return to that point later in this Chapter. To summarize, in the rest of our discussions we will not be concerned with the soft limit of the gluon-initiated sub-process.

We would like to make further comments on the light quark initiated coefficient functions at large  $z$ . Omitting terms that are not enhanced in the soft limit for *any* value of the mass ratio  $m^2/Q^2$ , one has:

$$H_i^q(z \rightarrow 1, \mu_F^2, \lambda) = H^{soft}(z, \mu_F^2, \lambda) \quad (4.31)$$

where:

$$\begin{aligned} H^{soft}(z, \mu_F^2, \lambda) &= 2C_F \left\{ 2 \left( \frac{\ln(1-z)}{1-z} \right)_+ - \left( \frac{\ln(1-\lambda z)}{1-z} \right)_+ \right. \\ &\quad \left. + \frac{1}{4} \left( \frac{1-z}{(1-\lambda z)^2} \right)_+ + \frac{1}{(1-z)_+} \left[ \ln \frac{Q^2 + m^2}{\mu_F^2} - 1 \right] \right\}. \end{aligned} \quad (4.32)$$

One immediately sees that the behavior of the coefficient function (4.32) at large  $z$  strongly depends on the value of the ratio  $m/Q$ . To illustrate that point,

we consider the two extreme regimes: the small- $m/Q$  limit, i.e.  $\lambda \approx 1$ , and the large- $m/Q$  limit, i.e.  $\lambda \ll 1$ .

In the first case, setting  $\lambda = 1$  in (4.32) one recovers the large- $N$  limit of the  $\overline{\text{MS}}$  massless coefficient function reported in [58]:

$$C_N^{soft}|_{\lambda=1} = 1 + \frac{\alpha_S(\mu^2)C_F}{\pi} \left\{ \frac{1}{2} \ln^2 N + \left[ \gamma_E + \frac{3}{4} - \ln \frac{Q^2}{\mu_F^2} \right] \ln N \right\}, \quad (4.33)$$

where  $\gamma_E = 0.577\dots$  is the Euler constant.

In the second case, for  $\lambda \rightarrow 0$  and  $z \rightarrow 1$ , one has  $\lambda z = \lambda$  in (4.32). As a result, the term  $\sim [(1-z)/(1-\lambda z)^2]_+$  is regular in the soft limit. The following expression holds:

$$C_N^{soft}|_{\lambda \ll 1} = 1 + \frac{\alpha_S(\mu^2)C_F}{\pi} \left\{ \ln^2 N + \left[ 2\gamma_E + 1 - \ln \left( \frac{\mathcal{M}^2}{\mu_F^2} \right) \right] \ln N \right\}. \quad (4.34)$$

For later convenience we have introduced the following scale:

$$\mathcal{M}^2 = m^2 \left( 1 + \frac{Q^2}{m^2} \right)^2. \quad (4.35)$$

In evaluating the Mellin transforms, we have made use of the results presented in the appendix.

It is obvious that the coefficient functions  $H_i^q$  are enhanced in the limit  $z \rightarrow 1$  and therefore must be resummed. Let us note, however, the very different behavior of the NLO result in the soft limit for small and large values of the ratio  $m/Q$  (see Eqns.(4.33) and (4.34)). That suggests that the resummed coefficient function may exhibit strong dependence on the value of  $m/Q$ . In the next section we will present our results for the resummation of the coefficient function with NLL accuracy for low transferred momentum  $Q^2 \sim m^2$ , and will discuss its relation to the well known massless limit  $m^2/Q^2 \rightarrow 0$ .

### 4.3 Soft-gluon Resummation for the Quark-initiated Coefficient Function

One can perform the soft-gluon (threshold) resummation with NLL accuracy for the coefficient function for the process (4.27) by applying the general methods developed in [53] that we presented in detail in Section (2.4.3). To that end, one first needs to collect the contributions from soft-gluon emission. That can be done using the eikonal techniques discussed also in Section (2.4.3). Second, one needs to identify and – if it is present – to collect the contribution from pure collinear radiation.

Let us start with the calculation of the soft contributions in the eikonal approximation. We consider the inclusive hard scattering process

$$q_1(p)W^*(q) \rightarrow q_2(p_2) + \text{soft gluons}, \quad (4.36)$$

where the momenta  $p$ ,  $q$  and  $p_2$  are hard and the momenta of the additional gluons are all soft. In c.m. co-ordinates we have:

$$2p^0 \cong \frac{Q^2 + m^2}{\sqrt{(1-z)Q^2 + m^2}}. \quad (4.37)$$

In the eikonal approximation the momentum of the outgoing hard quark is taken [53] to be  $\bar{p} = p + q$ , with  $\bar{p}^2$  given by:

$$\bar{p}^2 \simeq (1-z)(Q^2 + m^2) + m^2. \quad (4.38)$$

Next we calculate the contribution from real gluon emission to the eikonal cross-section at order  $\mathcal{O}(\alpha_S)$  and add the virtual contribution using unitarity, as in (2.73). The eikonal current (2.72) is constructed out of the hard momenta  $p$  and  $\bar{p}$ , and its square is given in [53]. We then express the result as an integral over the variables  $z$  and  $k^2 = (p + p_g)^2(1-z)$  with  $0 \leq k^2 \leq (2p^0)^2(1-z)^2$  and  $0 \leq z \leq 1$ .

Finally, the exponentiated result for the coefficient function for the process (4.36) in the soft limit and in the  $\overline{\text{MS}}$ -subtraction scheme reads:

$$\ln \Delta_N = \int_0^1 dz \frac{z^{N-1} - 1}{1 - z} \left\{ \int_{\mu_F^2}^{k_{\max}^2} \frac{dk^2}{k^2} A[\alpha_S(k^2)] + S[\alpha_S(k_{\max}^2)] \right\}. \quad (4.39)$$

The function  $A$  is defined in (2.77) and the function  $S$  in (3.30). To obtain the latter we used the relation <sup>3</sup> (2.75). The derivation of (4.39) proceeds in complete analogy with our discussions in Section (2.4.3) and Section (3.4), so we do not present each step in full detail here. In the present case, however, where the kinematics of the process we consider allows the ratio of the two mass parameters  $m^2/Q^2$  to vary widely, we encounter another complication that we discuss next.

Ideally, one would like to be able to describe the soft limit  $z \rightarrow 1$  of the coefficient function (4.29) with a single expression that is valid for any kinematically allowed value of the ratio  $m^2/Q^2$ . It principle that seems possible because the zero-mass limit  $m^2 \rightarrow 0$  of the coefficient function is regular for any value of the kinematical variable  $z$ . This follows from the fact that the inclusive quark-initiated coefficient function is free from mass singularities from the final state. However, as can be explicitly seen from the fixed order result we discussed in the previous section, the limit  $z \rightarrow 1$  of the coefficient function is strongly affected by the value of  $m^2/Q^2$ . The reason is obvious: if one wants to be able to cover all values of  $m^2/Q^2$ , effectively one has to deal with a two variable problem. As such one can consider  $z$  and  $\lambda z$  or, in the conjugated Mellin space,  $N$  and  $(1 - \lambda)N$  (recall the definition of  $\lambda$  in Eq.(4.14)).

Let us demonstrate our point in a simple example. Consider a term of the form  $\ln[(1 - \lambda)N]$ . We are interested in its behavior at large  $N$  for any  $\lambda \leq 1$ . Although such a term is formally divergent when  $N \rightarrow \infty$  for any  $\lambda < 1$ , it is clear that for values of  $\lambda$  sufficiently close to one, such a term cannot be considered large;

---

<sup>3</sup>After Eq.(4.40) has been used as well; see below.

in particular it cannot be considered on the same footing with pure  $\ln(N)$  terms. Another example is the scale  $k_{\max}^2$ . Its behavior strongly depends on the relative magnitude of  $m^2$  with respect to  $(1-z)Q^2$ . For small enough mass, that scale is  $\sim (1-z)$  while for sufficiently large mass it is  $\sim (1-z)^2$ :

$$k_{\max}^2 \cong (2p^0)^2(1-z)^2 = \begin{cases} Q^2(1-z) & \text{when } m^2 = 0, \\ \mathcal{M}^2(1-z)^2 & \text{when } m^2 \sim Q^2, \end{cases} \quad (4.40)$$

with  $\mathcal{M}$  defined in Eq.(4.35). That difference in the behavior of the scale  $k_{\max}^2$  influences significantly the soft limit of the coefficient function; we will see that the coefficient of the leading logarithmic term in the perturbative result (4.33) and (4.34) is in fact proportional to the value of the power of  $(1-z)$  in  $k_{\max}^2$ . Yet another illustration of the interplay between the large  $N$  limit and the value of the mass  $m$  (relative to  $Q$ ) is the result for the factor  $K$  (4.47), (4.58); the derivation of this factor is presented in some detail in the appendix.

In order to avoid the above mentioned subtleties and to be able to extract in a straightforward way the singular  $z$  dependence of the resummed coefficient function (4.39), in what follows we will consider separately the following two cases (each case effectively involves a single scale): the case of sufficiently large value of the ratio  $m^2/Q^2$  that we will refer to as “massive”, and the “massless” case  $m^2/Q^2 = 0$ . We will present separately results for both cases. We will treat these two results as complementing each other; we will apply the “massive” result for cases where  $m^2/Q^2 \gtrsim 1/5$  while we can certainly apply the massless result for  $m^2/Q^2 \lesssim 1/10$ . Supposedly in the intermediate region neither of the results is correct although the difference between the two results in that range is not large, i.e. the correct results also should not differ much.

Finally, in order to collect all contributions one must also account for possible collinear radiation from the final state. As we will see in a moment, that

contribution is also affected by the value of  $m^2/Q^2$ .

### 4.3.1 The case $m^2 \sim Q^2$

If the final-state quark is massive, the virtuality of the final state in the large- $z$  limit is given in Eq.(4.38) and is never small provided that  $m/Q$  is sufficiently large. As a result, there is no additional collinear enhancement for heavy quark production. Therefore in the case  $m^2/Q^2 \sim 1$ , by combining Eqns.(4.39) and (4.40), we get the following result for the quark-initiated coefficient function in the limit  $z \rightarrow 1$ :

$$\begin{aligned} \ln \Delta_N &= \int_0^1 dz \frac{z^{N-1} - 1}{1-z} \left\{ \int_{\mu_F^2}^{\mathcal{M}^2(1-z)^2} \frac{dk^2}{k^2} A \left[ \alpha_S(k^2) \right] \right. \\ &\quad \left. + S \left[ \alpha_S \left( \mathcal{M}^2(1-z)^2 \right) \right] \right\}. \end{aligned} \quad (4.41)$$

One can evaluate Eq.(4.41) with NLL accuracy with the help of Eq.(2.82). The result has the general form (2.80):

$$\Delta_N(\alpha_S(\mu^2), \mu^2, \mu_F^2, m^2, Q^2) = \exp \left[ \ln N g^{(1)}(L) + g^{(2)}(L, \mu^2, \mu_F^2) \right], \quad (4.42)$$

where similarly to Eq.(2.81) we have introduced:

$$L = b_0 \alpha_S(\mu^2) \ln N. \quad (4.43)$$

The functions  $g^{(1)}$  and  $g^{(2)}$  are given by

$$g^{(1)}(L) = \frac{A^{(1)}}{2\pi b_0 L} [2L + (1-2L) \ln(1-2L)], \quad (4.44)$$

$$\begin{aligned} g^{(2)}(L, \mu, \mu_F) &= \frac{A^{(1)}}{2\pi b_0} \left[ \ln \frac{\mathcal{M}^2}{\mu_F^2} - 2\gamma_E \right] \ln(1-2L) \\ &\quad + \frac{A^{(1)} b_1}{4\pi b_0^3} [4L + 2 \ln(1-2L) + \ln^2(1-2L)] \\ &\quad - \frac{1}{2\pi b_0} [2L + \ln(1-2L)] \left( \frac{A^{(2)}}{\pi b_0} + A^{(1)} \ln \frac{\mu^2}{\mu_F^2} \right) \\ &\quad + \frac{S^{(1)}}{2\pi b_0} \ln(1-2L). \end{aligned} \quad (4.45)$$

In Eq.(4.42) the term  $\ln Ng^{(1)}(L)$  accounts for the resummation of leading logarithms (LL)  $\alpha_S^n \ln^{n+1} N$  in the Sudakov exponent, while the function  $g^{(2)}(L, \mu^2, \mu_F^2)$  resums NLL terms  $\alpha_S^n \ln^n N$ .

Next, we present our final Sudakov-resummed coefficient function with matched NLO and NLL contributions:

$$H_{N,i}^S(\mu^2, \mu_F^2, m^2, Q^2) = \left[ 1 + \frac{\alpha_S(\mu^2) C_F}{2\pi} K_i(\mu_F^2, m^2, Q^2) \right] \times \exp \left[ \ln Ng^{(1)}(\lambda) + g^{(2)}(\lambda, \mu, \mu_F) \right]. \quad (4.46)$$

Furthermore, in analogy with the top decay case we considered in the previous Chapter and following [43], we include in our final Sudakov-resummed coefficient function also the terms  $K(\mu_F^2, m^2, Q^2)$  of the NLO coefficient function (4.29) which are constant in the limit  $N \rightarrow \infty$ :

$$K_i(\mu_F^2, m^2, Q^2) = \left( \frac{3}{2} - 2\gamma_E \right) \ln \left( \frac{Q^2 + m^2}{\mu^2} \right) + \ln(1 - \lambda) \left( 2\gamma_E + \frac{3\lambda - 2}{2\lambda} \right) + A_i - 2\text{Li}_2 \left( -\frac{Q^2}{m^2} \right) + 2(\gamma_E - 1)(\gamma_E + 2). \quad (4.47)$$

The evaluation of the factor (4.47) is detailed in the appendix. Following [94] we have defined the quantities  $A_i$ , which satisfy the following relations:

$$A_1 = A_3 = 0, \quad A_2 = \frac{1}{\lambda}(1 - \lambda) \ln(1 - \lambda). \quad (4.48)$$

We now match the resummed coefficient function to the exact first-order result: we add the resummed result to the exact coefficient function and, in order to avoid double counting, we subtract what they have in common. The final expression for the resummed coefficient function reads:

$$\begin{aligned} \hat{H}_{N,i}^{\text{res}}(\mu^2, \mu_F^2, m^2, Q^2) &= H_{N,i}^S(\mu^2, \mu_F^2, m^2, Q^2) \\ &\quad - \left[ H_{N,i}(\mu^2, \mu_F^2, m^2, Q^2) \right]_{\alpha_S} \\ &\quad + C_{N,i}^q(\mu^2, \mu_F^2, m^2, Q^2) \end{aligned} \quad (4.49)$$

where  $C_{N,i}^q$  is the Mellin transform of the perturbative result for the functions  $C_i^q$  introduced in (4.29).

Before closing the discussion of the threshold resummation in the massive case we would like to discuss a relation between the result Eq.(4.41) and the corresponding results for other processes.

One can relate our result Eq.(4.41) to the one for heavy quark decay. An example is the top quark decay Eq.(3.3) we discussed in the previous Chapter. One can easily see that the expression Eq.(4.41) can be obtained from the corresponding result in top decay – Eq.(3.29) – after the identification:

$$m_{top} \rightarrow m ; \quad m_W^2 \rightarrow -Q^2. \quad (4.50)$$

The relation (4.50) is not accidental. It can be understood in the following way: consider the coefficient functions for the following two processes:

$$\mathcal{Q} \rightarrow W + q, \quad (4.51)$$

$$q + W^* \rightarrow \mathcal{Q}. \quad (4.52)$$

By  $\mathcal{Q}$  and  $q$  we denote heavy and light quark, respectively, and the states in Eqns.(4.51), (4.52) are the initial/final states in those processes <sup>4</sup>. Ignoring details like spins and charges, the processes (4.51) and (4.52) are related <sup>5</sup> by time-inversion which, in turn, implies (4.50). Let us now generalize those processes and consider more particles (denoted generally by  $X$ ) in the final states:

$$\mathcal{Q} \rightarrow W + q + X, \quad (4.53)$$

$$q + W^* \rightarrow \mathcal{Q} + X. \quad (4.54)$$

---

<sup>4</sup>Clearly, that is unphysical in view of the Kinoshita-Lee-Nauenberg Theorem discussed in Section (2.4). However, one can think of Eqns.(4.51) and (4.52) as the Born approximation to the corresponding physical processes.

<sup>5</sup>Plus inversion of the sign of the mass of the  $W$ -boson since the latter is space-like in (4.52) and time-like (and on-shell) in (4.51).

Of interest to us are processes where  $X$  stands for a collection of soft gluons. In that case, up to contributions that are not singular in the limit  $N \rightarrow \infty$ , the processes (4.53) and (4.54) can also be related by Eq.(4.50). To see this, one needs to recall that the processes (4.53) and (4.54) can be described with the help of the eikonal cross-section discussed in Section (2.4.3). In this approximation the “back reaction” from soft gluon radiation on the hard radiating particles is neglected. To derive the soft coefficient function in the eikonal approximation, we integrate Eq.(2.68) over all of the radiated gluons. The resulting expression therefore depends only on the configuration of the hard scattering particles that in turn is encoded in Eqns.(4.51) and (4.52).

An explicit example is the one-loop evaluation of the eikonal amplitudes in our processes of interest: the results depend only on the square of the eikonal current for which (4.50) is manifest.

Of course the above considerations are complete only because there is no additional contribution due to collinear radiation in any of the processes (4.53) and (4.54). We would also like to note that the relation (4.50) is not restricted only to the NLL approximation. For that reason we expect that the function  $S$  appearing in both Eq.(4.41) and Eq.(3.29) is the same even beyond the NLL level.

Let us point out that soft resummation for the coefficient function in DIS has been first considered in [53, 58] and lately implemented in [61], but in the approximation in which all participating quarks are massless. Soft-gluon resummation for heavy quark production in DIS processes has been investigated in [96] and [97], where the authors have considered neutral current interactions.

### 4.3.2 The case $m^2 \ll Q^2$

In the limit  $m^2/Q^2 \rightarrow 0$  we recover the well known soft limit of the massless coefficient function (4.29) derived in [53]. As follows from Eq.(4.38), in this case the virtuality of the final-state jet vanishes like  $(1 - z)Q^2$ . Therefore the NLL coefficient function receives an additional contribution due to purely collinear radiation. As shown in [53], one can account for such a contribution by solving a modified evolution equation for the jet distribution associated with the final state. As a result, an additional term will contribute to the function  $S(\alpha_S)$  that enters the Sudakov exponent in Eq.(4.39). Taking also into account the zero-mass limit in Eq.(4.40), we get the well known massless result for the quark initiated  $\overline{\text{MS}}$  coefficient function [58]:

$$\ln \Delta_N|_{m/Q \rightarrow 0} = \int_0^1 dz \frac{z^{N-1} - 1}{1 - z} \left\{ \int_{\mu_F^2}^{Q^2(1-z)} \frac{dk^2}{k^2} A \left[ \alpha_S(k^2) \right] + \frac{1}{2} B \left[ \alpha_S \left( Q^2(1-z) \right) \right] \right\}. \quad (4.55)$$

The function  $B(\alpha_S)$  generalizes the function  $S$  from Eq.(4.39) and also includes the contribution from collinear radiation from the final state. It also can be expanded in powers of  $\alpha_S$ :

$$B(\alpha_S) = \sum_{n=1}^{\infty} \left( \frac{\alpha_S}{\pi} \right)^n B^{(n)} \quad (4.56)$$

and, to NLL level, one needs only the first term of the expansion:

$$B^{(1)} = -\frac{3}{2} C_F. \quad (4.57)$$

The explicit evaluation of Eq.(4.55) to NLL level can be found in [61], where functions analogous to our  $g^{(1)}$  and  $g^{(2)}$  are reported. Similarly to Eq.(4.49) in the massive case, we also match the resummed result (4.55) to the exact coefficient function (4.29), with functions  $H_i^q$  now evaluated in the limit  $m/Q \rightarrow 0$ , i.e.  $\lambda \rightarrow 1$ . The constant factors  $K_i$ , analogous to the one in Eq.(4.47), read in the

massless approximation (see the appendix for details):

$$K_i(\mu_F^2, m^2, Q^2)|_{m/Q \rightarrow 0} = \left( \frac{3}{2} - 2\gamma_E \right) \ln \left( \frac{Q^2}{\mu^2} \right) + \gamma_E^2 + \frac{3}{2}\gamma_E - \frac{\pi^2}{6} - \frac{9}{2}, \quad (4.58)$$

for  $i = 1, 2, 3$ .

Finally, one can check that the  $\mathcal{O}(\alpha_S)$  expansion of the resummed results correctly reproduces the large- $N$  limits of the coefficient function in both the massive and massless cases.

Before we move on to the phenomenological applications, let us compare our results on soft-gluon resummation for heavy quark decay Eq.(3.29) and for heavy-quark production in CC DIS Eq.(4.41) to the general results for soft-gluon resummation discussed in [21]. Both our results have the general form:

$$\ln \Delta_N^{\text{res}} = \ln \Delta_N^q + \ln J_N^q, \quad (4.59)$$

where the factor:

$$\ln \Delta_N^q = \int_0^1 dz \frac{z^{N-1} - 1}{1 - z} \int_{\mu_F^2}^{Q^2(1-z)^2} \frac{dk^2}{k^2} A \left[ \alpha_S(k^2) \right]. \quad (4.60)$$

is due to soft and collinear radiation from the final quark for the case of top-decay (similarly to the  $e^+e^-$  quark production in [43]) and from the initial quark in CC DIS. The scale  $Q^2$  appearing there is the corresponding characteristic hard scale. It equals  $m_t^2(1 - m_W^2/m_t^2)^2$  for the case of top-decay and  $m^2(1 + Q^2/m^2)^2$  for the case of massive quark production in CC DIS. The second term in Eq.(4.59)

$$\ln J_N^q = \int_0^1 dz \frac{z^{N-1} - 1}{1 - z} S \left[ \alpha_S(Q^2(1-z)^2) \right], \quad (4.61)$$

describes soft-gluon radiation that is not collinearly enhanced, and the scale  $Q^2$  is the same as the one in (4.60). Our result (4.61) however differs in an obvious way from the similar factors appearing in [21, 43]: in both of our cases (top decay and CC DIS) we have an observed massless quark and an unobserved massive quark.

For that reason in Eq.(4.61) we have the function  $S$  instead of the function  $1/2B$ , where the latter embodies collinear radiation from a massless quark. Also, the integral over the (eikonal) anomalous dimension that appears in those papers is also absent in our cases, since for us the two limits of that integral coincide, i.e. in the massive case we have:

$$\begin{aligned} \ln J_N^q &= \int_0^1 dz \frac{z^{N-1} - 1}{1 - z} \left\{ \int_{Q^2(1-z)^2}^{Q^2(1-z)^a} \frac{dk^2}{k^2} A \left[ \alpha_S(k^2) \right] \right. \\ &\quad \left. + J \left[ \alpha_S(Q^2(1-z)^a) \right] \right\}, \end{aligned} \quad (4.62)$$

where  $a = (1, 2)$  and  $J = (1/2B, S)$  in the massless and massive cases respectively. Again,  $Q$  stands for the relevant hard scale for the process under consideration.

## 4.4 Phenomenological Results for Charm Quark Production

In this section we apply our results for soft-gluon (threshold) resummation to the study of charm quark production in charged current (CC) events. Measurements of the charm quark structure functions in the CC regime are in fact important in order to probe the density of strange quarks and gluons in the proton.

Charged-current Deep Inelastic Scattering processes  $\nu_\mu N \rightarrow \mu X$  were recently studied at the NuTeV experiment at Fermilab, where neutrino and antineutrino beams collide with an iron fixed target (see, e.g., Ref. [98] for the updated results). In particular, production of two oppositely-charged muons at NuTeV [99] is mainly associated with a CC event with a charm quark in the final state. The first generation of the H1 and ZEUS experiments on electron-proton DIS at the HERA collider at DESY (HERA I) did detect charged-current events  $ep \rightarrow \nu_e X$  [100, 101], but it did not have sufficiently-high statistics to reconstruct heavy

quarks in the CC regime. However, such measurements are foreseen in the current improved-luminosity run (HERA II) and at the possible future generation of HERA III experiments [102], which should be able to investigate the proton structure functions also at low  $Q^2$  values.

The structure functions are given as a convolution of  $\overline{\text{MS}}$  coefficient functions and parton distribution functions. Since the resummed coefficient function is given in  $N$ -space, in principle one would like to use parton distribution functions in Mellin space as well, in order to get the resummed structure function in moment space and finally invert it numerically from  $N$ - to  $x$ -space. However, all modern sets of parton distribution functions [29, 103, 26] are given numerically in the form of a grid in the  $(x, Q^2)$  space.

In order to overcome this problem, we follow the method proposed in Ref. [104] in the context of joint resummation, which allows one to use  $x$ -space parton distributions, even when performing resummed calculations in Mellin space.

This method consists of rewriting the integral of the inverse Mellin transform of the resummed structure functions as follows:

$$\begin{aligned}\mathcal{F}_i^{\text{res}}(\chi, Q^2) &= \frac{1}{2\pi i} \int_{\Gamma_N} dN \chi^{-N} q_N(\mu_F^2) H_{N,i}^{\text{res}}(\mu^2, \mu_F^2, m^2, Q^2) \\ &= \frac{1}{2\pi i} \int_{\Gamma_N} dN \chi^{-N} [(N-1)^2 q_N(\mu_F^2)] \frac{H_{N,i}^{\text{res}}(\mu^2, \mu_F^2, m^2, Q^2)}{(N-1)^2} (4.63)\end{aligned}$$

where  $q_N(\mu_F^2)$  is the parton distribution of the initial-state quark  $q_1$ , as if it were available in  $N$  space, and  $\Gamma_N$  is the integration contour in the complex plane, chosen according to the Minimal Prescription [63].

One can integrate out the term with the parton distribution function observing that the following relation holds:

$$\frac{1}{2\pi i} \int_{\Gamma_N} dN \xi^{-N} (N-1)^2 q_N(\mu_F^2) = \frac{d}{d\xi} \left\{ \xi \frac{d}{d\xi} [\xi q(\xi, \mu_F^2)] \right\} = \Phi(\xi, \mu_F^2). \quad (4.64)$$

Due to Eq.(4.64), one no longer needs the  $N$ -space parton distributions, but one should just differentiate the  $x$ -space ones, which is numerically doable.

As one has the analytical expression for  $H_{N,i}^{\text{res}}$  in  $N$ -space (4.49), the following inverse Mellin transform is straightforward:

$$\mathcal{H}(\xi, \mu_F^2) = \frac{1}{2\pi i} \int_{\Gamma_N} dN \xi^{-N} \frac{H_{N,i}^{\text{res}}(\mu^2, \mu_F^2, m^2, Q^2)}{(N-1)^2} \quad (4.65)$$

which, thanks to the suppressing factor  $1/(N-1)^2$  in the integrand function, turns out to be smooth for  $\xi \rightarrow 1$ .

The resummed structure function will be finally expressed as the following convolution

$$\mathcal{F}_i^{\text{res}}(x, Q^2) = \int_x^1 \frac{d\xi}{\xi} \mathcal{H}(\xi, \mu^2, \mu_F^2) \Phi\left(\frac{\chi}{\xi}, \mu_F^2\right). \quad (4.66)$$

After having clarified how we are dealing with the parton distribution functions, we are able to present results for soft-resummed structure functions. We shall consider charm quark production, i.e.  $q_2 = c$  in Eq.(4.27), since processes with charm quarks in the final state play a role for structure function measurements at NuTeV and in HERA experiments.

As for the choice of the parton distribution set, in principle, once data on heavy quark production CC DIS were to be available, one should use the CC NLL coefficient function when performing the parton distribution global fits and get NLL parton densities as well. For the time being, we can just use one of the most-updated NLO sets and convolute it with the fixed-order or resummed coefficient function.

We shall present results based on the new generation of CTEQ NLO  $\overline{\text{MS}}$  parton distribution functions [29], the so-called CTEQ6M set, but similar results can be obtained using, e.g., the MRST [103] or the GRV [26] sets.

The elementary scattering processes which yield the production of charm quarks in CC DIS are  $dW^* \rightarrow c$  and  $sW^* \rightarrow c$ . For  $e^+(e^-)p$  scattering at HERA,

our parton distribution function  $q_1(\xi, Q^2)$  in Eq.(4.24) will hence be:

$$q_1(\xi, Q^2)|_{\text{HERA}} = |V_{cd}|^2 d(\xi, Q^2) + |V_{cs}|^2 s(\xi, Q^2), \quad (4.67)$$

where  $V_{cd}$  and  $V_{cs}$  are the relevant Cabibbo–Kobayashi–Maskawa matrix elements. For neutrino scattering on an isoscalar target, that will have to be modified in order to account for the possibility of an interaction with a neutron as well:

$$q_1(\xi, Q^2)|_{\text{NuTeV}} = |V_{cd}|^2 \frac{d(\xi, Q^2) + u(\xi, Q^2)}{2} + |V_{cs}|^2 s(\xi, Q^2), \quad (4.68)$$

where  $d(\xi, Q^2)$ ,  $u(\xi, Q^2)$  and  $s(\xi, Q^2)$  are still the proton parton distribution functions and we have applied the isospin symmetry (2.3).

In order to be consistent with the use of the CTEQ parton distribution functions, we shall use for the QCD scale in the  $\overline{\text{MS}}$  renormalization scheme the values  $\Lambda_4 = 326$  MeV and  $\Lambda_5 = 226$  MeV, for four and five active flavors respectively. This corresponds to  $\alpha_S(m_Z) = 0.118$ . The charm and bottom quark masses have been set to  $m_c = 1.3$  GeV and  $m_b = 4.5$  GeV, as done in [29].

Since mass effects are important for large values of the ratio  $m_c/Q$ , we would like to have  $Q$  as small as possible to be able to apply our massive resummation. The NuTeV experiment is indeed able to measure structure functions at small  $Q^2$  values [98, 99], as they are able to detect the final-state muon produced in the  $\nu_\mu N \rightarrow \mu X$  processes. In our phenomenological analysis we shall consider charm production at  $Q^2 = 2$  GeV $^2$  and  $Q^2 = 5$  GeV $^2$ , which are values reachable at NuTeV and such that  $m_c^2/Q^2$  is relatively large.

The detection of CC events at HERA is more problematic, due to backgrounds and to the presence of a neutrino, instead of a charged lepton, in the final state. The current HERA II experiments make it possible to detect heavy quarks in CC events, but the  $Q^2$  values for such events are still supposed to be much larger than the charm quark squared mass, typically  $Q^2 \gtrsim 100$  GeV $^2$ . We shall present

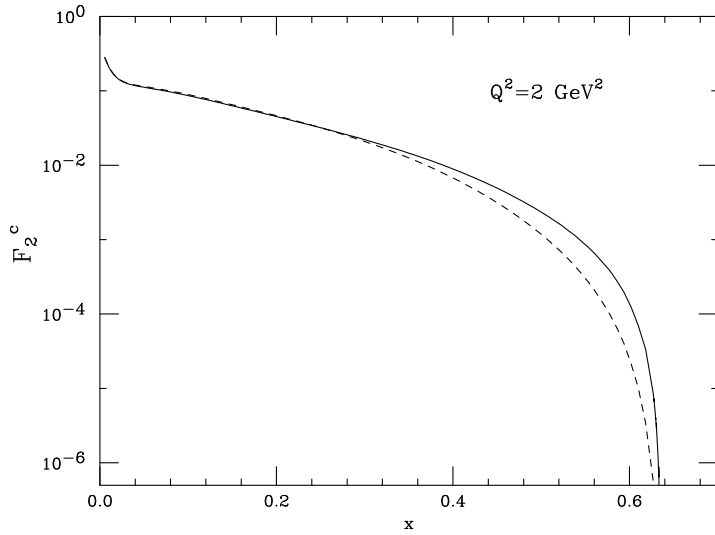


Figure 4-2: Results for  $F_2^c(x, Q^2)$  for charm quark production in neutrino scattering at  $Q^2 = 2 \text{ GeV}^2$  with (solid) and without (dashed) soft resummation in the coefficient function. We have set  $\mu_F = \mu = Q$ .

nonetheless results for charm quark production at HERA, but in this case we shall have to use the massless result for the resummed  $\overline{\text{MS}}$  coefficient function, i.e. Eq.(4.55) and the formulas reported in [61]. We shall consider the typical HERA values  $Q^2 = 300 \text{ GeV}^2$  and  $1000 \text{ GeV}^2$ .

We shall present results for the structure function  $F_2^c(x, Q^2)$ , but we can already anticipate that the effect of the resummation is approximately the same on all three structure functions  $F_1^c$ ,  $F_2^c$  and  $F_3^c$  and on the single-differential cross section  $d\sigma/dx$ , obtained from Eq.(4.10), after integrating over  $y$ .

For the sake of comparison with the experiments, we shall plot the structure function  $F_2^c$  in terms of Bjorken  $x$ , which is the quantity which is measured. For most of our plots, we shall set the renormalization and factorization scales equal to  $Q$ , i.e.  $\mu_F = \mu = Q$ . Afterwards, we shall also investigate the dependence of our results on the choice of these scales.

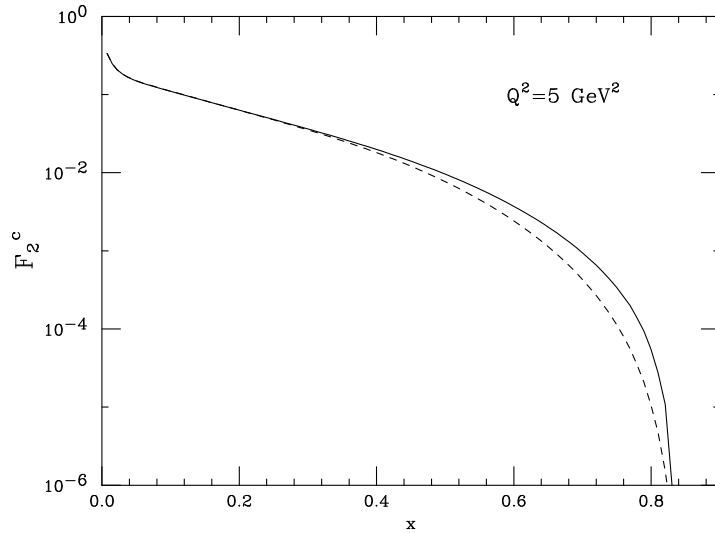


Figure 4-3: As in Fig. 4-2, but for  $Q^2 = 5 \text{ GeV}^2$ .

In Figs.(4-2) and (4-3) we show  $F_2^c(x, Q^2)$  in neutrino scattering at  $Q^2 = 2 \text{ GeV}^2$  and  $5 \text{ GeV}^2$  and compare the results obtained using fixed-order and soft-resummed  $\overline{\text{MS}}$  coefficient functions. We have set the target mass to  $M = 1 \text{ GeV}$ , which is a characteristic nucleon mass. We observe a relevant effect of the implementation of soft resummation: the two predictions agree up to  $x \simeq 0.2 - 0.3$ ; afterwards one can see an enhancement of the structure function due to the resummation. At very large  $x$  resummed effects are indeed remarkable: for  $Q^2 = 2 \text{ GeV}^2$  one has an enhancement of a factor of 2 at  $x = 0.5$  and a factor of 5 at  $x = 0.6$ . For  $Q^2 = 5 \text{ GeV}^2$  one gets a factor of 2 at  $x = 0.7$  and 5 at  $x = 0.8$ .

In Figs.(4-4) and (4-5) we present results for  $F_2^c(x, Q^2)$ , but for charm production at HERA, in particular for positron-proton scattering at  $Q^2 = 300$  and  $1000 \text{ GeV}^2$ . In this case, since  $m_c/Q \ll 1$ , we use the massless result (4.55) for the resummed coefficient function. We observe that the impact of the resummation is smaller than in the case of low  $Q^2$  values. This is a reasonable result: in fact, leading and next-to-leading logarithms in the Sudakov exponent are weighted by

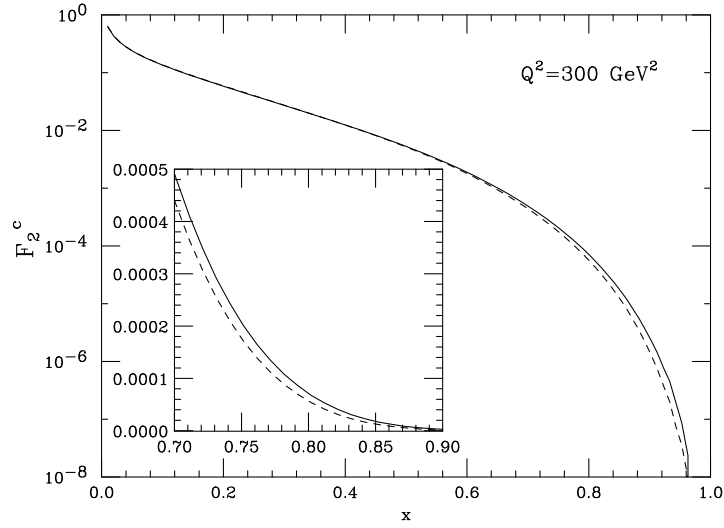


Figure 4-4: Results for  $F_2^c(x, Q^2)$  for charm quark production in positron-proton scattering at HERA. for  $Q^2 = 2 \text{ GeV}^2$  We have set  $\mu_F = \mu = Q$ . In the inset figure, we show the same plots at large  $x$  and on a linear scale.

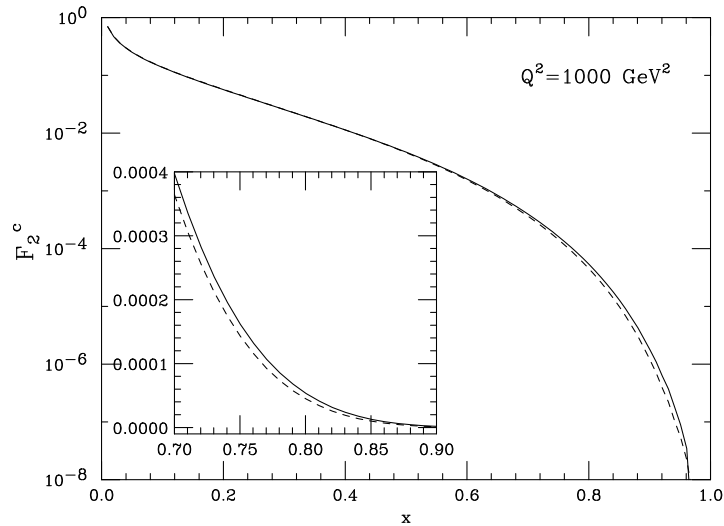


Figure 4-5: As in Fig. 4-4, but for  $Q^2 = 1000 \text{ GeV}^2$ .

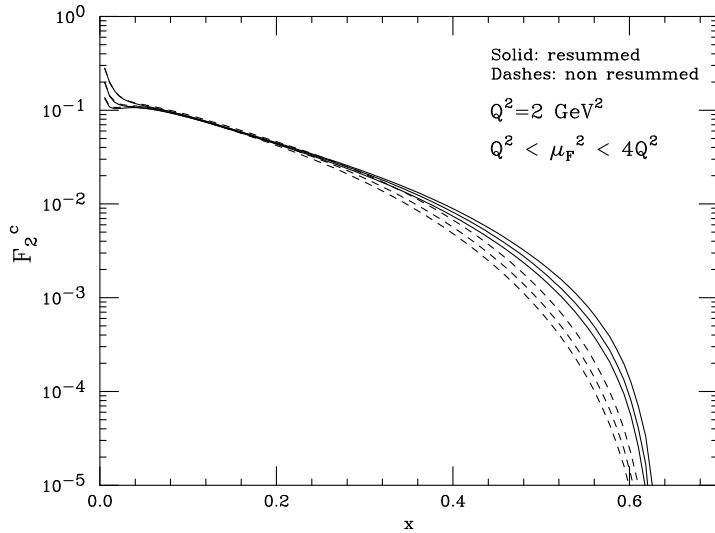


Figure 4-6: Dependence of  $F_2$  on the factorization scale for neutrino scattering at NuTeV. Solid lines include soft resummation in the coefficient function, dashed lines are fixed-order predictions

powers of  $\alpha_S(\mu^2)$ . As, e.g.,  $\alpha_S(2 \text{ GeV}^2) \simeq 3 \alpha_S(300 \text{ GeV}^2)$ , resummed effects are clearly more important when  $Q^2$  is small. Moreover, the larger  $Q^2$  is, the larger the values of  $x$  are at which one is sensitive to Sudakov effects.

We note in Figs.(4-4) and (4-5) that, at about  $x > 0.6$ , the fixed-order and resummed predictions start to be distinguishable. We estimate the overall impact of large- $x$  resummation on  $F_2^c(x, Q^2)$  at  $Q^2 = 300 \text{ GeV}^2$  and  $Q^2 = 1000 \text{ GeV}^2$  to be between 10% and 20%.

In Figs.(4-6) and (4-7) we investigate the dependence on the factorization and renormalization scales. We still keep  $\mu = \mu_F$ , which we allow to assume the values  $Q^2$ ,  $2Q^2$  and  $4Q^2$ . We consider  $Q^2$  values of 2 and 300 GeV $^2$  for the experimental environments of NuTeV and HERA respectively. We see that the curves which implement soft resummation in the coefficient function show a weaker dependence on the chosen value for the factorization/renormalization

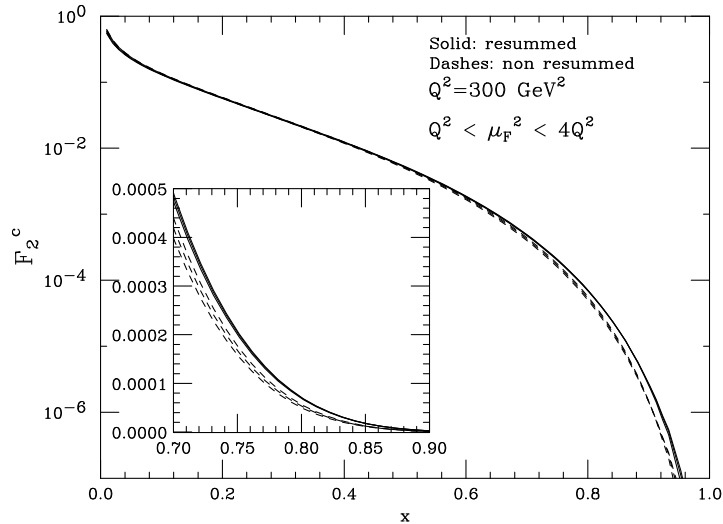


Figure 4-7: As in Fig. 4-6, but at HERA for  $Q^2 = 300 \text{ GeV}^2$ . In the inset figure, we plot the same curves at large  $x$  and on a linear scale.

scales. In Fig. (4-6) one can see that one still has a visible effect of the value of such scales, but the overall dependence on  $\mu_F$  and  $\mu$  of the resummed prediction is smaller than for the fixed-order. The plots at large  $Q^2$  exhibit in general a weak dependence on  $\mu_F$  and  $\mu$  even at NLO, as shown in Fig. (4-7). However, while the NLO structure function still presents a residual dependence on the scales, the resummed predictions obtained with three different values of  $\mu_F$  are basically indistinguishable. A smaller dependence on such scales implies a reduction of the theoretical uncertainty of the prediction and is therefore a remarkable effect of the implementation of soft gluon resummation.

We finally would like to compare the impact that mass effects and soft-gluon resummation have on the charm structure functions. To achieve this goal, we plot in Fig.(4-8) the theoretical structure function  $\mathcal{F}_2^c(\chi, Q^2)$  defined in Eq.(4.24) as a function of the variable  $\chi$  (see Eq.(4.19)), for neutrino scattering at  $Q^2 = 2 \text{ GeV}^2$ . We compare fixed-order massive (dashed line), fixed-order massless (dots)

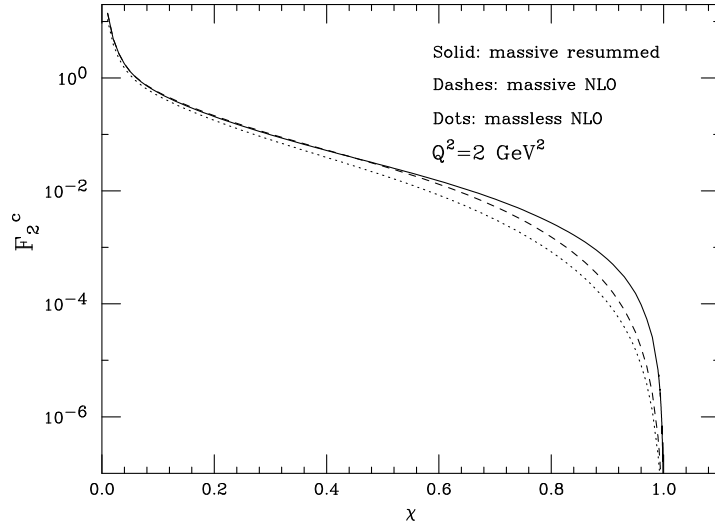


Figure 4-8: Comparison of massive (dashes) and massless (dots) fixed-order calculations with the resummed massive result (solid) for  $Q^2 = 2 \text{ GeV}^2$  and  $\mu = \mu_F = Q$ . Plotted is the theoretical structure function  $\mathcal{F}_2^c(\chi, Q^2)$  defined in Eq.(4.22).

and massive resummed (solid) predictions. We observe that the two fixed-order calculations yield different predictions throughout the full  $\chi$  range, which is a consequence of the implementation of mass effects; however, at large  $\chi$ , where one starts to be sensitive to the resummation, the impact of soft resummation is competitive with that of mass contributions.

Before closing this section, we would like to point out that, although we have improved our perturbative prediction by implementing soft-gluon resummation in the coefficient function, non-perturbative corrections are still missing. Non-perturbative effects are important especially at small values of  $Q^2$  and large  $x$ . In fact, a more accurate investigation of the very-large  $x$  limit of the structure functions shows that they exhibit an oscillatory behavior once  $x$  gets closer to the maximum value which is kinematically allowed.

# Chapter 5

## Conclusions

In this Thesis we have applied perturbative QCD to make precision predictions for processes like top decay and heavy quark production in charged-current DIS.

We have first discussed the general properties of QCD as a theory of the strong interactions. The discussion is organized in a way that emphasizes certain problems that arise in processes involving heavy quarks, like the appearance of large quasi-collinear logs and large soft-logs. Furthermore, in addition to the factorization theorem and parton evolution, we presented a general description of the resummation methods used to treat those problems.

Our first application was to  $b$  quark fragmentation in top decay, since this will be an important observable for the study of the top quark once enough experimental data is available. We first presented the results of our NLO QCD calculation for this process and we commented on its shortcomings: the need for all-order resummation of quasi-collinear and soft logs. Our NLO perturbative result reproduces the known universal initial condition for the perturbative fragmentation function as well as the NLO result for the total top decay width. We performed the resummation of the quasi-collinear logs  $\ln(m_b^2/m_t^2)$  applying the formalism

of perturbative fragmentation function with NLL accuracy. The resummation of those logs leads to very serious improvement of the  $b$ -quark spectrum. To further improve the behavior of the  $b$ -spectrum towards the region of large  $b$ -momentum fraction, we have evaluated the soft-gluon resummed expression for the top-decay coefficient function with NLL accuracy. The combined result of the two types of all-order resummations that we have performed is significant: the validity of our result is extended towards higher values of the  $b$ -quark energy fraction  $x_b$ . The resulting expression has very little dependence on the unphysical factorization and renormalization scales. Finally, we used our improved perturbative result for  $b$ -quark fragmentation to make a prediction for the energy spectrum of certain  $b$ -flavored hadrons in top decay. To that end we extracted information about the non-perturbative transition  $b$ -quark to  $b$ -flavored hadron from  $e^+e^-$  collision data. We performed that extraction in two ways: first we extracted the non-perturbative fragmentation function by fitting  $e^+e^-$  data with the fragmentation function of three different functional forms having one or two fittable parameters. We have observed that working this way, the largest uncertainty in the prediction comes from the fits to the data. The second approach we pursued in order to extract information for the non-perturbative fragmentation, is to extract from data the four lowest moments of the fragmentation function by working directly in the space of Mellin moments. That way we do not have to extract the non-perturbative function, i.e. no fit with its corresponding uncertainty is involved.

The second application that we considered in this Thesis is heavy quark production in inclusive CC DIS. We started by making the observation that the NLO light quark initiated coefficient function for heavy quark production in CC DIS contains terms that become arbitrarily large towards high values of the Bjorken variable. That fact signals the need for soft-gluon resummation for that coefficient function. We carefully identified the sources of such large contributions. Then

we performed the soft-gluon resummation separately in the kinematical regimes of large values of the ratio of the mass of the heavy quark with respect to the transferred momentum and small values of that ratio (i.e. the massless regime). Our calculation reproduces the known results in the limit of zero mass and of the NLO evaluation of the coefficient function. We applied our result to charm production in CC DIS. The most relevant application is to charm production in neutrino-nucleon DIS at NuTeV, since that experiment can reach low values of momentum transfer where our resummed result is most relevant. We made a prediction for the charm-component of the structure functions with full account for target mass effects. We observed that at large Bjorken  $x$ , although the absolute value of the structure function is small, the relative impact of the resummation we performed is significant. The dependence on factorization/renormalization scales is reduced as a result of the resummation. We have checked that at low  $Q$ , the size of the effect of the threshold resummation (at large  $x$ ) is comparable or even larger than the effect of the power corrections of the charm mass. This is clearly another indication of the significance of our result. It will be very interesting to compare our prediction with the forthcoming data from NuTeV.

# Bibliography

- [1] N. Arkani-Hamed, S. Dimopoulos and G. Dvali, Phys. Lett B 429 (1998) 263.
- [2] L. Randall and R. Sundrum, Phys. Rev. Lett. 83 (1999) 3370.
- [3] S. Weinberg, Phys. Rev. Lett. 19 (1967) 1264; A. Salam, in *Elementary Particle Physics*, ed. N. Svartholm (Almqvist and Wiksell, Stockholm, 1968), p.367.
- [4] K. Hagiwara et al, Phys. Rev. D 66 (2002) 010001.
- [5] T. Muta, *Foundations of QCD*, (World Scientific, Singapore, 1998).
- [6] R. K. Ellis, W. J. Stirling and B. R. Webber, *QCD and Collider Physics*, Cambridge Univ. Press, 1996.
- [7] A. Bassutto, M. Ciafaloni and G. Marchesini, Phys. Rep. 100 (1983) 201.
- [8] Yu. L. Dokshitzer, D. I. Dyakonov and S. I. Troyan, Phys. Rept. 58 (1980) 269.
- [9] Yu. L. Dokshitzer, V. A. Khoze, A. H. Mueller and S. I. Troyan, *Basics of Perturbative QCD*, Editions Frontieres, Gif-sur-Yvette, 1991.
- [10] M. Gell-Mann, Phys. Lett. 8 (1964) 214; G. Zweig, Preprints CERN-TH 401 and 412.

- [11] M. Han and Y. Nambu, Phys. Rev. 139B (1965) 1006; M. Gell-Mann, Acta Phys. Austriaca Suppl. 9 (1972) 733.
- [12] R. Feynman, Phys. Rev. Lett. 23 (1969) 1415.
- [13] J. Bjorken, Phys. Rev. 179 (1969) 1547.
- [14] M. Breidenbach et al., Phys. Rev. Lett. 23 (1969) 935.
- [15] C. Callan and D. Gross, Phys. Rev. Lett. 22 (1969) 156.
- [16] G. 't Hooft, Nucl. Phys. B 33 (1971) 173.
- [17] H. Fritzsch, M. Gell-Mann and H. Leutwyler, Phys. Lett. B 47 (1973) 365.
- [18] O. V. Tarasov, A. A. Vladimirov and A. Yu. Zharkov, Phys. Lett. B 93 (1980) 429; S. A. Larin and J. A. M. Vermaseren, Phys. Lett. B 303 (1993) 334; T. van Ritbergen, J. A. M. Vermaseren and S. A. Larin, Phys. Lett. B 400 (1997) 379.
- [19] W. Bernreuther, Ann. Phys. (NY) 151 (1983) 127; Erratum Nucl. Phys. B 513 (1998) 758.
- [20] D. Gross and F. Wilczek, Phys. Rev. D 8 (1973) 3497; H. D. Politzer, Phys. Rev. Lett. 26 (1973) 1346.
- [21] S. Catani, M. L. Mangano and P. Nason, JHEP 9807 (1998) 024.
- [22] J. C. Collins, D. E. Soper and G. Sterman, in *Perturbative QCD*, edited by A. H. Mueller (World Scientific, Singapore, 1989), p.1.
- [23] J. C. Collins, Phys. Rev. D 66 (1998) 094002.
- [24] J. C. Collins and D. E. Soper, Nucl. Phys. B 194 (1982) 445.

- [25] G. Curci, W. Furmanski and R. Petronzio, Nucl. Phys. B 175 (1980) 27; W. Furmanski and R. Petronzio, Phys. Lett. B97 (1980) 437.
- [26] M. Gluck, E. Reya and A. Vogt, Eur. Phys. J. C 5 (1998) 461.
- [27] J. C. Collins, F. Wilczek and A. Zee, Phys. Rev. D 18 (1978) 242.
- [28] M. Aivazis, J. C. Collins, F. I. Olness and Wu-Ki Tung, Phys. Rev. D 50 (1994) 3102.
- [29] J. Pumplin, D. R. Stump, J. Huston, H. L. Lai, P. Nadolsky and Wu-Ki Tung, JHEP 0207 (2002) 012.
- [30] S. Libby and G. Sterman, Phys. Rev. D 18 (1978) 3252; 18 (1978) 4737.
- [31] G. Altarelli and G. Parisi, Nucl. Phys. B 126 (1977) 298.
- [32] V. N. Gribov and L. N. Lipatov, Sov. J. Nucl. Phys. 15 (1972) 438; L. N. Lipatov, Sov. J. Nucl. Phys. 20 (1975) 94; Yu. L. Dokshitzer, Sov. Phys. JETP 46 (1977) 641.
- [33] E. G. Floratos, D. A. Ross and C. T. Sachrajda, Nucl. Phys. B 129 (1977) 66; ibid. B 139 (1978) 545 (erratum); ibid. B 152 (1979) 493; A. Gonzales-Arroyo, C. Lopez and F. J. Yndurain, Nucl. Phys. B 153 (1979) 161; E. G. Floratos, R. Lacaze and C. Kounnas, Nucl. Phys. B 192 (1981) 417.
- [34] H. Georgi and H. D. Politzer, Phys. Rev. D 9 (1974) 416.
- [35] D.J. Gross and F. Wilczek, Phys. Rev. D 9 (1974) 980.
- [36] G. Sterman, Phys. Rev. D 17 (1978) 2773; ibid 2789.
- [37] F. Bloch and A. Nordsieck, Phys. Rev. 52 (1937) 54; A. Nordsieck, Phys. Rev. 52 (1937) 59.

- [38] T. Kinoshita, *J. Math. Phys.* 3 (1962) 650; T. D. Lee and M. Nauenberg, *Phys. Rev.* 133 (1964) 1545.
- [39] S. Weinberg, *Phys. Rev.* 140B (1965) 516.
- [40] S. Catani and M. Grazzini, *Nucl. Phys. B* 570 (2000) 287.
- [41] S. Kretzer and I. Schienbein, *Phys. Rev. D* 58 (1998) 094035.
- [42] B. Mele and P. Nason, *Nucl. Phys. B* 361 (1991) 626.
- [43] M. Cacciari and S. Catani, *Nucl. Phys. B* 617 (2001) 253.
- [44] G. Colangelo and P. Nason, *Phys. Lett. B* 285 (1992) 167.
- [45] M. Cacciari and M. Greco, *Phys. Rev. D* 55 (1997) 7134.
- [46] P. Nason and C. Oleari, *Nucl. Phys. B* 565 (2000) 245.
- [47] M. Cacciari and P. Nason, *Phys. Rev. Lett.* 89 (2002) 122003.
- [48] M. Cacciari and M. Greco, *Nucl. Phys. B* 421 (1994) 530.
- [49] M. Cacciari, M. Greco, S. Rolli and A. Tanzini, *Phys. Rev. D* 55 (1997) 2736.
- [50] M. Cacciari and M. Greco, *Z. Phys. C* 69 (1996) 459.
- [51] G. Corcella and A. D. Mitov, *Nucl. Phys. B* 623 (2002) 247.
- [52] S. Keller and E. Laenen, *Phys. Rev. D* 59 (1999) 114004.
- [53] S. Catani and L. Trentadue, *Nucl. Phys. B* 327 (1989) 323.
- [54] G. Sterman, *Nucl. Phys. B* 281 (1987) 310.
- [55] S. Catani and L. Trentadue, *Nucl. Phys. B* 353 (1991) 183.

- [56] J. Frenkel, P. Sorensen and J. C. Taylor, *Z. Phys. C* 35 (1987) 361.
- [57] D. Amati, A. Bassetto, M. Ciafaloni, G. Marchesini and G. Veneziano, *Nucl. Phys. B* 173 (1980) 429.
- [58] S. Catani, G. Marchesini and B. R. Webber, *Nucl. Phys. B* 349 (1991) 635.
- [59] J. Kodaira and L. Trentadue, *Phys. Lett. B* 112 (1982) 66; S. Catani, E. D'Emilio and L. Trentadue, *Phys. Lett. B* 211 (1988) 335.
- [60] W. L. van Neerven and A. Vogt, *Phys. Lett. B* 490 (2000) 111.
- [61] A. Vogt, *Phys. Lett. B* 497 (2001) 228.
- [62] U. Aglietti and G. Ricciardi, *Phys. Rev. D* 66 (2002) 074003.
- [63] S. Catani, M. L. Mangano, P. Nason and L. Trentadue, *Nucl. Phys. B* 478 (1996) 273.
- [64] M. Beneke, V. M. Braun, *Nucl. Phys. B* 454 (1995) 253.
- [65] M. Cacciari, G. Corcella and A. D. Mitov, *JHEP* 12 (2002) 015.
- [66] F. Abe et al. (CDF Collaboration), *Phys. Rev. Lett.* 74 (1995) 2626; S. Abachi et al. (DØ Collaboration), *Phys. Rev. Lett.* 74 (1995) 2632.
- [67] L. Demortier et al., (CDF and DØ Collaborations), Fermilab-TM-2084 (1999).
- [68] U. Baur, M. Buice and L. H. Orr, *Phys. Rev. D* 64 (2001) 094019.
- [69] D. Chakraborty, J. Konigsberg and D. Rainwater, hep-ph/0303092 and references therein.

- [70] M. Beneke et al., in Proceedings of 1999 CERN Workshop on Standard Model Physics (and more) at the LHC, CERN 2000-004, G. Altarelli and M. L. Mangano eds., p. 419, hep-ph/0003033.
- [71] J. A. Aguilar-Saavedra et al., ECFA/DESY LC Physics Working group, hep-ph/0106315; T. Abe et al., American Linear Collider Working Group, Part 3, Studies of Exotic and Standard Model Physics, hep-ex/0106057; K. Abe et al., ACFA Linear Collider Working group, hep-ph/0109166.
- [72] L. H. Orr and J. L. Rosner, Phys. Lett. B 246 (1990) 221; I. Bigi, Yu. L. Dokshitzer, V. A. Khoze, J. H. Kuhn and P. M. Zerwas, Phys. Lett. B 181 (1986) 157.
- [73] DØ Collaboration, B. Abbott et al., Phys. Rev. D58 (1998) 052001; CDF Collaboration, T. Affolder et al., Phys. Rev. D63 (2001) 032003.
- [74] A. Kharchilava, Phys. Lett. B476 (2000) 73.
- [75] CDF Collaboration, T. Affolder et al., Phys. Rev. Lett. 86 (2001) 3233.
- [76] A. Czarnecki, Phys. Lett. B252 (1990) 467.
- [77] G. Passarino, M. Veltman, Nucl. Phys. B 160 (1979) 151.
- [78] A. Czarnecki, K. Melnikov, Nucl. Phys. B 544 (1999) 520.
- [79] C. S. Li, R. J. Oakes and T. C. Yuan, Phys. Rev. D 43 (1991) 855.
- [80] G. P. Korchemsky and G. Sterman, Phys. Lett. B 340 (1994) 96.
- [81] R. Akhoury and I. Z. Rothstein, Phys. Rev. D 54 (1996) 2349; A. K. Leibovich and I. Z. Rothstein, Phys. Rev. D 61 (2000) 074006; A. K. Leibovich, I. Low and I. Z. Rothstein, Phys. Rev. D 62 (2000) 014010.

- [82] U. Aglietti, Phys. Lett. B 515 (2001) 308; U. Aglietti, Nucl. Phys. B 610 (2001) 293; U. Aglietti, R. Sghedoni and L. Trentadue, Phys. Lett. B 522 (2001) 83.
- [83] V. G. Kartvelishvili, A. K. Likehoded and V.A. Petrov, Phys. Lett. B 78 (1978) 615.
- [84] C. Peterson, D. Schlatter, I. Schmitt and P. M. Zerwas, Phys. Rev. D 27 (1983) 105.
- [85] G. Altarelli, R. K. Ellis, G. Martinelli and S.-Y Pi, Nucl. Phys. B 160 (1979) 301; W. Furmanski and R. Petronzio, Z. Physik C 11 (1982) 293.
- [86] ALEPH Collaboration, A. Heister et al., Phys. Lett. B 512 (2001) 30.
- [87] SLD Collaboration, K. Abe et al., Phys. Rev. Lett. 84 (2000) 4300.
- [88] OPAL Collaboration, G. Abbiendi et al., CERN-EP/2002-051.
- [89] DELPHI Collaboration, ICHEP 2002 Note, DELPHI 2002-069 CONF 603.
- [90] G. Corcella and A. D. Mitov, hep-ph/0308105.
- [91] M. Aivazis, F. I. Olness and Wu-Ki Tung, Phys. Rev. D 50 (1994) 3085.
- [92] S. Kretzer and M. H. Reno, Phys. Rev. D 66 (2002) 113007.
- [93] O. Nachtmann, Nucl. Phys. B 63 (1973) 237.
- [94] M. Glück, S. Kretzer and E. Reya, Phys. Lett. B380 (1996) 171; ibid. B405 (1997) 391.
- [95] T. Gottschalk, Phys. Rev. D23 (1981) 56.
- [96] E. Laenen and Sven-Olaf Moch, Phys.Rev. D 59 (1999) 034027.

- [97] P. M. Nadolsky, N. Kidonakis, F. I. Olness and C.-P. Yuan, Phys. Rev. D 67 (2003) 074015.
- [98] NuTeV Collaboration, D. Naples et al., hep-ex/0306035; M. Tzanov et al., hep-ex/0306035.
- [99] NuTeV Collaboration, M. Goncharov et al., Phys. Rev. D64 (2001) 112006.
- [100] H1 Collaboration, C. Adloff et al., hep-ex/0304003.
- [101] ZEUS Collaboration, S. Chekanov et al., Phys. Lett. B545 (2002) 244.
- [102] H. Abramowicz et al., “A New Experiment for the HERA Collider”, MPI-PhE/2003-06.
- [103] A. D. Martin, R. G. Roberts, W. J. Stirling and R. S. Thorne, Eur. Phys. J. C23 (2002) 73.
- [104] A. Kulesza, G. Sterman and W. Vogelsang, Phys. Rev. D 66 (2002) 014011.
- [105] L. Lewin, “Dilogarithms and Associated Functions”, MacDonald, London, 1958.

# Appendix A

## Some Supplementary Results

### A.1 Relevant Feynman Rules

We can specify the Feynman rules that we have used by presenting the relevant amplitude for one of the diagrams with real gluon emission.

$$M = \bar{u}_{\sigma, c_1}(p_b) \left[ -i \frac{g_S}{2} \gamma^\nu \lambda_{c_1, c_2}^a \right] G_\nu^a(p_g, \kappa) \frac{i (\not{p}_b + \not{p}_g + m)}{(p_b + p_g)^2 - m_b^2 + i\varepsilon} \\ \times \left[ -i \frac{g}{\sqrt{8}} V_{tb} \delta_{c_2, c_3} \gamma^\mu (1 - \gamma^5) \right] \epsilon_\mu^*(p_W, \rho) u_{\lambda, c_3}(p_t). \quad (\text{A.1})$$

The terms in square brackets correspond to the boson-quark vertexes,  $c_{1,2,3}$  are the quark color indexes,  $\sigma, \kappa, \rho$  and  $\lambda$  are the polarizations (spins) of the  $b$ -quark, the gluon,  $W^+$ -boson and the top-quark respectively. Also, the propagator for a gluon with loop momentum  $q$  is (we choose to work in Feynman gauge):

$$-i \delta_{ab} \frac{g_{\mu\nu}}{q^2 + i\varepsilon}. \quad (\text{A.2})$$

We work with cross-section that is summed over the final states and averaged over the initial ones. The relevant results (for the example of Eq.(A.1)) are:

$$\overline{\sum}_{in} \sum_{out} = \frac{1}{3} \sum_{c_1, c_2} \sum_a \frac{1}{2} \sum_\lambda \sum_\sigma \sum_\rho \sum_\kappa, \quad (\text{A.3})$$

$$\sum_{\kappa} G_{\nu}^a(p, \kappa) G_{\mu}^a(p, \kappa) = -g_{\nu\mu}, \quad (\text{A.4})$$

$$\sum_{\sigma} u_{\sigma, \alpha}(p) \bar{u}_{\sigma, \beta}(p) = (\not{p} + m)_{\alpha\beta}, \quad (\text{A.5})$$

$$\sum_{\rho} \epsilon_{\mu}^*(p, \rho) \epsilon_{\nu}(p, \rho) = -g_{\nu\mu} + \frac{p_{\mu} p_{\nu}}{m_W^2}, \quad (\text{A.6})$$

Our conventions for working in  $D$  space-time dimensions are:

$$\begin{aligned} \epsilon &= \frac{4 - D}{2} \\ \{\gamma_{\mu}, \gamma_{\nu}\} &= 2g_{\mu\nu} \\ \text{tr}(\gamma_{\mu}\gamma_{\nu}) &= 4g_{\mu\nu} \\ \gamma_{\mu}\gamma^{\mu} &= D \\ \gamma_{\mu}\gamma_{\nu}\gamma^{\mu} &= (2 - D)\gamma_{\nu} \\ g_{\mu}^{\mu} &= D \\ \frac{d^D k}{(2\pi)^D} &= \text{measure for the loop integrals.} \end{aligned} \quad (\text{A.7})$$

Also, only the strong coupling picks up the usual mass dimension:

$$g_S \rightarrow g_S \mu^{\epsilon}.$$

## A.2 Phase Space for Top Decay at NLO

We consider the three particle top decay  $t \rightarrow bWg$  in  $D$  space-time dimensions, where each of the particles in that reaction is on-mass-shell. The masses are  $m_t, m_W, m_b$  and 0 respectively. For simplicity, we work in the top rest frame. One has:

$$\begin{aligned} d\Gamma &= N_D \overline{|\mathcal{M}|^2}(p_t; p_b, p_g, p_W) \delta^D(p_t - p_b - p_g - p_W) \\ &\times \delta(p_b^2 - m_b^2) \delta(p_W^2 - m_W^2) \delta(p_g^2) d^D p_b d^D p_g d^D p_W, \end{aligned} \quad (\text{A.8})$$

with:

$$N_D = \frac{1}{2m_t} \frac{1}{(2\pi)^{5-4\epsilon}}. \quad (\text{A.9})$$

With the help of the delta-functions, one can reduce (A.8) to:

$$\begin{aligned} d\Gamma &= N_D \overline{|M|^2} \delta \left( 2(p_b \cdot p_g) - 2(p_t \cdot p_g) - 2(p_t \cdot p_b) + m_t^2 + m_b^2 - m_W^2 \right) \\ &\times \frac{d^{D-1} p_b}{2E_b} \frac{d^{D-1} p_g}{2E_g}, \end{aligned} \quad (\text{A.10})$$

The matrix element  $\overline{|M|^2}$  is given in Eq.(3.7); we have used the relations implied by the delta functions to simplify it.

Next, it will be convenient to work in spherical co-ordinates with the  $z$ -axis along the  $D-1$  dimensional vector  $\vec{p}_g$ . Clearly, nothing depends on its orientation; the only nontrivial integrations are over the energies  $E_b$  and  $E_g$  and over  $\cos \theta = \cos(\vec{p}_g, \vec{p}_b)$ .

To carry out the trivial angular integrations, one may use the following results: in  $d$ -dimensional Euclidean space (see also [5]),

$$d^d x = r^{d-1} dr d\Omega_d, \quad d\Omega_d = \prod_{l=1}^{d-1} (\sin \theta_l)^{d-l-1} d\theta_l. \quad (\text{A.11})$$

The trivial angular integrations (all for the  $p_g$  case and all but one for the  $p_b$  case) amount to the factor  $S_d \mathcal{S}_d$ , where:

$$\begin{aligned} S_d &= \int d\Omega_d, \\ \mathcal{S}_d &: d\Omega_d = \mathcal{S}_d (\sin \theta)^{d-2} d\theta, \end{aligned} \quad (\text{A.12})$$

i.e., the factor  $\mathcal{S}_d$  contains all the angular integrations but the azimuthal one.

To evaluate those factors, it is convenient to introduce:

$$J^{(n)} = \int_0^\pi \sin^n \theta d\theta = \frac{\pi}{2^n} \frac{\Gamma(n+1)}{\Gamma(n/2+1)^2}.$$

The latter satisfy the relation  $J^{(n)} = (n-1)/n J^{(n-2)}$  with  $J^{(0)} = \pi$ ,  $J^{(1)} = 2$ . Then one can easily show that  $S_d = 2 \prod_{n=0}^{d-2} J^{(n)}$  and  $\mathcal{S}_d = 2 \prod_{n=0}^{d-3} J^{(n)}$ . The relevant result for us is:

$$\begin{aligned} S_{D-1} &= 2 \frac{\pi^{3/2-\epsilon}}{\Gamma(3/2-\epsilon)}, \\ \mathcal{S}_{D-1} &= 2 \frac{\pi^{1-\epsilon}}{\Gamma(1-\epsilon)}, \\ S_{D-1} \mathcal{S}_{D-1} &= 8\pi^2 \left[ 1 + 2\epsilon(1 - \gamma_E - \ln(2\pi)) + \mathcal{O}(\epsilon^2) \right]. \end{aligned} \quad (\text{A.13})$$

Finally, we can write the final result containing the two non-trivial integrations over the two energies:

$$d\Gamma = \frac{N_D}{8} m_t^{2-4\epsilon} S_{D-1} \mathcal{S}_{D-1} \frac{\overline{|M|^2}}{(Ay^2 + By + C)^\epsilon} dx_E dy, \quad (\text{A.14})$$

where  $x_E = E_b/m_t$ ,  $y = E_g/m_t$ ,  $A = x_E^2 - b - (1-x_E)^2$ ,  $B = 2(1-x_E)(s-x_E)$ ,  $C = -(x_E - s)^2$ . The squared matrix element (3.7) should be evaluated using:

$$\cos(\vec{p}_b, \vec{p}_g) = \frac{m_t^2}{|\vec{p}_g| |\vec{p}_b|} (x_E y - x_E - y + s).$$

The limits on the two variables are (see also the notation introduced in (3.4)):

$$\begin{aligned} \sqrt{b} &\leq x_E \leq s, \\ y_- &\leq y \leq y_+ ; \quad y_\pm = \frac{s - x_E}{1 - x_E \mp \sqrt{x_E^2 - b}}. \end{aligned}$$

To obtain the desired differential distribution  $d\Gamma/dx_b$  one must integrate over  $y$  and use  $x_b = x_E/s$  as implied by (3.5). In the integration over  $y$  the so-called plus prescription appears. It is discussed in Section (A.4).

### A.3 Spence Functions

We present some relations between the Spence functions (or di-logarithms) that we have used. Most are taken from [105] where more details about the properties of those functions can be found.

That function is defined through the integral:

$$\text{Li}_2(z) = - \int_0^z \frac{dt}{t} \ln(1-t), \quad (\text{A.15})$$

and has a cut from  $z = 1$  to  $\infty$ . Some particular values are:

$$\text{Li}_2(1) = \frac{\pi^2}{6}, \quad \text{Li}_2(-1) = -\frac{\pi^2}{12}. \quad (\text{A.16})$$

The Spence function satisfies the following relations [105]:

$$\begin{aligned} \text{Li}_2\left(-\frac{1}{x}\right) &= -\text{Li}_2(-x) - \frac{1}{2} \ln^2(x) - \frac{\pi^2}{6}, \\ \text{Li}_2(x) &= -\text{Li}_2\left(\frac{-x}{1-x}\right) - \frac{1}{2} \ln^2(1-x), \\ \frac{1}{2}\text{Li}_2(x^2) &= \text{Li}_2(x) + \text{Li}_2(-x), \\ \text{Li}_2\left(\frac{x}{1-x} \frac{y}{1-y}\right) &= \text{Li}_2\left(\frac{x}{1-y}\right) + \text{Li}_2\left(\frac{y}{1-x}\right) \\ &\quad - \text{Li}_2(x) - \text{Li}_2(y) - \ln(1-x) \ln(1-y), \\ \text{Li}_2\left(\frac{y(1-x)}{x(1-y)}\right) &= \text{Li}_2(x) - \text{Li}_2(y) + \text{Li}_2\left(\frac{y}{x}\right) + \text{Li}_2\left(\frac{1-x}{1-y}\right) \\ &\quad - \frac{\pi^2}{6} + \ln(x) \ln\left(\frac{1-x}{1-y}\right). \end{aligned}$$

Combining the above relations one can derive other relations:

$$\begin{aligned} \text{Li}_2(x) &= -\text{Li}_2(1-x) + \frac{\pi^2}{6} - \ln(x) \ln(1-x), \\ \text{Li}_2(x) &= \text{Li}_2\left(\frac{1}{1-x}\right) + \ln(1-x) \ln\left(\frac{1-x}{-x}\right) - \frac{1}{2} \ln^2(1-x) - \frac{\pi^2}{6}, \\ \text{Li}_2\left(\frac{1-x}{-x}\right) &= 2\text{Li}_2\left(\frac{-x}{1-x}\right) - 3\text{Li}_2(1-x) - 2 \ln(x) \ln(1-x) \\ &\quad + \ln^2(1-x) - \frac{1}{2} \ln^2(x) + \frac{\pi^2}{3}. \end{aligned} \quad (\text{A.17})$$

## A.4 Plus Prescription

Here we discuss some properties of the so-called plus prescription  $[f(x)]_+$  defined through:

$$\int_0^1 [f(x)]_+ g(x) dx = \int_0^1 f(x) (g(x) - g(1)) dx \quad (\text{A.18})$$

where  $g$  is a sufficiently regular function, while the function  $f$  typically is non-integrable in the point  $x = 1$ . The plus prescriptions are strictly distributions; for  $x < 1$  they can be thought as the function itself i.e.:

$$[f(x)]_+ = f(x) \text{ for } x < 1.$$

Those distributions appear through the following identity:

$$\lim_{\epsilon \rightarrow 0} \frac{(x - x_{min})^{2\epsilon}}{(1 - x)^{1+2\epsilon}} = -\frac{1}{2\epsilon} \delta(1 - x) + \frac{1}{(1 - x)_+} + \mathcal{O}(\epsilon). \quad (\text{A.19})$$

One can prove it by multiplying both sides with a test function, use the definition (A.18) and then compare the terms multiplying the different powers of  $\epsilon$ . The lower limit can be any number  $x_{min} : 0 \leq x_{min} < 1$ . In the massless case,  $m_b = 0$ , one needs the identity (A.19) including the term linear in  $\epsilon$ , the latter being:

$$\left( \frac{\ln(1 - x)}{1 - x} \right)_+ - \frac{\ln(x)}{1 - x}.$$

Using Eq.(A.18), one can easily prove the following important distributional identities:

$$\begin{aligned} [f(x)]_+ g(x) &= f(x)g(x) - \left( g(1) \int_0^1 f(y) dy \right) \delta(1 - x), \\ [f(x)g(x)]_+ &= [f(x)]_+ g(x) - \left( \int_0^1 [f(y)]_+ g(y) dy \right) \delta(1 - x), \\ [f(x)]_+ g(x) &= [f(x)]_+ g(1) + f(x) (g(x) - g(1)). \end{aligned} \quad (\text{A.20})$$

All of these identities are applicable to functions  $f, g$  for which the identities themselves make sense. As an example, using the above relations, one can write

the splitting function  $P_{qq}^{(0)}(x)$  in Eq.(2.34) as:

$$P_{qq}^{(0)}(x) = C_F \left( \frac{1+x^2}{1-x} \right)_+ = C_F \left( \frac{2}{(1-x)_+} - (1+x) + \frac{3}{2}\delta(1-x) \right) \quad (\text{A.21})$$

## A.5 Mellin-Space Results

The Mellin transformation is defined through Eq.(2.39). That transformation has the factorization property (2.40). The inverse Mellin transform is given in Eq.(2.65). The following functions are often encountered:

$$\begin{aligned} \int_0^1 dz z^{N-1} \frac{1}{(1-z)_+} &= -S_1(N-1), \\ \int_0^1 dz z^{N-1} \frac{\ln z}{(1-z)_+} &= -\psi_1(N), \\ \int_0^1 dz z^{N-1} \left[ \frac{\ln(1-z)}{1-z} \right]_+ &= \frac{1}{2} [S_1^2(N-1) + S_2(N-1)], \\ \int_0^1 dz z^{N-1} \ln(1-x) &= -\frac{S_1(N)}{N}, \end{aligned} \quad (\text{A.22})$$

where (we correct a typo in that definition in Eq.(B.2) in [51]):

$$\psi_k(x) = \frac{d^{k+1} \ln \Gamma(x)}{dx^{k+1}} \quad (\text{A.23})$$

and

$$\begin{aligned} S_1(N) &\equiv \psi_0(N+1) - \psi_0(1) = S_1(N-1) + \frac{1}{N}, \\ S_2(N) &\equiv -\psi_1(N+1) + \psi_1(1) = S_2(N-1) + \frac{1}{N^2}, \\ S_3(N) &\equiv \frac{1}{2} [\psi_2(N+1) - \psi_2(1)]. \end{aligned} \quad (\text{A.24})$$

The large  $N$  behavior of some of the often encountered singular functions is [53]:

$$\int_0^1 dz z^{N-1} \frac{1}{(1-z)_+} = -\ln(N) - \gamma_E + \mathcal{O}(1/N),$$

$$\begin{aligned}
\int_0^1 dz z^{N-1} \left[ \frac{\ln(1-z)}{1-z} \right]_+ &= \frac{1}{2} \ln^2(N) + \gamma_E \ln(N) \\
&+ \frac{1}{2} (\gamma_E^2 + \zeta(2)) + \mathcal{O}(1/N).
\end{aligned} \tag{A.25}$$

## A.6 $N$ -space Result for the Coefficient Function and $D_q^{ini}$

The  $N$ -space expression for the coefficient function (3.21) is [51]:

$$\begin{aligned}
\hat{\Gamma}_N(m_t, m_W, \mu, \mu_F) &= 1 + \frac{\alpha_S(\mu) C_F}{2\pi} \left\{ \ln \frac{m_t^2}{\mu_F^2} \left[ \frac{1}{N(N+1)} - 2S_1(N) + \frac{3}{2} \right] \right. \\
&+ [1 + 2\ln(1-w)] \frac{1}{N(N+1)} - 2\psi_1(N) - 2\psi_1(N+2) \\
&+ \frac{4w(1-w)}{1+2w} \left[ \frac{_2F_1(1, N+1, N+2, 1-w)}{N+1} \right. \\
&- \left. \frac{2F_1(1, N+2, N+3, 1-w)}{N+2} \right] + S_1^2(N-1) + S_1^2(N+1) \\
&+ S_2(N-1) + S_2(N+1) + 2[1 - 2\ln(1-w)]S_1(N) \\
&+ 2\ln w \ln(1-w) - 2 \frac{1-w}{1+2w} \ln(1-w) - \frac{2w}{1-w} \ln w \\
&+ \left. 4\text{Li}_2(1-w) - 6 - \frac{2\pi^2}{3} \right\}.
\end{aligned} \tag{A.26}$$

The  $N$ -space expression for the quark initiated initial condition (2.58) for the perturbative fragmentation function is [42]:

$$\begin{aligned}
D_{q,N}^{ini}(\mu_0, m) &= 1 + \frac{\alpha_S(\mu_0^2) C_F}{2\pi} \left[ \ln \left( \frac{\mu_0^2}{m^2} \right) \left( \frac{3}{2} + \frac{1}{N(N+1)} - 2S_1(N) \right) \right. \\
&- 2S_1^2(N) + \frac{2}{N(N+1)} S_1(N) - \frac{2}{(N+1)^2} \\
&- \left. 2S_2(N) + 2 - \frac{1}{N(N+1)} + 2S_1(N) \right]
\end{aligned} \tag{A.27}$$

One can derive those transformations with the use of the results in Section (A.5).

## A.7 $N$ -space Expressions for the Kernels $P_N^{(0,1)}$

Applying the results in Section (A.5) one has the following  $N$ -space expression for the leading order splitting function:

$$P_N^{(0)} = C_F \left( \frac{3}{2} + \frac{1}{N(N+1)} - 2S_1(N) \right). \quad (\text{A.28})$$

The result for the non-singlet NLO kernel is reported in [42] and reads:

$$P_N^{(1)} = C_F^2 [P_F(N) + \Delta(N)] + \frac{1}{2} C_F C_A P_G(N) + \frac{1}{2} C_F n_f P_{NF}(N), \quad (\text{A.29})$$

where  $C_F$  and  $C_A$  are given in (2.10),  $n_f$  is the number of the active flavors, and

$$\begin{aligned} P_F(N) &= \left( 2S_1(N) - \frac{1}{N(N+1)} \right) (2S_2(N) - 2\zeta(2)) - \frac{2(2N+1)}{N^2(N+1)^2} S_1(N) \\ &\quad + 4S_3(N) - 3S_2(N) + 3\zeta(2) + \frac{3N^3 + N^2 - 1}{N^3(N+1)^3} - \frac{23}{8}, \\ P_{NF}(N) &= \frac{20}{9}S_1(N) - \frac{4}{3}S_2(N) - \frac{1}{6} - 2\frac{11N^2 + 5N - 3}{9N^2(N+1)^2}, \\ P_G(N) &= -P_F(N) + S_1(N) \left( -\frac{134}{9} - 2\frac{2N+1}{N^2(N+1)^2} \right) + 4S_1(N)S_2(N) \\ &\quad + S_2(N) \left( \frac{13}{3} - \frac{2}{N(N+1)} \right) + \frac{43}{24} + \frac{151N^4 + 263N^3 + 97N^2 + 3N + 9}{9N^3(N+1)^3}, \\ \Delta(N) &= 2 \left( -2S_1(N) + \frac{3}{2} + \frac{1}{N(N+1)} \right) \left( 2S_2(N) - \frac{1}{3}\pi^2 - \frac{2N+1}{N^2(N+1)^2} \right). \end{aligned}$$

## A.8 Derivation of the Factors $K_i$ in Eqns.(4.47)

### and (4.58)

Here we present in some detail the derivation of the factor  $K_i$  given in Eqns.(4.47) and (4.58). We introduce a functional  $\Delta$ , such that to a function  $f(N)$ :

$$\lim_{N \rightarrow \infty} f(N) = \sum_{i>0} \ln^i(N) + f_0 + \mathcal{O}(1/N),$$

it assigns the constant  $f_0$ , i.e.:

$$\Delta[f(N)] = f_0.$$

Then the desired coefficient  $K_i$  is defined as:

$$\Delta[H_i^q(z, \mu_F^2, \lambda)] = C_F K_i(\mu_F^2, \lambda).$$

To calculate the action of  $\Delta$ , one first has to extract the singular dependence of a function using the results in (A.20). For example, making use of the relations (A.25), one gets for the leading order splitting function in Eq.(A.21):

$$\Delta[P_{qq}^{(0)}(z)] = C_F \left( \frac{3}{2} - 2\gamma_E \right).$$

We next calculate explicitly one of the more complicated terms in the coefficient function  $H_i^q$  that can be found in [92]:

$$\Delta[(f_\lambda(z))_+] = \begin{cases} \frac{1}{\lambda^2} (\lambda + \ln(1 - \lambda)), & \lambda < 1; \\ -\gamma_E, & \lambda = 1, \end{cases} \quad (\text{A.30})$$

where

$$f_\lambda(z) = \frac{1 - z}{(1 - \lambda z)^2}.$$

To demonstrate that result, one needs to separately consider the cases  $\lambda < 1$  and  $\lambda = 1$ . The action of  $\Delta$  in the latter case is obvious. When  $\lambda < 1$ ,  $f_\lambda(z)$  is integrable and we extract the  $z \rightarrow 1$  singular contribution using (A.20):

$$[f_\lambda(z)]_+ = f_\lambda(z) + \frac{1}{\lambda^2} (\lambda + \ln(1 - \lambda)) \delta(1 - z), \quad \lambda < 1. \quad (\text{A.31})$$

However, one must ensure that the first term in (A.31) vanishes in the large  $N$  limit. One can show that this term is indeed  $1/N$  suppressed and does not contribute. However, for large but fixed  $N$ , in the limit  $\lambda \rightarrow 1$ :

$$f_\lambda(z) \simeq \frac{\ln(1 - \lambda)}{N},$$

i.e. although the first term in (A.31) is formally  $1/N$  suppressed, it is no longer small in the limit of vanishing quark mass.